Design and Analysis of a Miniature Linear Compressor

by

Uğur Birbilen

A Thesis Submitted to the

Graduate School of Engineering

in Partial Fulfillment of the Requirements for

the Degree of

Doctor of Philosophy

in

Mechanical Engineering

Koc University

March 2018

Koc University

Graduate School of Sciences and Engineering

This is to certify that I have examined this copy of a doctoral thesis by

Uğur Birbilen

and have found that it is complete and satisfactory in all respects,

and that any and all revisions required by the final

examining committee have been made.

Committee Members:

____

Ismail Lazoğlu, Ph. D. (Advisor)

____

Erdem Alaca, Ph. D.

____

Mustafa Bakkal, Ph. D.

____

Metin Muradoğlu, Ph. D.

____

Ata Muğan, Ph. D.

Date: ______________________________

TO MY FAMILY

ABSTRACT

Linear compressors are good alternatives for the conventional rotary compressors which usually have to deal with the conversion of rotational motion to reciprocating motion before the compression step, whereas linear compressors directly generate linear motion to be used for the compression step right away. This offers many advantages over rotary compressors. While linear compressor technology is nothing new, miniature-scale linear compressor is a recent favorite. The compactness in linear compressor design combined with the smallness in scale makes this type of compressor a very interesting candidate for many practical applications, for example in the cooling of electronic equipment or in building mini refrigerators. This research deals with the detailed analysis of a prototype miniature-scale linear compressor. Basically, a linear compressor can be said to consist of two main parts: the linear actuator part which enables the reciprocating motion to the piston directly attached to it and the cylinder-valve assembly part where the interaction with the piston causes compression.

The linear actuator is moving-magnet type, which, compared to the other two types, namely moving-iron and moving-coil, provides higher thrust and efficiency and lower losses. To further enhance the compactness of the design, a tubular structure is selected. An analytical model is first presented and the formulation for the magnetic flux density and the generated thrust force is shown. Then an FEM analysis is conducted, where the axisymmetric approach is used in order to have a conformity with the tubular structure. The magnetic fluxes generated inside the actuator are again calculated and the generated thrust force is demonstrated accordingly. These results are compared with the ones coming from the analytical model. The experimental setup for the linear actuator is presented and the thrust force generated is compared with the analytical results.

The cylinder-valve assembly is presented and the selection and application steps as well as the estimated valve performance analysis is shown. The according manufacturing processes for the said assembly and the selection of the seal equipment for the miniature-scale problem at hand is presented.

The dynamic parameters of the entire compressor assembly are presented. This is shown for both the mechanical and electromagnetic cases. The governing system dynamics equations, which includes the thrust generated by the actuator and the stiffness and damping coming from both the mechanical equipment and the compressed gas, are provided. Motor constant and

excitation frequency effects are discussed. The frequency response function is shown in order to find the optimal operating point with the best system efficiency.

ÖZET

Doğrusal kompresörler, sıkıştırma adımından önce dönme hareketinin karşılıklı harekete dönüşümü ile uğraşmak zorunda kalan geleneksel döner kompresörler için iyi alternatiflerdir, çünkü lineer kompresörler sıkıştırma aşamasında kullanılacak doğrusal hareketi doğrudan üretebilirler. Bu, döner kompresörlere kıyasla birçok avantaj sağlar. Doğrusal kompresör teknolojisi yeni bir teknoloji olmamakla birlikte, minyatür ölçekli lineer kompresör özellikle son zamanlarda önem kazanmıştır. Doğrusal kompresör tasarımındaki kompaktlık, ölçeğin küçültülmesi ile birleştiğinde, bu kompresörü, elektronik ekipmanların soğutulması veya mini buzdolaplarının inşası gibi birçok pratikte uygulama için çok ilginç bir aday haline getirmektedir. Bu araştırma, bir prototip minyatür ölçekli doğrusal kompresörün detaylı analizi ile ilgilidir. Temelde doğrusal bir kompresörün iki ana bölümden oluştuğu söylenebilir: doğrudan doğruya tutturulmuş bir pistona ileri geri hareketi sağlayan lineer aktüatör kısmı ve pistonla etkileşimin gaz sıkışmasına neden olduğu silindir-valf kısmı.

Doğrusal aktüatör, hareketli-mıknatıs tipi olup, diğer iki tipe göre, yani hareketli-demir ve hareketli-bobin tipi aktüatörlerle karşılaştırıldığında daha yüksek itme kuvveti, verimlilik ve daha düşük kayıplar sağlar. Tasarımın kompaktlığını daha da artırmak için silindirik bir yapı seçilmiştir. Öncelikle bir analitik model sunulmuş ve manyetik akı yoğunluğu ve oluşturulan itki kuvveti için formülasyonlar verilmiştir. Daha sonra silindirik yapıya uygunluk sağlamak için eksenel simetrik yaklaşımın kullanıldığı bir sonlu elemanlar analizi yapılmıştır. Aktüatör içinde üretilen manyetik akılar bu yöntemle tekrar hesaplanmış ve buna göre üretilen itme kuvveti gösterilmiştir. Bu sonuçlar analitik modelden gelen sonuçlar ile karşılaştırılmıştır. Doğrusal aktüatör için deney düzeneği sunulmuş ve oluşan itki kuvveti analitik sonuçlar ile karşılaştırılmıştır.

Silindir-valf düzeneği sunulmuş ve valf seçimi ve uygulama adımlarının yanı sıra tahmini valf performans analizi gösterilmiştir. Söz konusu montaj için uygun imalat prosesleri ve mevcut minyatür ölçekli problem için conta donanımının seçimi sunulmuştur.

Kompresör yapısının bütün olarak dinamik parametreleri sunulmuştur. Bu hem mekaniksel hem de elektromanyetik durumlar için gösterilmiştir. Aktüatör tarafından üretilen itki ve hem mekanik ekipmandan hem de sıkıştırılmış gazdan gelen rijitlik ve sönümleme katsayılarını içeren sistem dinamiği denklemleri verilmiştir. Motor sabiti ve uyarılma frekansı etkileri

hakkında bilgi verilmiştir. En iyi sistem verimi ile en uygun çalışma noktasını bulmak için frekans tepki fonksiyonu gösterilmiştir.

ACKNOWLEDGEMENTS

I would like to thank Prof. Ismail Lazoglu for his never-ending support and for the excellent opportunity to work in Manufacturing and Automation Research Center, where I was always provided with the state-of-the-art equipment. I also would like to thank Koc University for the facilities provided for me.

I would like to thank all the jury members for sparing time to evaluate my thesis.

I would like to thank all my colleagues in the lab, especially Muzaffer Bütün for his support.

I would like to thank my family members for their support and for believing in me during the completion of my thesis.

May all of you have a wonderful life full of exciting experiences.

TABLE OF CONTENTS

LIST OF TABLES

LIST OF FIGURES

NOMENCLATURE

a_0	Fourier coefficient for initial gas force
a_1	Fourier coefficient concerning gas stiffness coefficient
a_2	Fourier coefficient concerning gas damping coefficient
A	magnetic vector potential [V s m^{-1}]
A_{cond}	total cross-sectional area of the conductor [m^2]
A_{cp}	cross-sectional area of the piston [m^2]
A_{total}	total area of the slot [m^2]
B	magnetic flux density [T]
B_g	air gap flux density [T]
B_x, B_y, B_z	magnetic flux density along the axes x, y, z [T]
B_r	magnetic flux density, radial component [T]
B_z	magnetic flux density, axial component [T]
B_{rem}	remanent flux density [T]
c_{fr}	viscous damping coefficient of friction [N s m^{-1}]
c_{gas}	damping coefficient of gas [N s m^{-1}]
D	electric flux density [C m^{-2}]
E	electric field intensity [V m^{-1}]
emf	electromotive force [V]
f	force per unit volume [N m^{-3}]
F_{em}	electromagnetic force [N]
F_{gas}	gas force [N]
F_{mover}	thrust force per pole on the mover [N]
F_0	peak force amplitude [N]
F_{th}	thrust force [N]
h_m	permanent magnet height [m]
H	magnetic field intensity [A m^{-1}]
i	current [A]
J	current density [A m^{-2}]
J_s	source current density [A m^{-2}]
J_i	induced current density [A m^{-2}]

J_θ	current density, azimuthal component [A m^{-2}]
k_{spr}	spring coefficient of flexures [N m^{-1}]
K	back-emf coefficient
K_f	slot filling ratio
l	length [m]
L	inductance [H]
M	magnetization [A m^{-1}]
M_r	magnetization, radial component [A m^{-1}]
M_z	magnetization, axial component [A m^{-1}]
m_{mover}	mover mass [kg]
N	number of turns
$P_{cylinder}$	cylinder pressure [Pa]
P_{dc}	dc copper loss [W]
P_e	Pointing vector [W m^{-2}]
P_e	eddy loss [W]
P_h	hysteresis loss [W]
$P_{suction}$	suction pressure [Pa]
q	charge [C]
r_0	mover inner radius [m]
r_{in}	stator inner radius [m]
r_m	permanent magnet outer radius [m]
r_{out}	stator outer radius [m]
r_s	gap outer radius [m]
R	resistance [Ohm]
R_{ref}	reference resistance [Ohm]
R_m	reluctance [H^{-1}]
S	surface [m^2]
T	temperature [^{0}C]
T_{ref}	reference temperature [^{0}C]
u_x, u_y, u_z	unit vectors along the axes x, y, z
U	speed [m s^{-1}]
V	potential difference [V]
V_{back}	back-emf [V]
W_E	energy stored in the electrostatic fields [J]
W_M	energy stored in the magnetic fields [J]
z	mover displacement [m]
$\dot{z}$	mover velocity [m s^{-1}]
$\ddot{z}$	mover acceleration [m s^{-2}]
Z	peak stroke amplitude [m]

Greek letters

α	thermal resistance coefficient [Ohm ^{0}C^{-1}]

α	pole pitch correction factor
ε	permittivity [F m^{-1}]
ζ	damping ratio
λ	total flux linkage [Wb]
μ_0	permeability of free space [H m^{-1}]
ρ	volume charge density [C m^{-3}]
σ	electric conductivity [S m^{-1}]
τ_m	magnet pole pitch [m]
τ_p	pole pitch [m]
ϕ	magnetic flux [Wb]
Ʊ	magneto-motive force [ampere-turn]
ω	frequency [rad s^{-1}]
ω_n	natural frequency [rad s^{-1}]

Chapter 1

ABOUT LINEAR COMPRESSORS

1.1 Overview

Before refrigeration people relied on techniques such as salting, drying or canning to preserve their food, however, they came to realize that refrigeration was the best way to do so, because it was the only way to preserve the food and not to have its taste changed. While the earliest refrigeration techniques were realized through the usage of ice, later mechanical refrigeration techniques were introduced [1]. Today, a refrigerator is an indispensable part of daily life. It is the most widely used cooling process in general. According to data taken from 2005, Turkey is the fifth most manufacturer of refrigerators with an annual production number of 4,867,000. China is first with 29,871,000, followed by United States with 11,639,000, Italy with 7,201,000 and South Korea with 7,122,000 [2].

Refrigeration is simply the process to force heat transfer from a low temperature region to a high temperature region. This can be achieved using the so-called refrigeration cycle, which in turn is based on the reverse Carnot cycle. The basic schematic of the reverse Carnot cycle is given in Figure 1.1(a). The working fluid in the cycle, known as refrigerator goes through an evaporator while extracting heat from a colder medium, changing from liquid to gaseous state, then goes through a compressor where its temperature rises, then goes through a condenser, becoming liquid again while expelling heat to a warmer medium, then goes through a turbine, expanding back to the state at the beginning of the cycle. In an ideal Carnot cycle, the evaporation and condensation phases are isothermal, whereas the compression and expansion phases are isentropic. In practice, the isothermal parts of the cycle can be achieved very closely, however, in a Carnot cycle, in order for the isentropic parts to be realizable, the cycle must be executed in saturation region. This means a compressor and turbine should be used which can handle two phases at once, which is not possible. Thus, in an actual refrigeration cycle, there are some slight changes. The schematic for the refrigeration cycle is given in Figure 1.1(b). The turbine is replaced with an expansion valve or a capillary tube. The refrigerant enters the compressor as saturated vapor, gets compressed isentropically to superheated vapor, enters the condenser, expelling heat to the warmer medium and becoming saturated liquid, then gets throttled by the expansion valve, becoming a saturated mixture, enters the evaporator, extracting heat from the colder medium and becoming saturated vapor, completing the cycle [3].

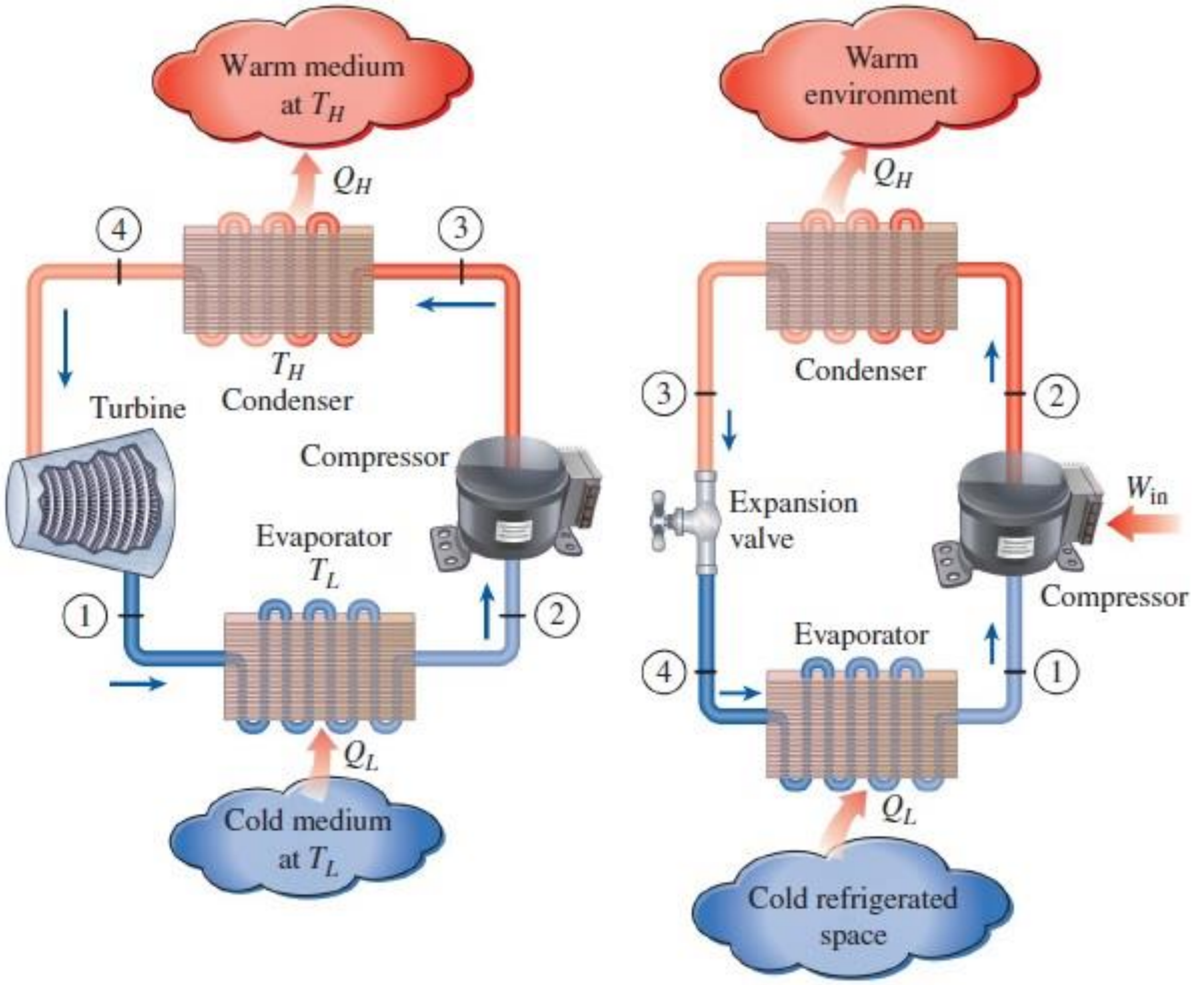

(a) (b)

Figure 1.1: The refrigeration cycles: (a) reverse Carnot cycle (b) actual refrigeration cycle [3]

As stated above, the compression part in the refrigeration cycle is handled by a compressor. What a compressor basically does is the conversion of mechanical excitation energy to potential energy stored in a compressed gaseous medium. Conventional compressors usually employ an intermediary mechanism which converts the rotational motion generated by the motor to reciprocating motion which in turn is used for the compression step. The mechanism that is usually employed here is a slider-crank mechanism which consists of a rotating shaft, crank arm and slider. The slider is connected to a piston, which travels inside a cylinder. The cylinder is connected to a suction and a discharge valve. As the piston moves back and forth inside the cylinder, suction of low-pressure refrigerant with only the suction valve open and the discharge of compressed refrigerant with only discharge valve open is accomplished. The schematic for a common refrigerator compressor is given in Figure 1.2.

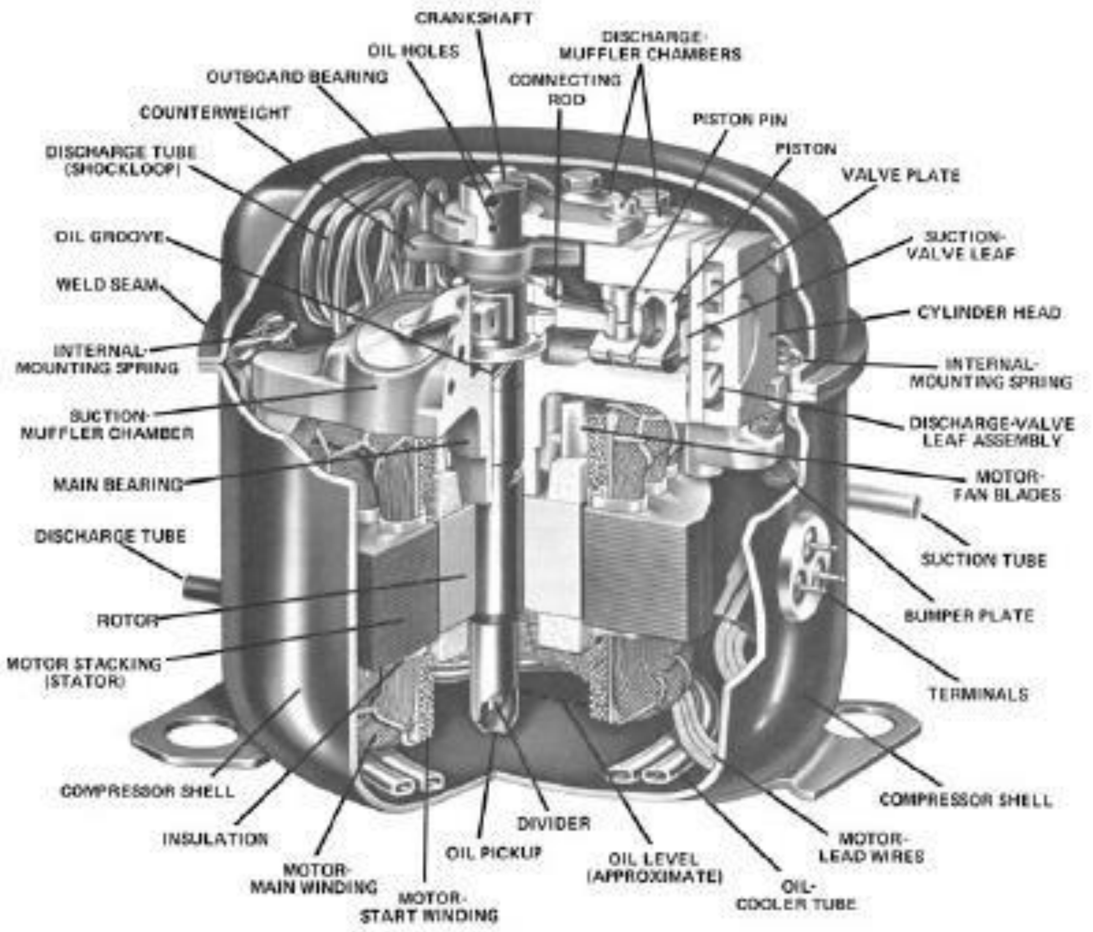

Figure 1.2: Schematic view of a common refrigerator compressor [4]

A linear compressor is an attractive alternative to the conventional rotary compressor due to the many advantages it offers.

1.2 Linear Compressor

In a conventional rotary compressor the mechanical excitation is provided by a rotary motor. In a linear compressor the rotary motor is replaced with a linear motor. The armature of the linear motor, is connected directly to the piston, and the intermediary crank mechanism is removed. This is because the motion provided by the linear motor to its armature is already a reciprocating one, thus the need for a conversion mechanism is eliminated. Such a compressor introduces many advantages over conventional ones. The main advantage of a linear compressor is less mechanical parts due to the elimination of conversion mechanism. This means the force output of the motor is used a lot more efficiently. The force is transmitted only at the axial direction, this means no side forces occur. Since the conversion mechanism is eliminated, the friction forces associated with such a mechanism are no longer present. In addition to this efficient use of force, the noise generated by the friction is also lessened. A linear compressor also enables oil-free operation, which greatly improves the heat transfer performance in condensation and evaporation phases in the cycle. One other advantage a linear compressor offers is the active stroke control. By controlling the thrust generated by the linear motor, the stroke can be changed easily. This means that the output power of the compressor can be actively controlled.

An example linear compressor from the literature is given in Figure 1.3. The performance of this compressor is compared with a conventional rotary compressor in terms of motor efficiency in Figure 1.4(a), and the thermodynamic and overall efficiencies are compared in Figure 1.5(b). From Figure 1.4(a) it can be observed that the motor efficiency of a linear compressor is much higher. In order to generate the same output power, a higher input power for the conventional rotary compressor is required. As the input power goes higher, the parasitic losses, which are core loss, copper losses and other minor losses, especially core losses increase drastically for the induction motor used in the conventional rotary compressor [5].

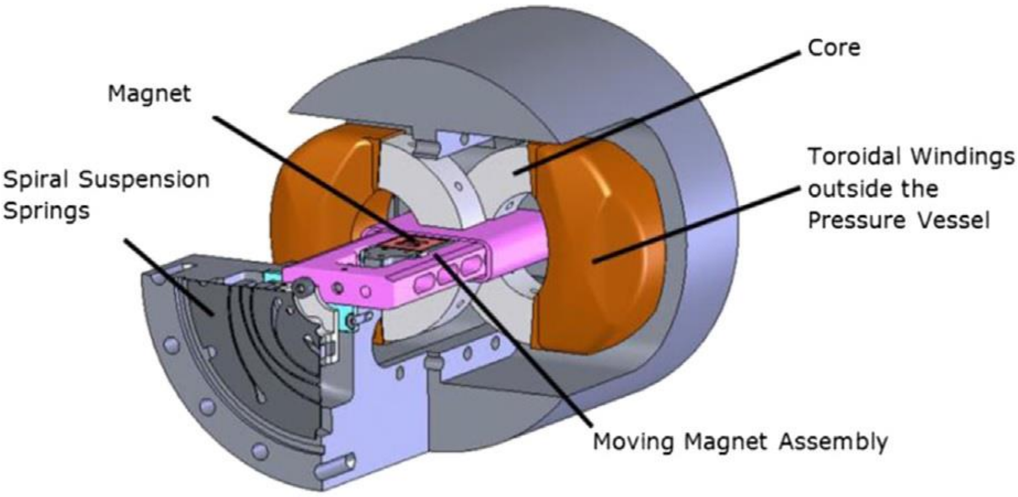

(a)

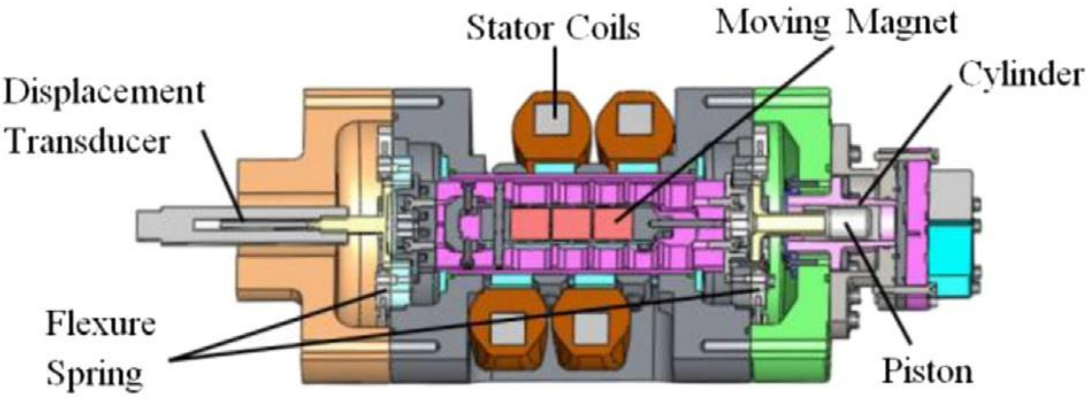

(b)

Figure 1.3: Schematic of a linear compressor: (a) motor design (b) cross-sectional view of the compressor [5]

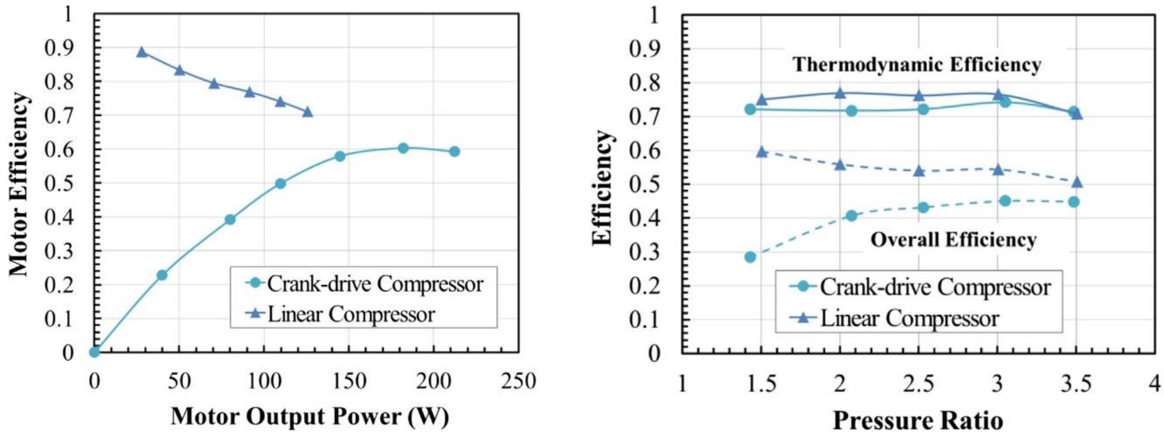

Figure 1.4: Comparison of efficiencies of a conventional rotary compressor and a linear compressor: (a) motor efficiency (b) overall efficiency [5]

As mentioned above, compared to a conventional rotary compressor a linear compressor generates less noise. A comparison made by [6] in terms of noise is given in Figure 1.4. From the figure it is obvious that the compared linear compressor operates at lower noise levels.

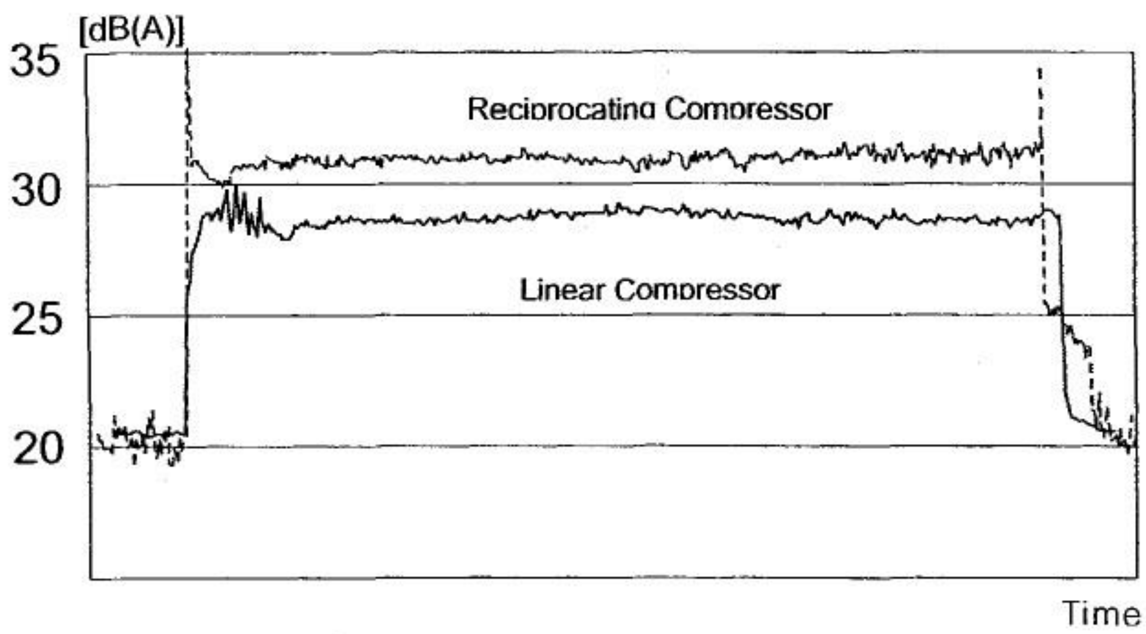

Figure 1.5: Noise level comparison of a reciprocating compressor and a linear compressor [6].

Some other linear compressor designs are given in Figure 1.6 to 1.8. As it will be discussed in Chapter 3, there are three types of linear compressors: moving-iron, moving-magnet and moving-coil. In the figures, examples for each type are provided.

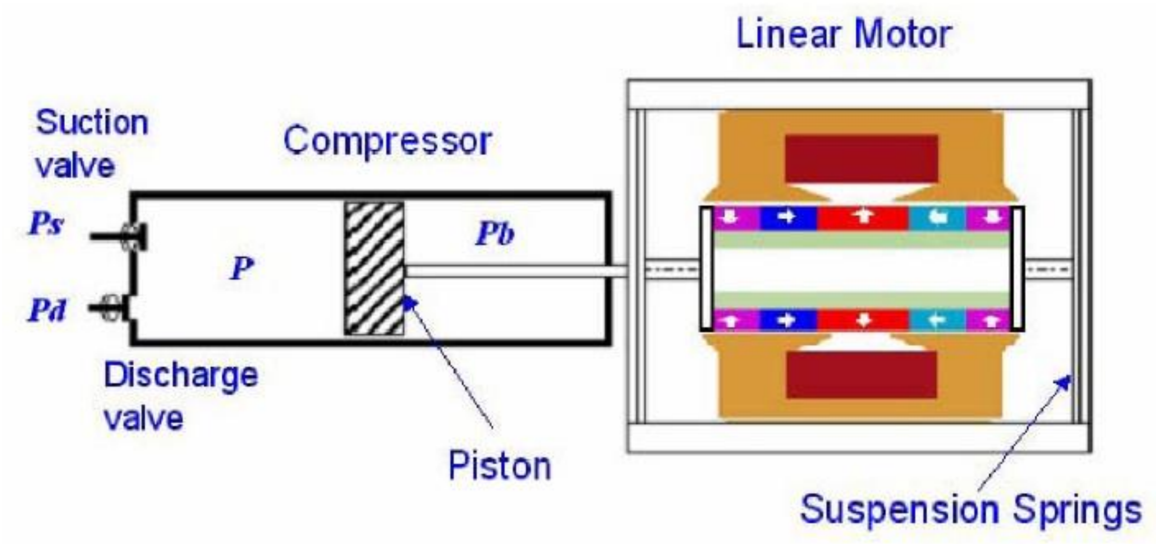

Figure 1.6: Moving-magnet type linear compressor [7]

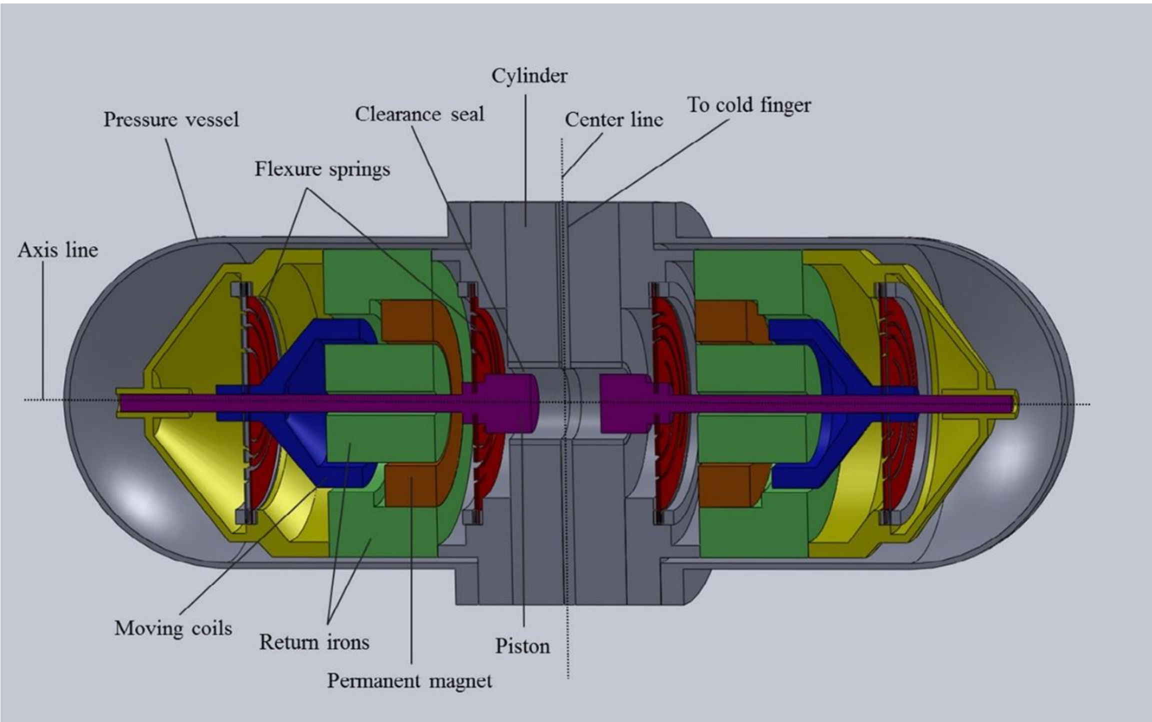

Figure 1.7: Moving-coil type linear compressor [8]

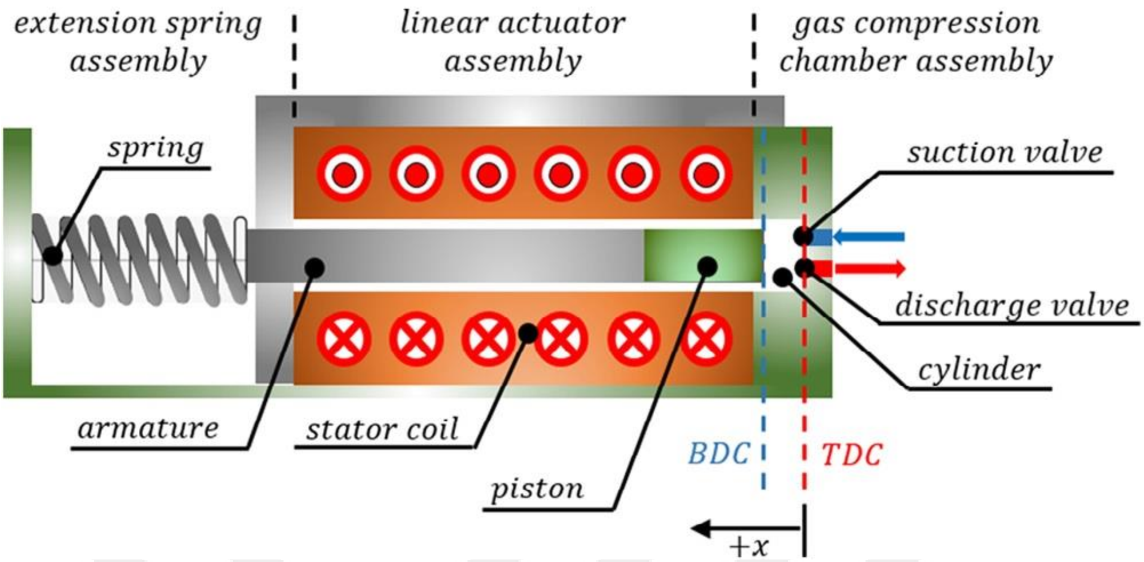

Figure 1.8: Moving-iron type linear compressor [9]

1.3 Miniature Linear Compressor

The research presented deals with the miniaturization of linear compressor technology. As discussed in the previous section, compared to a conventional compressor a linear compressor has less mechanical parts and consequently less frictional loss, which means that a linear compressor is much better suited to miniaturization than a conventional compressor, because at smaller scales friction has a more detrimental effect on the system. On top that the linear motor in the compressor is designed to work at resonant frequency, which makes the reduction of size easily realizable.

In the literature many electrostatically actuated linear compressors have been suggested, because this kind of actuation is easily achievable at small scales, in particular, many MEMS devices of the sort have been proposed. An example for the electrostatically actuated linear compressor is given in Figure 1.9.

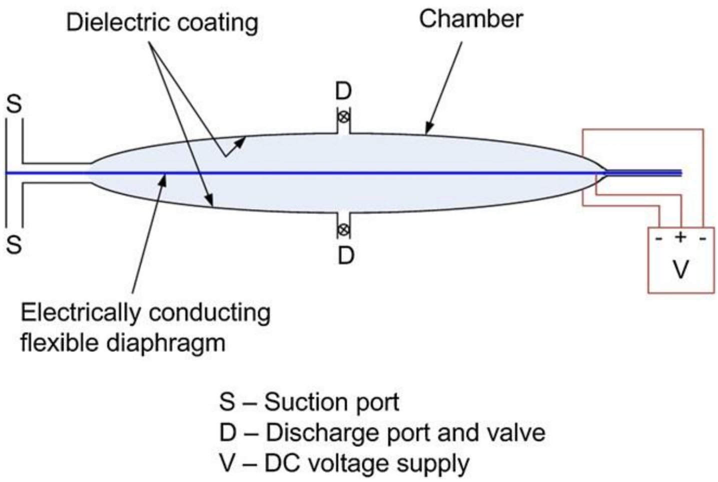

Figure 1.9: An electrostatically actuated miniature compressor [10]

Naturally, compared to an electromagnetic actuator an electrostatic actuator offers comparably low thrust and stroke. This makes an electromagnetically actuated linear compressor still an attractive candidate for miniature scale application. In Figure 1.10 one such actuator is presented. It is designed for the purpose of electronics cooling.

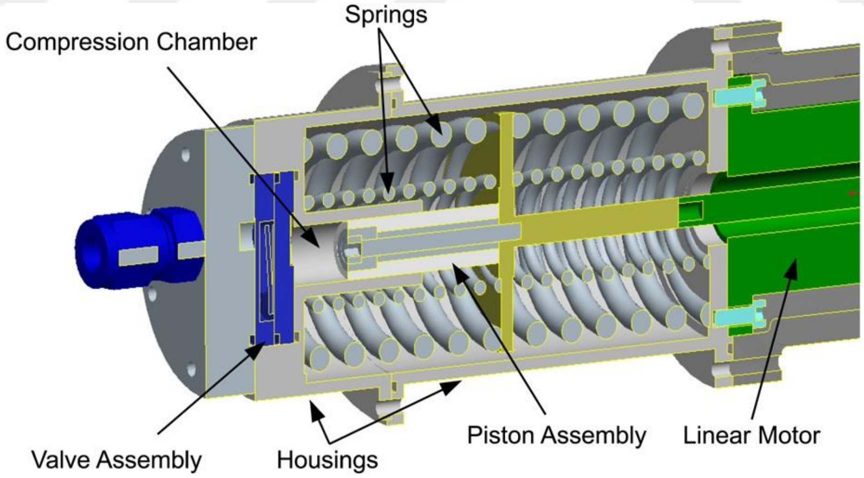

Figure 1.10: Cross-sectional view of a miniature-scale linear compressor for electronics cooling [11]

In short, the miniaturization advantage a linear compressor offers makes it a very strong candidate for electronics cooling or miniature scale refrigerator applications.

Chapter 2

QUICK REVIEW OF ELECTROMAGNETICS PRINCIPLES

2.1 Introduction

In this chapter the general concepts associated with magnetism and electromagnetic field theory will be presented.

The basic laws concerning electromagnetic fields are defined by Maxwell's equations. Charged particles, when exposed to electric and magnetic fields, experience a force. The Lorentz force equation defines this force as

$$\boldsymbol{F} = q(\boldsymbol{E} + \boldsymbol{U} \times \boldsymbol{B}) = \boldsymbol{F_E} + \boldsymbol{F_B} \tag{2-1}$$

where q is the charge, U is its speed (m/s), E is the electric field intensity (V/m), and B is the magnetic flux density (Wb/m^2).

The potential difference dV between two points placed at a distance $\boldsymbol{dl}$ is

$$dV = -\boldsymbol{E} \cdot \boldsymbol{dl} \tag{2-2}$$

This can be rewritten using gradient $\boldsymbol{\nabla}$:

$$\boldsymbol{E} = -\boldsymbol{\nabla} V = -\frac{\partial V}{\partial x}\boldsymbol{u_x} - \frac{\partial V}{\partial y}\boldsymbol{u_y} - \frac{\partial V}{\partial z}\boldsymbol{u_z} \tag{2-3}$$

with $\boldsymbol{u_x}$, $\boldsymbol{u_y}$, $\boldsymbol{u_z}$ the unit vectors along the axes x, y, z, respectively.

The total magnetic flux ϕ through a surface S is defined as

$$\phi = \iint_S \boldsymbol{B} \cdot \boldsymbol{dS} \tag{2-4}$$

Faraday's law states that if in a closed circuit the magnetic flux changes with time and electromotive force (emf) is induced. For a coil closed circuit with N turns for the coil this relationship can be defined as

$$emf = -N\frac{d\phi}{dt} \tag{2-5}$$

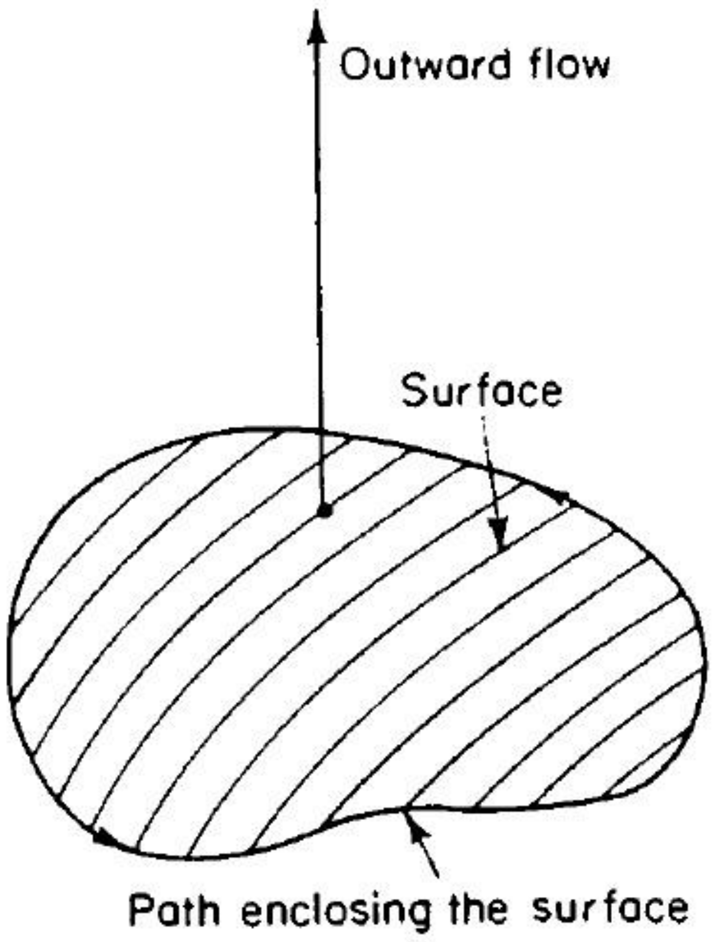

Figure 2.1: Direction of circulation about a closed path according to Lenz' law [12]

the negative sign indicating Lenz' law which states the generated emf should create a flux which opposes the originator flux (Figure 2.1). This emf can also be defined in terms of the electric field as

$$emf = \int \boldsymbol{E} \cdot \boldsymbol{dl} \tag{2-6}$$

Combining the electric field and magnetic flux expressions,

$$\int \boldsymbol{E} \cdot \boldsymbol{dl} = -\frac{\partial}{\partial t} \iint_{S} \boldsymbol{B} \cdot \boldsymbol{dS} \tag{2-7}$$

Using Stokes theorem, this can be rewritten as

$$\int_{\Gamma} \mathbf{E} \cdot \mathbf{dl} = \iint_{S} (\boldsymbol{\nabla} \times \mathbf{E}) \cdot \mathbf{dS} \tag{2-8}$$

where the surface $\boldsymbol{S}$ is enclosed by the path Γ. Using (2-8) in (2-7),

$$\boldsymbol{\nabla} \times \boldsymbol{E} = -\frac{\partial \boldsymbol{B}}{\partial t} \tag{2-9}$$

Taking divergence for both sides in (2-9), and remembering from vector algebra divergence of a curl is zero,

$$div\ \boldsymbol{B} = \frac{\partial \boldsymbol{B_x}}{\partial x} + \frac{\partial \boldsymbol{B_y}}{\partial y} + \frac{\partial \boldsymbol{B_z}}{\partial z} = 0 \tag{2-10}$$

These equations, of course, do not take the relative motion between the closed circuit and the magnetic field. If the charge is at a relative velocity $\boldsymbol{U'}$ with respect to a moving reference of velocity $\boldsymbol{U}$ the force equation becomes

$$\boldsymbol{F} = q[\boldsymbol{E} + \boldsymbol{U} \times \boldsymbol{B} + \boldsymbol{U'} \times \boldsymbol{B}] \tag{2-11}$$

and (2-9) becomes

$$\boldsymbol{\nabla} \times \boldsymbol{E} = -\frac{\partial \boldsymbol{B}}{\partial t} + \boldsymbol{\nabla} \times (\boldsymbol{U} \times \boldsymbol{B}) \tag{2-12}$$

The left hand side of (2-12) is the transformer emf and the right hand side is the motional emf. In a linear electric machine a mover is present so the motional emf is necessary for force production.

If there is an electric current already present, Ampere's law states that there is a relationship with it and the resulting magnetic field intensity $\boldsymbol{H}$ (A/m):

$$\int \boldsymbol{H} \cdot \boldsymbol{dl} = I \tag{2-13}$$

The current can be defined as enclosed by a path of integration:

$$I = \iint_S \boldsymbol{J} \cdot \boldsymbol{dS} \tag{2-14}$$

with $\boldsymbol{J}$ being the surface current density (A/m^2). Using Stokes' theorem,

$$\boldsymbol{\nabla} \times \boldsymbol{H} = \boldsymbol{J} \tag{2-15}$$

Taking the divergence for both sides in (2-15) should yield zero, however the divergence of the right hand side is in relation with the volume charge density ρ by the continuity equation:

$$\boldsymbol{\nabla} \cdot \boldsymbol{J} = -\frac{\partial \rho}{\partial t} \tag{2-16}$$

In order to counter this inconsistency the term $\partial \boldsymbol{D}/\partial t$ that is also known as the displacement current density is added to (2-15):

$$\boldsymbol{\nabla} \times \boldsymbol{H} = \boldsymbol{J} + \frac{\partial \boldsymbol{D}}{\partial t} \tag{2-17}$$

The inconsistency is now removed, considering $\boldsymbol{\nabla} \cdot \boldsymbol{D} = \rho$, which is actually, Gauss' law with $\boldsymbol{D}$ being the electric flux density.

Maxwell's equations are thus:

$$\begin{aligned}
&\boldsymbol{\nabla} \times \boldsymbol{E} = -\frac{\partial \boldsymbol{B}}{\partial t} + \boldsymbol{\nabla} \times (\boldsymbol{U} \times \boldsymbol{B}) \\
&\boldsymbol{\nabla} \times \boldsymbol{H} = \boldsymbol{J} + \frac{\partial \boldsymbol{D}}{\partial t} \\
&\boldsymbol{\nabla} \cdot \boldsymbol{B} = 0 \\
&\boldsymbol{\nabla} \cdot \boldsymbol{D} = \rho
\end{aligned} \tag{2-18}$$

Material constitutive laws Ohm's law,

$$\boldsymbol{J} = \sigma \boldsymbol{E} \tag{2-19}$$

permittivity law,

$$\boldsymbol{D} = \varepsilon \boldsymbol{E} \tag{2-20}$$

and permeability law,

$$\boldsymbol{B} = \mu \boldsymbol{H} \tag{2-21}$$

define the relationship between E, B, J, D and H. Electric conductivity σ (S/m), permittivity ε (F/m), and permeability μ (H/m) can be considered scalar for isotropic materials, but for anisotropic materials they should be considered as tensors.

There is also one important thing that should be considered for linear electric machines: in their case there are no free charges, the motion of charges constitutes the current flow. So, Lorentz force can be expressed as

$$\boldsymbol{f} = \boldsymbol{J} \times \boldsymbol{B} \tag{2-22}$$

with $\boldsymbol{f}$ being force per unit volume (N/m^3).

For the solution of electromagnetic field distribution equations, a general tool can be defined. In order to do this, a quantity that can be called the magnetic vector potential $\boldsymbol{A}$ can be defined where

$$\boldsymbol{B} = \boldsymbol{\nabla} \times \boldsymbol{A} \tag{2-23}$$

again considering that the divergence of a curl is zero. Thus:

$$\boldsymbol{\nabla} \times \boldsymbol{H} = \boldsymbol{\nabla} \times \frac{\boldsymbol{B}}{\mu} = \boldsymbol{\nabla} \times \left(\frac{1}{\mu}\boldsymbol{\nabla} \times \boldsymbol{A}\right) = \boldsymbol{J} \tag{2-24}$$

$$\boldsymbol{\nabla}^2\boldsymbol{A} = \ \boldsymbol{\nabla} \times (\boldsymbol{\nabla} \times \boldsymbol{A}) = \ \mu\boldsymbol{J} \tag{2-25}$$

(2-23) is the Poisson equation. The Laplacian $\boldsymbol{\nabla}^2\boldsymbol{A}$ is

$$\begin{aligned}\boldsymbol{\nabla}^2\boldsymbol{A} = \ &\left(\frac{\partial^2 A_x}{\partial x^2} + \frac{\partial^2 A_x}{\partial y^2} + \frac{\partial^2 A_x}{\partial z^2}\right)\boldsymbol{u_x} + \left(\frac{\partial^2 A_y}{\partial x^2} + \frac{\partial^2 A_y}{\partial y^2} + \frac{\partial^2 A_y}{\partial z^2}\right)\boldsymbol{u_y} \\ &+ \left(\frac{\partial^2 A_z}{\partial x^2} + \frac{\partial^2 A_z}{\partial y^2} + \frac{\partial^2 A_z}{\partial z^2}\right)\boldsymbol{u_z}\end{aligned} \tag{2-26}$$

For the case where $\boldsymbol{J}$ becomes zero in a domain, (2-24) becomes

$$\boldsymbol{\nabla}^2\boldsymbol{A} = \ 0 \tag{2-27}$$

(2-26) is the Laplace equation.

If $\boldsymbol{H}$ and $\boldsymbol{J}$ are sinusoidals and μ and σ are considered uniform, $\boldsymbol{J}$ is actually the sum of source current density $\boldsymbol{J_s}$ and the induced current density $\boldsymbol{J_i}$ with $\boldsymbol{J_i}$ being

$$\dot{\boldsymbol{J}}_{\boldsymbol{i}} = \sigma\dot{\boldsymbol{E}}_{\boldsymbol{i}} = -\sigma\frac{\partial\dot{\boldsymbol{A}}}{\partial t} = -j\omega\sigma\dot{\boldsymbol{A}} \tag{2-28}$$

So, (2-24) becomes

$$\boldsymbol{\nabla}^2\dot{\boldsymbol{A}} - j\omega\sigma\dot{\boldsymbol{A}} \ = \ \mu\boldsymbol{J_s} \tag{2-29}$$

(2-28) is the Helmholtz equation.

Poisson, Laplace and Helmholtz equations are particular cases for a general equation:

$$L\big(\phi(P,t)\big) = f(P,t) \tag{2-30}$$

where L is a differential operator and ϕ is a general function, becoming $\boldsymbol{A}$ in this case. P is the position in space.

For electrostatic fields, ϕ becomes a scalar potential V. Electrostatic fields are irrotational, so

$$\boldsymbol{E} = -\boldsymbol{\nabla}V \tag{2-31}$$
$$-\boldsymbol{\nabla}\cdot(\varepsilon\boldsymbol{\nabla}V) = \rho$$

In order to find a solution, boundary conditions are also needed. Considering (2-29), the value $\phi(P,t)$ gets on a boundary Γ is the boundary condition.

Energy relations can also be defined. The energy stored in the field for electrostatic fields can be written as

$$W_E = \frac{1}{2}\iiint_V (\boldsymbol{D}\cdot\boldsymbol{E})dV \tag{2-32}$$

For magnetic fields it becomes

$$W_M = \frac{1}{2}\iiint_V (\boldsymbol{B}\cdot\boldsymbol{H})dV \tag{2-33}$$

Power density is defined by the Poynting vector $\boldsymbol{P_e}$ (W/m^2):

$$\boldsymbol{P_e} = \boldsymbol{E}\times\boldsymbol{H} \tag{2-34}$$

W_E and W_M are used to find the thrust in a linear electromagnetic machine whereas $\boldsymbol{P_e}$ is for the steady state and the losses.

For a coil with N turns the total flux linkage λ can be expressed as

$$\lambda = N \iint_S \boldsymbol{B} \cdot \boldsymbol{dS} = NBS \tag{2-35}$$

The inductance L can be expressed as

$$L = \frac{\lambda}{I} = \frac{\mu S N^2}{l_n} = \frac{N^2}{R_m}$$
$$R_m = \frac{l_n}{\mu S} \tag{2-36}$$

Here, l_n is the flux path, and the expression R_m introduced above is the so-called magnetic reluctance. The reason for the introduction of this expression is to liken it to electric resistance R in order to make an analogy between the magnetic circuit and an electric circuit.

Finally, the stored magnetic energy W_m and the stored electric energy W_e can be expressed as

$$W_m = \int_0^i \lambda di = \int_0^i (Li) di = \frac{Li^2}{2}$$
$$W_e = \int_0^V \rho dV = \int_0^V (CV) dV = \frac{CV^2}{2} \tag{2-37}$$

2.2 Materials

2.2.1 Ferromagnetic Materials

Within the permeability law (2-21) the quantity μ called the permeability should be considered according to the medium being dealt with. Thus, this quantity can be expressed as

$$\mu = \mu_0 \mu_R \tag{2-38}$$

$\mu_0 = 4\pi 10^{-7} H/m$ is called the permeability of free space. μ_R is the so-called relative permeability, and it is a nondimensional, material specific constant. There are three major classifications for materials in terms of their magnetic behavior: a material is considered paramagnetic if its relative permeability is slightly greater than 1.0, diamagnetic if it is slightly less than 1.0, and ferromagnetic with much larger values for the relative permeability. One other thing to consider is the isotropy in a material. The permeability in a material can be considered scalar only for homogeneous and isotropic (same properties regardless from direction). If not, permeability should be taken as a tensor. Furthermore, the relationship in (2-21) is not always linear, as μ changes with B. In such a case, the relationship between B and H should be demonstrated graphically in a so-called B-H curve [12].

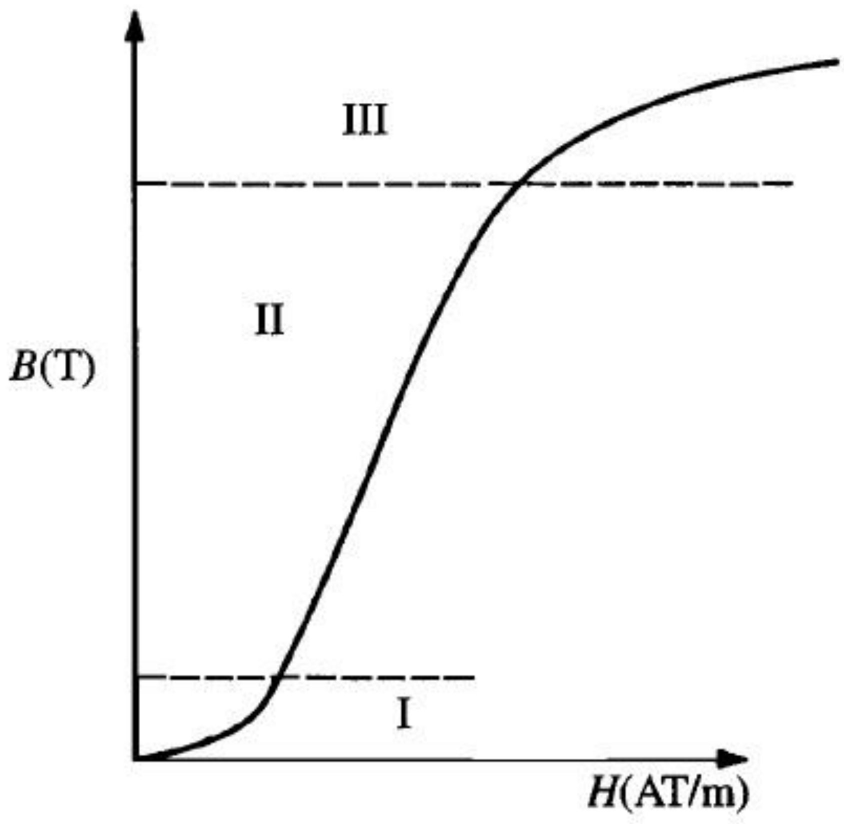

Figure 2.2: B-H curve for a magnetic material [12]

A typical B-H curve can be seen in Figure 2.2. There are three regions of importance. A ferromagnetic material consists of domains of a few micrometers in size where all dipole moments are aligned. For a fully demagnetized material, these domains all have a random orientation, so the net flux density is zero. If an external magnetization force H is applied, the domains align themselves in the direction of increasing H. This results in an increase of B. For region I this change is abrupt as more and more domains participate in the alignment. In region

II the trend becomes stable and around region III almost all domains have taken part in the alignment with only a few remaining yet to be aligned, resulting in a slowed increase in B. The increase is slowed down until all domains are aligned and B reaches the saturation density B_s. At this point, magnetic saturation is reached. In order to obtain the permeability at a certain level, the slope of this B-H curve should be calculated.

One other factor that should be considered is the hysteresis that occurs between magnetization and demagnetization of a material. During a continuous magnetization and demagnetization of a material, there is a hysteresis between the B-H behavior of magnetization and demagnetization. Such a curve is given in Figure 2.3. The area inside the hysteresis loop is called the hysteresis loss, because that represents the energy required to reverse the magnetic domain walls with the reversal of magnetizing force [12]. The loop area increases if the magnetization-demagnetization sequence occurs at higher frequencies [13]. This is a very important criterion to be considered when designing linear electric machines because of their specific excitation frequencies, and material selection must be done according to the calculated losses.

As stated above, there are three types of materials in terms of magnetic behavior. For both paramagnetic materials with relative permeability slightly higher than 1.0 and diamagnetic with slightly lower than 1.0 the value can be taken as 1.0 for practical purposes. Examples for paramagnetic materials are magnesium, molybdenum and lithium, and some diamagnetic materials are copper, silver and gold. Ferromagnetic materials, as the name suggests, are usually ferrous materials, such as iron, cobalt and nickel. In linear machines, they are used as magnetic cores. Stainless steel is the widely preferred type of ferromagnetic material. Steel 430FR, 431, and silicon steel are among steel types with very high relative permeability. When designing an electric machine, the parts which will not require to have ferromagnetic capacity, nonmagnetic materials such as aluminum or polymers can be selected to reduce the overall weight of the machine.

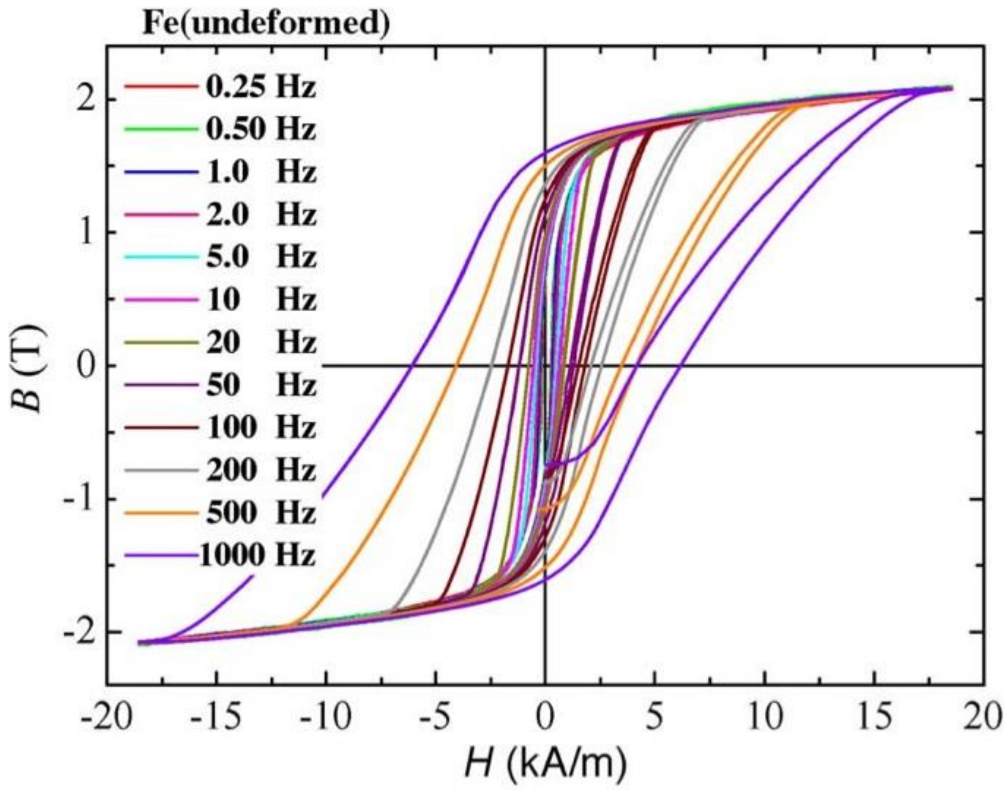

Figure 2.3: Hysteresis loop with changing frequency [13]

2.2.2 Permanent Magnets

Permanent magnets are hard magnetic materials with a very large hysteresis loop. When analyzing their characteristics, usually the second quadrant of their B-H curve is used. Such a graph comparing several magnet types is given in Figure 2.4.

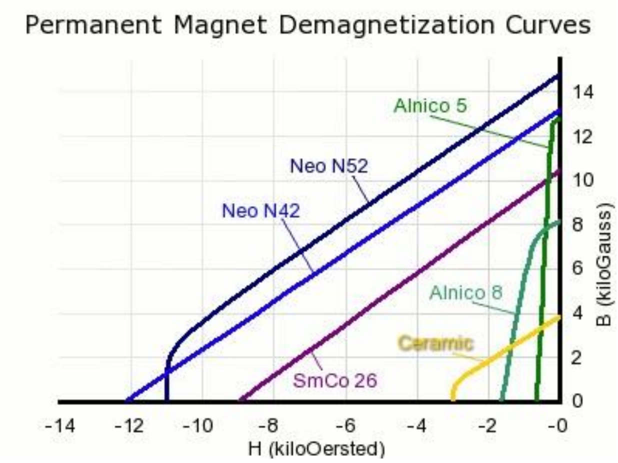

(a)

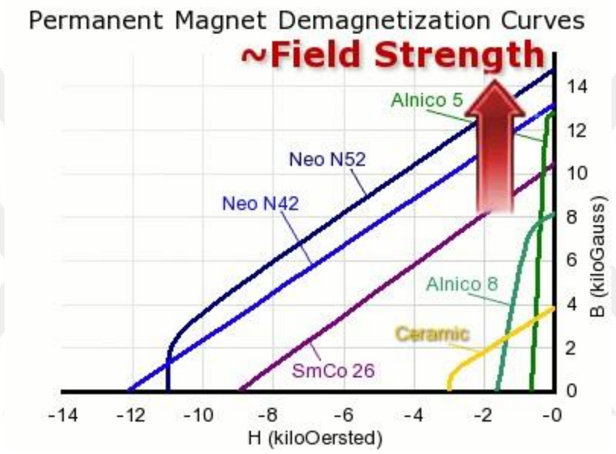

(b)

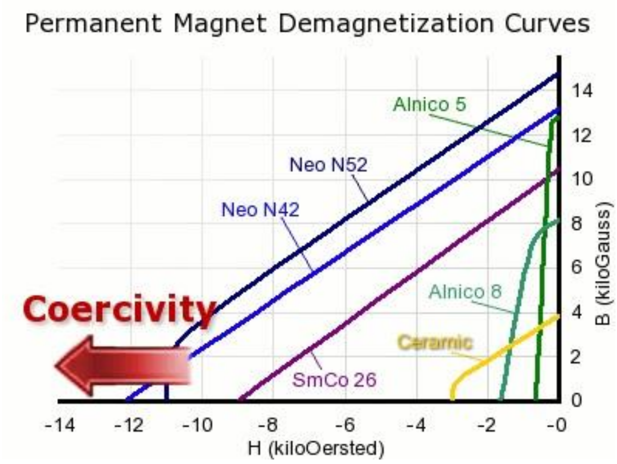

(c)

Figure 2.4: (a) B-H curves of several permanent magnets (b) Field strength increases going up at B axis (c) Coercivity increases going left at H axis [14]

At the graph given in Figure 2.4(a) for the point at which $H = 0$, the corresponding value of B is called remanent flux density (B_{rem}). This is the magnetic flux density that remains in the material even after the external magnetizing force is removed, which is a key point for permanent magnets. Going up at the B-axis, the remanent flux density increases (Figure 2.4(b)). For the point at which $B = 0$, the corresponding value of H is called the coercive field (H_c). This is the external magnetizing strength needed to bring the magnetic flux density remaining inside the material back to zero. Going left at the H-axis the coercivity values increase (Figure 2.4(c)). The negativity for H_c values indicates a reversal in the magnetization (demagnetization) in order remove the remanent flux. The pull-force of a permanent magnet is proportional to the area under the B-H curve for a permanent magnet.

Ambient temperature also has an effect on magnet performance. Usually at lower temperatures a wider hysteresis loop is observed. The B-H curve comparison for N42 grade NdFeB (Neodymium-Iron-Boron) magnet at different temperatures is given in Figure 2.5.

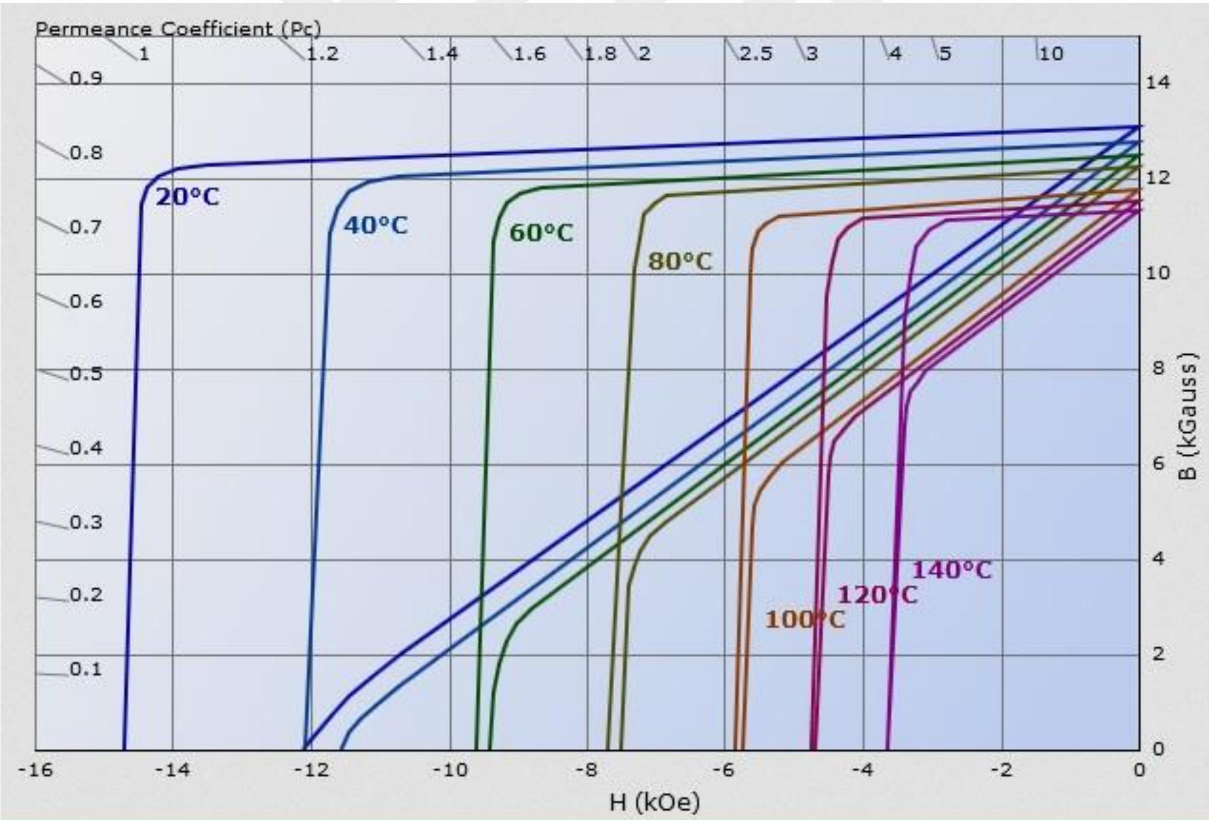

Figure 2.5: B-H curve for N42 grade NdFeB magnet for different temperatures [15]

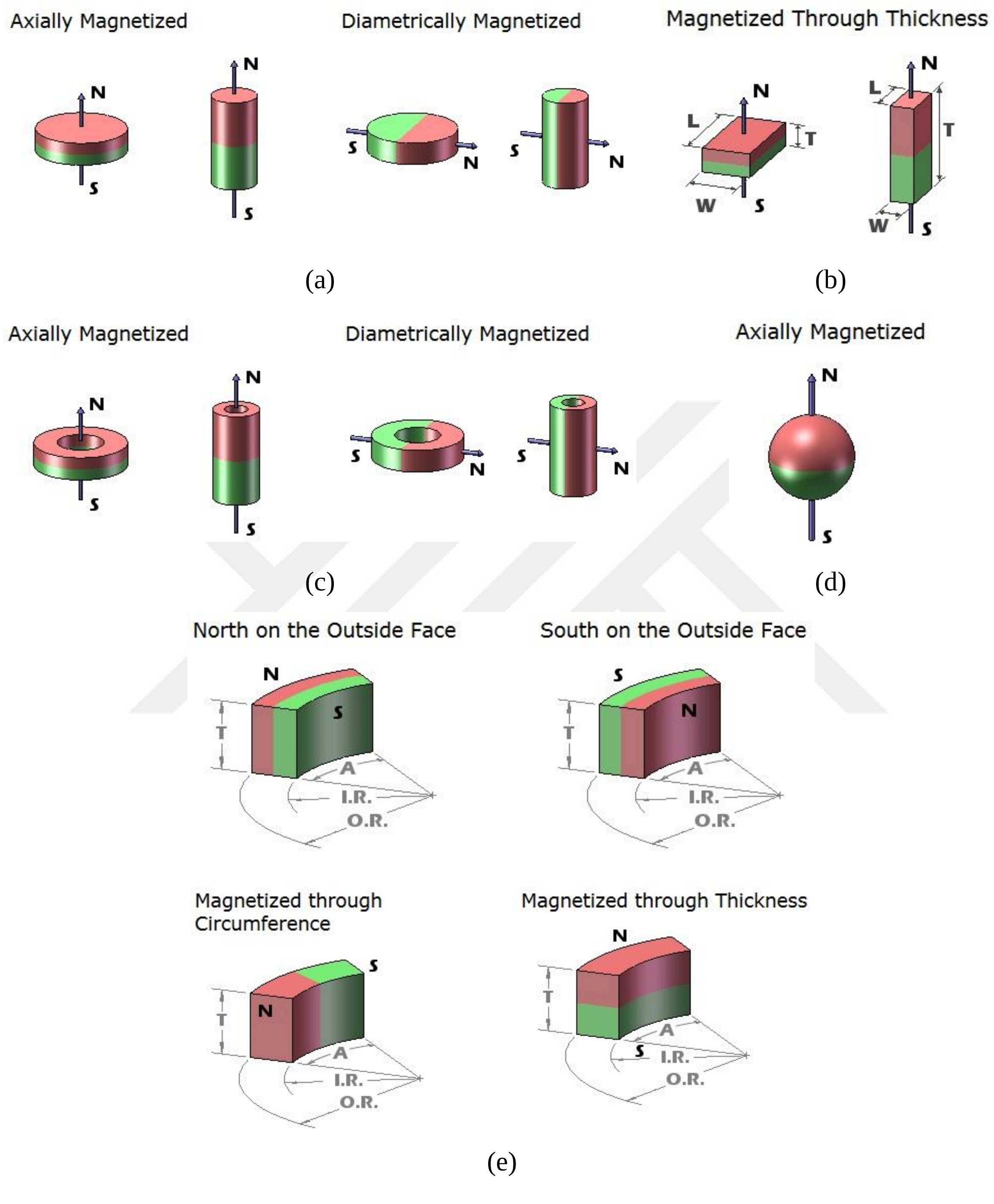

Figure 2.6: Magnetization directions for different types of magnets (a) Disc (cylinder) magnets (b) Block magnets (c) Ring magnets (d) Spherical magnets (e) Arc magnets [16]

There are several types of permanent magnets differing in their magnetization direction. This is naturally dependent on the magnet shape. For a cubical magnet three directions are possible for magnetization, each direction corresponding to one of the three axes defining the cube. So, for a cubical (block) magnet, the magnetization is through the thickness. Disc magnets or cylindrical magnets can be either axially or diametrically magnetized and spherical magnets can only be axially magnetized. One very interesting magnet type is the ring magnet. This is basically a disc magnet with a hole in it, so like disc magnets they can be axially or diametrically magnetized. In addition to that, the hole in the middle makes radial magnetization a possibility. However, this is a very difficult process to overcome, so arc magnets are used instead, several of them being radially magnetized and put together in order to form a complete ring for operations where radially magnetized magnets are needed. Of course, flux lines are straight lines and do not curve around the geometry, so a perfectly radial magnetization is not possible even for arc segments, which means that the more arcs (arcs of lesser degrees) are used, the closer the closed ring will approximate a radially magnetized magnet. Same goes for the circumferential magnetization of an arc magnet. The possible magnetization directions are given in Figure 2.6 and the flux lines appearing in an arc magnet are demonstrated in Figure 2.7. Inside the material the flux lines go from south pole to north pole, which also shows the direction at which the magnetizing force is acting.

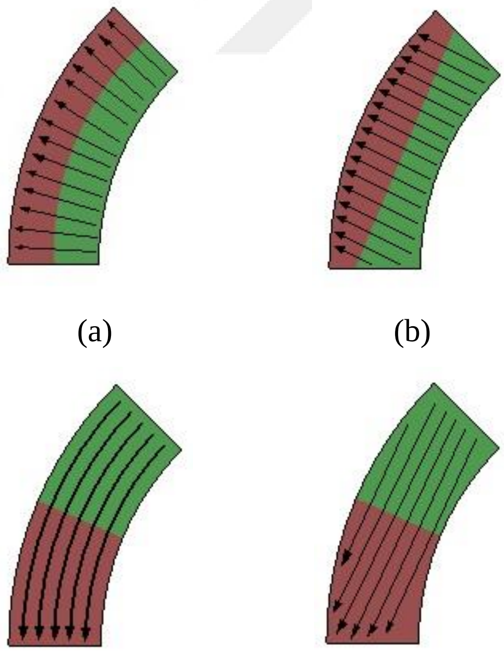

(a) (b)

(c) (d)

Figure 2.7: Flux lines in an arc magnet (a) Desired flux lines for a radially magnetized arc magnet (b) Actual flux lines for a radially magnetized arc magnet (c) Desired flux lines for a

circumferentially magnetized arc magnet (d) Actual flux lines for a circumferentially magnetized arc magnet

2.2.3 Stator Core

Solid cores of high permeability are used as the stator in order to further enhance the magnetic field generated by the stator windings. In an electric machine, two designs are usually employed. The most preferred design is the slotted type where the windings are placed around stator teeth. In this configuration the air gap is small, therefore the torque/force and the acceleration is strong. In order to remedy the eddy current losses, laminations of silicon steel are usually employed. The laminated stack and windings make the stator assembly. The return path that completes the magnetic circuit are the slots and the motor housing. Since the teeth help the stator to be closer to the armature, the air gap is very small and the magnetic circuit is efficiently closed. This results in a stronger thrust output. However, slotted stators are subject to very large cogging forces, which occurs when the armature tries to align itself with the stator teeth instead of the windings. This causes ripple effects and consequently reduces motor efficiency. For a smoother operation, slotless designs are proposed. Here windings take a cylindrical shape and held together with epoxy resin. In this configuration cogging is completely eliminated and smooth and quiet operation is obtained. One other advantage the slotless design offers is the reduction of eddy losses, because the back iron-armature distance is greater in a slotless motor. Ripple is greatly reduced magnetic saturation is lowered. This enables the motor to operate at higher values than the rated power for short intervals. Moreover, the teeth in a slotted motor increase the inductance, so the absence of it helps to improve current bandwidth, since the current dragging is reduced. In order to remedy the thrust problem in a slotless motor, strong permanent magnets such as SmCo (Samarium-Cobalt) or NdFeB (Neodymium-Iron-Boron) are employed [17]. The schematic comparison of a slotted and slotless brushless motor can be seen in Figure 2.8.

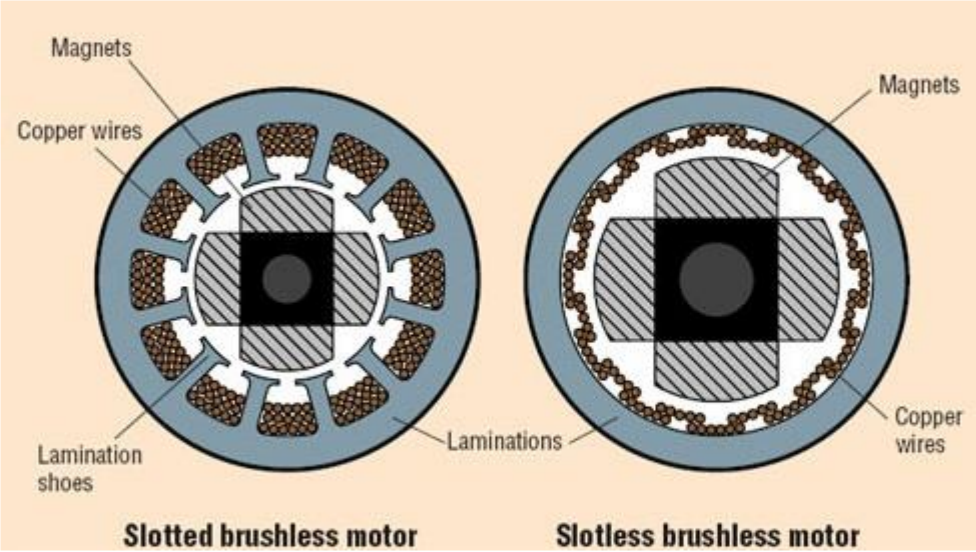

Figure 2.8: Comparison of a slotted motor and its slotless counterpart [17]

In summary, a slotted motor offers high thrust and acceleration, whereas a slotless motor offers smooth operation with low ripple and an almost linear motor constant.

The core losses are divided in two categories, the first being the hysteresis losses

$$P_h = k_h f {B_m}^{1.5\ to\ 2.5} \left[\frac{W}{kg}\right] \tag{2-39}$$

and the second eddy losses

$$P_e = k_e f^2 {B_m}^2 \left[\frac{W}{kg}\right] \tag{2-40}$$

where k_h is a constant, k_e is a constant, f is frequency, and B_m is the maximum flux density [12].

Especially for slotted designs, the eddy current losses are reduced by using laminations of silicon steel. This divides the core into thin sheets where a very thin layer of insulator is added in-between the sheets. The sheets are oriented parallel to the flow of magnetic flux (Figure 2.9). The eddy loss is proportional to the square of lamination thickness and conductivity of the material. Laminations increase the total volume, and efficient methods of stacking are important for keeping this increase at tolerable levels. The so-called stacking factor, which is a measure for this matter, important for calculating the flux density, is the ratio of the volume actually occupied by the material to the total volume. It increases with thicker lamination sizes, approaching 1.0 [12].

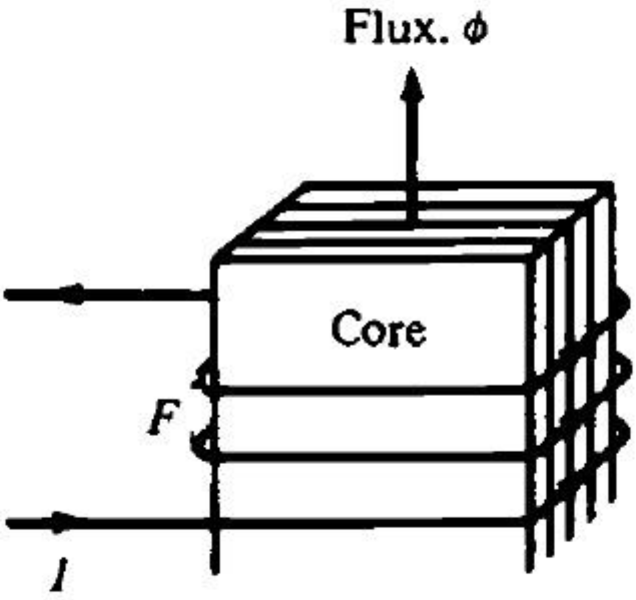

Figure 2.9: A lamination segment [12]

2.2.4 Electric Conductors

The electrical conductors used in an electric machine are copper wires that are insulated from each other with insulation coating and from the magnetic core with insulation sheets. Sometimes aluminum wires can also be used instead of copper ones due to aluminum’s lesser density contributing to weight reduction and aluminum being a cheaper material.

One important physical quantity when analyzing a conductor performance is the electrical resistivity, which is a measure of how strongly a wire opposes the applied electric current. A low resistivity points to a wire that allows easy passage of electrical charge. Copper with a resistivity of 0.0171 Ohm · mm^2/m is one of the best conductors of electric current (slightly behind pure silver). Resistivity can be extracted from the resistance formula

$$R = \rho \frac{l}{A} \tag{2-41}$$

where R is the resistance, ρ is the resistivity of the conductor, l is the length of the conductor, and A is the cross-sectional area of the conductor.

The resistance of a conductor increases with temperature according to the relationship

$$R_T = R_{ref}[1 + \alpha(T - T_{ref})] \tag{2-42}$$

where α is the thermal resistance coefficient, R_{ref} the resistance of the conductor at a reference temperature T_{ref} (usually $20\ °C$), and R_T the resistance of the conductor at the temperature T.

The conductor can either be fed dc or ac. The current density distribution is uniform if the current is dc, non-uniform if it is ac. Conductors with circular cross-section are usually up to 3 mm in diameter, for larger cross-sections, rectangular cross-sections are used to increase the slot filling ratio. This is a measure of the effective filling of a conductor coil its designated slot and can be roughly defined as

$$K_f = \frac{A_{cond}}{A_{total}} \tag{2-43}$$

where A_{cond} is the total cross-sectional area of the conductor, and A_{total} is the total area of the slot.

The copper loss for dc is

$$P_{dc} = R_{dc}{I_{dc}}^2 \tag{2-44}$$

In the case of ac, penetration depth of a single copper wire is much larger than its diameter, however coils are placed in slots of laminated core. The current density in the single conductor decreases in amplitude along slot depth. Therefore, with increasing frequency, the resistance increases and the inductance decreases.

The frequency and slot height therefore contribute to decrease in penetration depth, introducing skin effects during conduction. This can be countered by introducing layers or breaking the conductor down to thinner wires.

2.3 Magnetic Circuit Analogy

As stated in Section 2.1, the reluctance R_m can be used in order to make an analogy of an electric circuit to the magnetic flux. In this approach the so-called magnetic potential

$$F = \int \boldsymbol{H} \cdot \boldsymbol{dl} \tag{2-45}$$

is used analogous to the potential in an electric circuit, with the its special case, the magnetomotive force (mmf) acting as the source. The magnetic flux ϕ is analogous to the current flowing through an electric circuit, and the reluctance R_m replaces the resistance.

The analogy is demonstrated for a magnetic circuit in Figure 2.10. Applying Ampere's law to this circuit,

$$\oint \boldsymbol{H} \cdot \boldsymbol{dl} = NI = H_i l_i + H_g l_g = \phi(R_{m_i} + R_{m_g}) \tag{2-46}$$

Here the index i represents iron and the index g represents the air gap. In this magnetic circuit analogy, saturation, leakage flux or fringing effects are neglected.

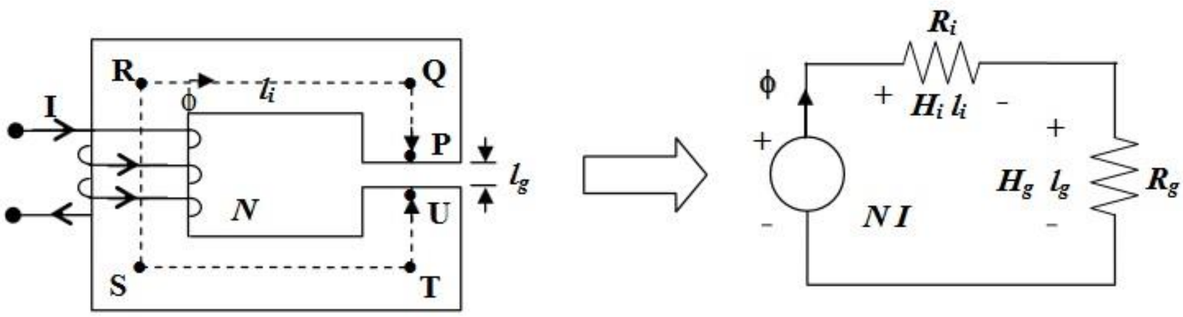

Figure 2.10: Magnetic circuit analogy [18]

The same analogy can be applied when dealing with more complicated circuits where flux paths are divided. In such cases (2-46) can be applied just like using Kirchhoff's Voltage Law or Kirchhoff's Current Law and considering individual nodes of importance or meshes where a certain part of the divided total flux "flows" through.

Chapter 3

TYPES OF LINEAR OSCILLATORY MACHINES

3.1 Introduction

In applications where linear motion is needed, linear electromagnetic machines offer a great alternative to systems where a conventional rotary motor is coupled to a rotary to linear motion conversion mechanism. A linear machine in principle operates under the same principles as the rotary machine. Both convert electrical excitation energy to mechanical work (motor), or the other way around (generator). In the case of rotary machines the mechanical work shows itself in the form of torque and angular displacement, whereas for linear machines it is force and axial displacement.

A linear motor basically uses electromagnetic forces according to the laws described in the previous chapter, to produce linear motion. Depending on the topology of the motor, this motion may be progressive or oscillatory. In general the topology of the progressive machines is different from that of the oscillatory machine; progressive machines are usually three-phase brushless ac machines, whereas oscillatory machines are single phase machines. Progressive machines can be operated at variable voltage and frequency, but oscillatory machines usually operate at a fixed frequency, because it is common practice to design oscillatory machines to operate at resonance, that is, to excite them at a frequency that matches the mechanical eigenfrequency (mode) of the moving part. This results in a higher efficiency.

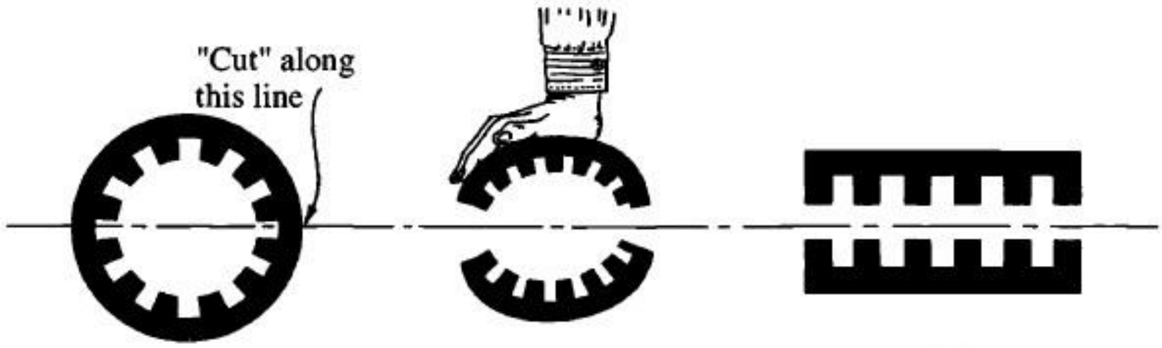

(a)

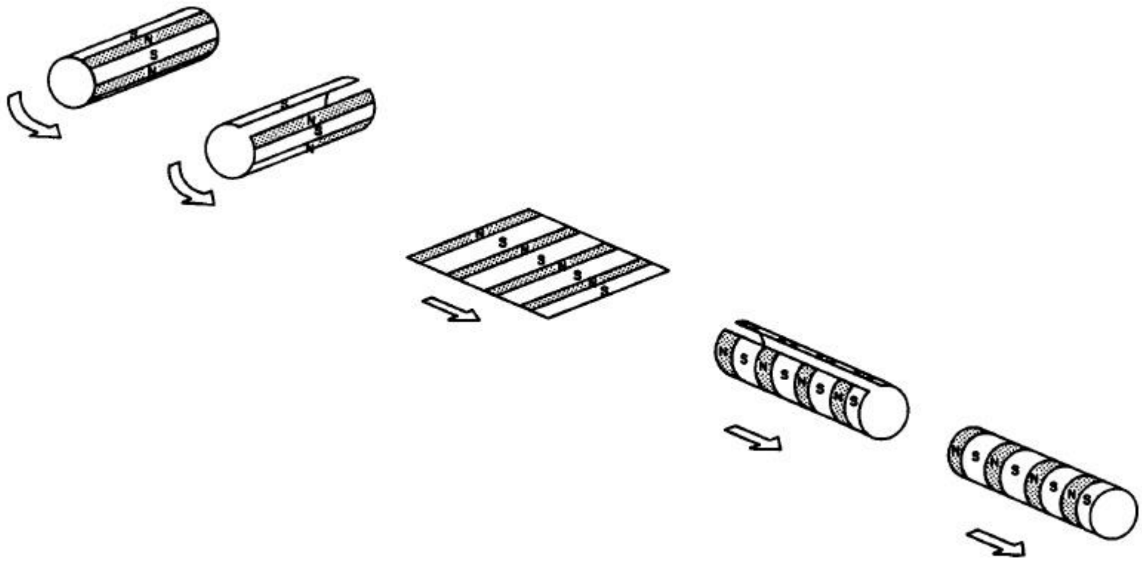

(b)

Figure 3.1: (a) Unrolling to receive a flat topology (b) Rerolling to receive a tubular topology [20]

The working principle is, thus, very similar to a regular induction motor. The moving part has windings on it, which, when energized create a magnetic field. This traveling magnetic field induces current on the windings on the stationary plate due to relative motion, and this current interacts with the original magnetic field, producing thrust.

The synchronous linear machine topology is obtained the same way as illustrated in Figure 3.1. The difference here is that the synchronous machine topology is used as a template. Similar to a conventional synchronous machine there is a DC excited or permanent magnet moving part placed on a track with three phase winding. Just like in the rotary case, linear synchronous motors offer more efficiency over linear induction motors. They have more initial cost, but the relative simplicity of the mover enables weight reduction and lower maintenance costs.

The energy efficiency of the linear induction motor is lower than its counterpart and the synchronous induction motor. Especially in the case of MAGLEV applications, the air gap between the mover and the stator is much larger for an induction motor, which reduces the efficiency even further. Compared to a synchronous motor the mover is usually heavier which limits the speed capability. However, the simplicity in design and low initial cost makes the induction motor attractive [21].

The low weight of the mover in a linear synchronous motor enables fast acceleration and high speeds. However, similar to the case of rotary synchronous motor the exact position of the mover is needed to ensure synchronous operation. The position and velocity sensing equipment is essential and adds to the total cost. The track structure of linear synchronous motor is much more complicated than the linear induction motor. This results in an overall rise in the initial cost and the motor must be very carefully designed to meet the given criteria, since design flexibility is not offered [22].

(a)

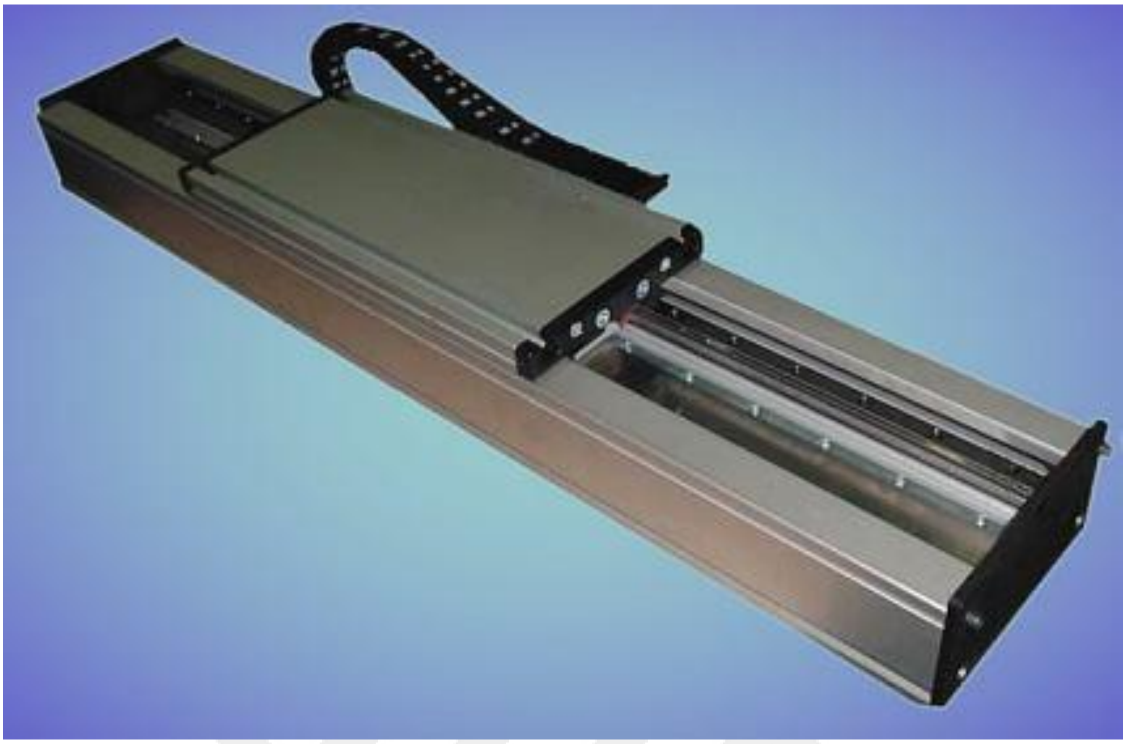

(b)

(c)

Figure 3.2: Some commercial progressive motors (a) Linear induction motor by H2W Tech [23] (b) Linear synchronous motor by System Management Welfare [24] (c) Tubular permanent magnet linear synchronous motor by Oswald Motors [25]

Linear oscillatory machines produce a limited thrust in an oscillatory back-and-forth manner. This kind of movement is useful in applications such as vibrators, speakers, compressors, pumps and linear generators. The basic idea behind an oscillatory machine is that a magnetic field generated by a permanent magnet piece interacts with an air-core coil that is excited by a current, producing thrust according to the force law. Oscillation is achieved and augmented with the help of a mechanical element, which is usually a mechanical spring assembly. In applications where continuous oscillations are not needed, plunger solenoids are usually used. Some examples of these applications are electronic locks, relays, and magnetic suspension systems. In plunger solenoids, permanent magnets can be replaced by iron plungers to reduce cost. The electromagnetic effect pulls the plunger inside the air-core coil, and once the coil current is cut, the spring connected to the plunger pushes it back to its original position. A schematic for a plunger solenoid is given in Figure 3.3.

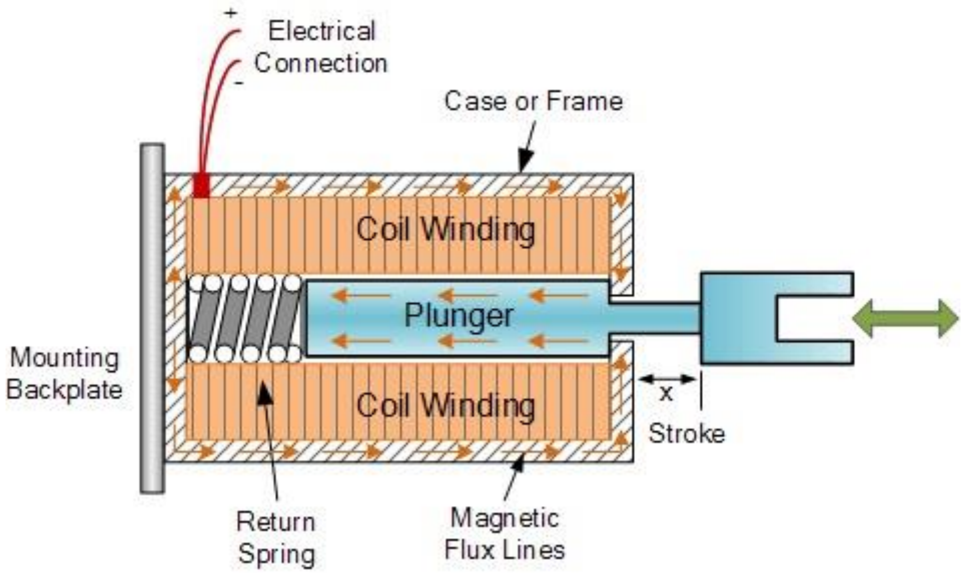

Figure 3.3: Schematic for a plunger solenoid [26]

As previously mentioned, linear oscillatory machines use a fixed frequency to generate a continuous oscillation. In applications such as pumps, compressors, linear vibrators and speakers a linear oscillatory motor is used. These are single-phase excited motors which employ permanent magnets. Used the other way around they act as single-phase linear oscillatory generators. A Stirling engine uses such a generator. In both cases the oscillatory machine offers simplicity in design with elimination of conversion mechanisms, and high efficiency (as a result of both compactness and operation at resonance frequency).

There are three main types of linear oscillation machines:

- Moving-coil,
- Moving-magnet,
- Moving-iron.

Just as progressive machines, oscillatory machines can be either flat or tubular. Tubular ones offer the advantage of more surface area being involved between stator and armature, enabling higher thrust and better heat dissipation. They are also better at dealing radial forces due to being circular, whereas in flat configurations those forces become a serious problem. Double-sided flat machine topologies are suggested in order to deal with this issue.

The linear oscillatory motors will be investigated in more detail, because they are the preferred choice of linear actuator for the use of linear compressors.

3.2 Moving-Coil Linear Oscillatory Motors

Moving-coil linear motors can either come as single-coil or multiple-coil configurations which are placed on the moving part with the permanent magnets placed in the stator. Single-coil types are used for high force outputs or as voice-coil speakers. Multiple-coil types are used for weight reduction in the core, because such an arrangement leads to multiple permanent magnet poles in the core in return, which reduces the weight. Usually in single coil topologies the length of permanent magnet is larger than the coil by stroke length l_{stroke}. For multiple-coil cases, the coils can be designed to be longer than the permanent magnets by l_{stroke} or the other way around. It all depends on the design criteria, of which the overall weight is the most important one. Both topologies are demonstrated schematically in Figure 3.4.

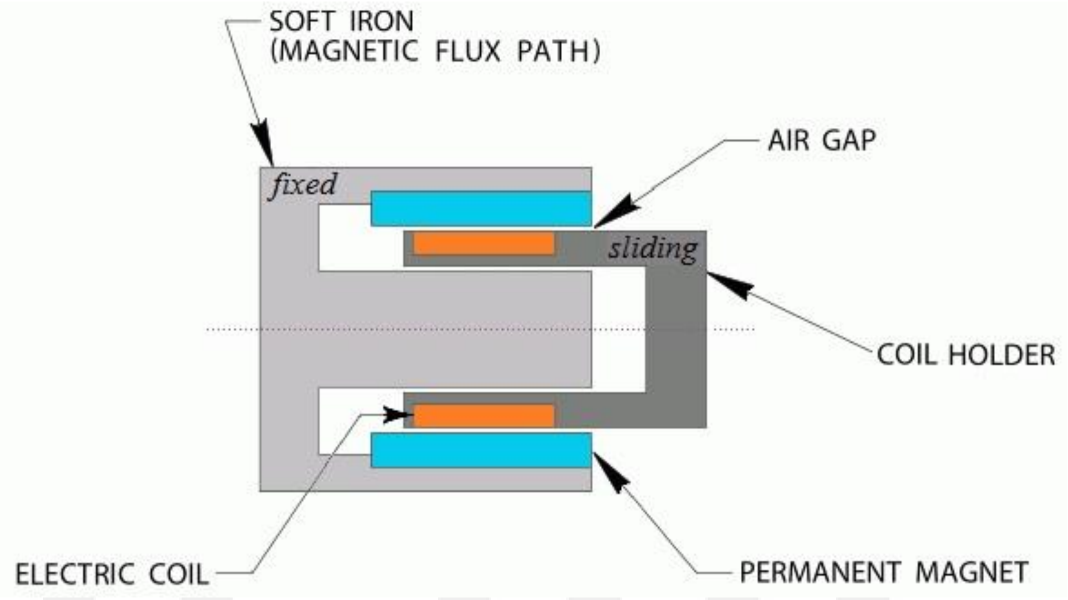

(a)

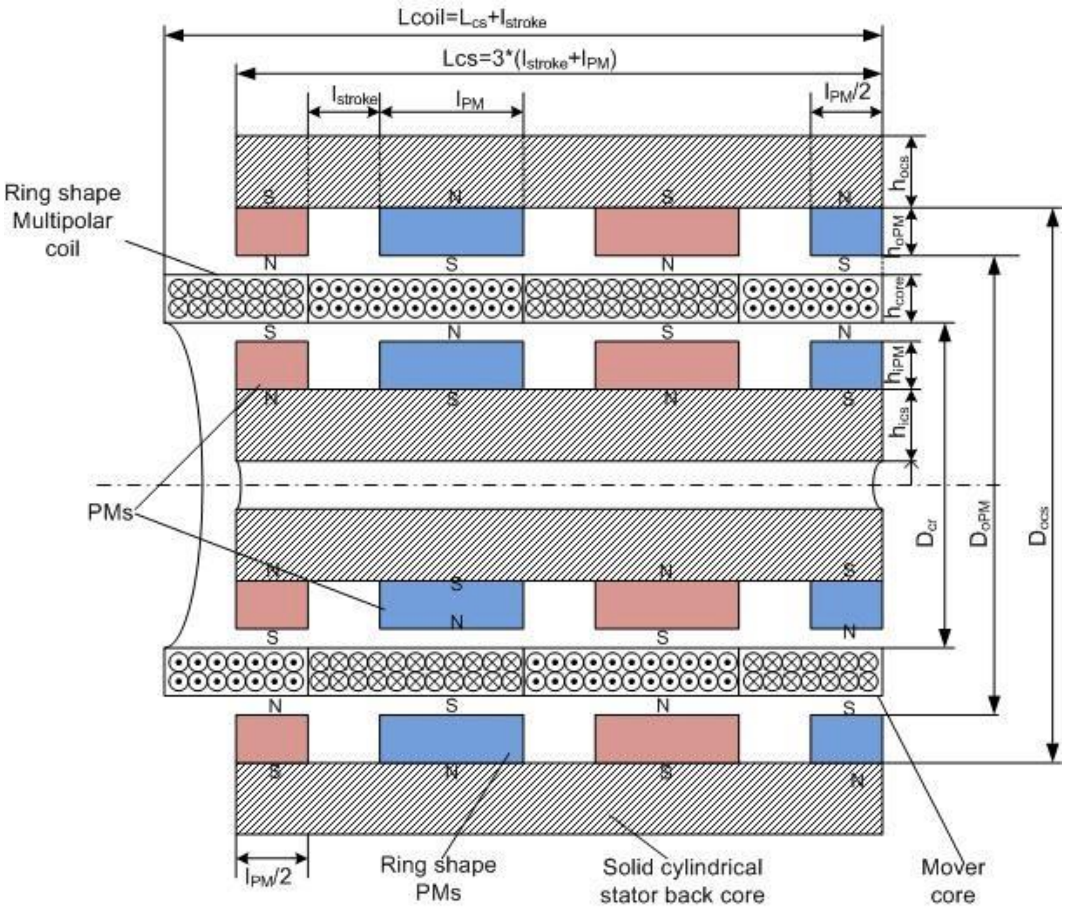

(b)

Figure 3.4: Moving-coil linear oscillation motor topologies (a) Single-coil [27] (b) Multi-coil [28]

The low inductance in the coils leads to a low thrust density. In order to overcome this problem, multiple-coil solutions are proposed. As mentioned above, this means multiple permanent magnet poles in the stator core, reducing its weight, however the multiple-coil configuration in the mover may lead to an increase in weight. In order to get the same resonant frequency, the spring coefficient should also be increased, further adding to the overall cost and still not getting a considerable increase in thrust force.

3.3 Moving-Iron Linear Oscillatory Motors

Essentially, plunger solenoids that operate at a fixed frequency to generate oscillatory motion can be classified as moving-iron linear oscillatory motors. Oscillatory motion is achieved by using on-off supply, that is, a PWM square wave with a designated duty cycle. At “ON” electromagnetic force propels the mover forward and at “OFF” the mechanical spring pulls it back. Doing this continuously at a fixed frequency generates an oscillating motion in the moving part. As with the other oscillatory motors, operation at resonance frequency is targeted in order to obtain higher efficiency.

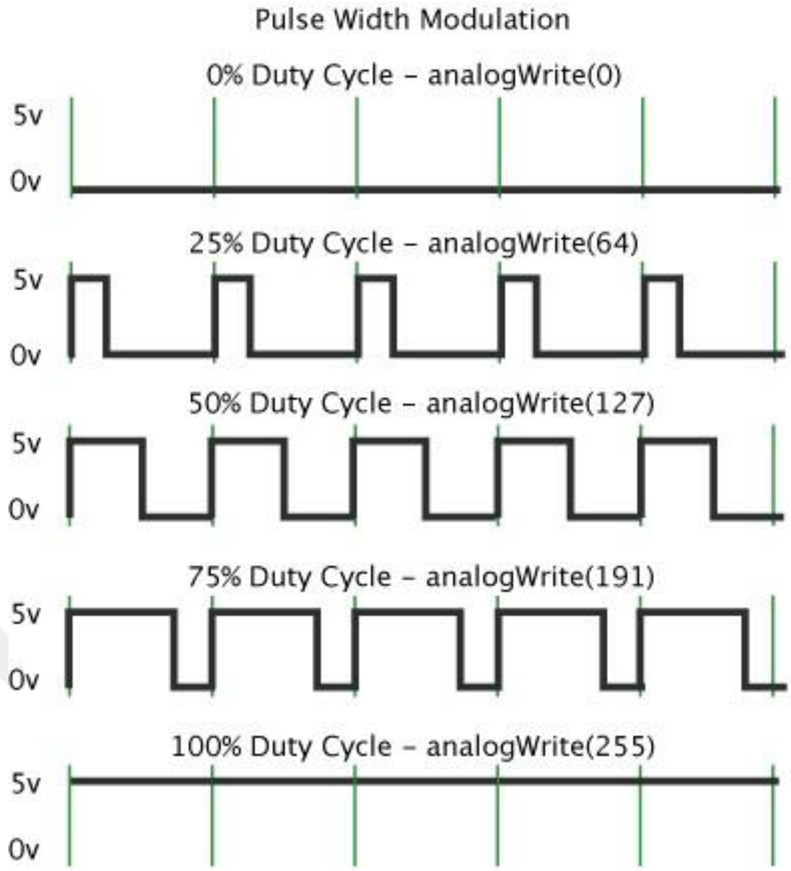

Figure 3.5: PWM square wave generated by Arduino [29]

Compared to the other oscillatory motors, the moving-iron type uses a mover of larger weight for the same frequency and thrust. This is especially prominent for the case of mover that is not a permanent magnet. In order to decrease the reluctance through the mover a magnetic material must be employed, and magnetic materials are high density materials. The single-pole coil introduces a rather large inductance, reducing response speed and power factor. Bouncing of the mover and non-uniformity in back emf leads to unwanted vibrations.

The schematic for a novel hybrid-flux-path moving-iron linear oscillatory machine is given in Figure 3.6.

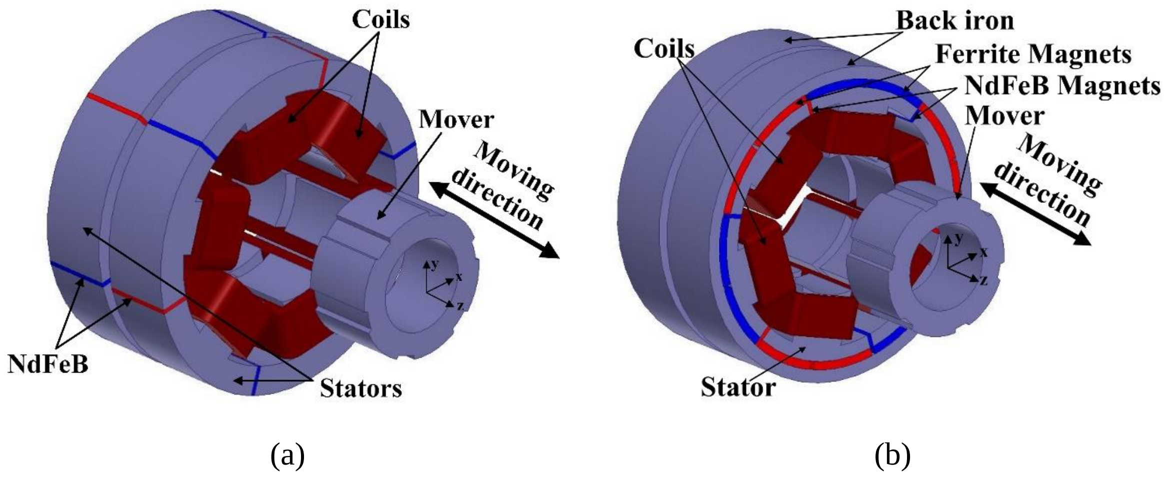

Figure 3.6: Schematic for a hybrid-flux-path moving-iron linear oscillatory machine [30]

3.4 Moving-Magnet Linear Oscillatory Motors

Moving-magnet linear oscillatory machines employ a moving part that consists of permanent magnets. Thrust is achieved by their interaction with the coils in the stator. Either the coils or the magnets or both can be single-pole or multi-pole. Flat or tubular configurations are available with tubular type usually preferred for compactness and larger power factor. Multiple-pole topologies are preferred if the machine size (diameter in tubular case) is desired to be kept small.

There are many moving-magnet motor designs in the literature that are used in compressor and pump applications. As mentioned above, the tubular type offers a compact, circular design where flexures can be employed to act as springs all the while also offering the possibility of serving as linear bearings for the mover. A tubular single-pole design from the literature is given in Figure 3.7. The resonance frequency for this motor is 100 Hz and at 10 W input power it generates a stroke slightly over 2 mm [31].

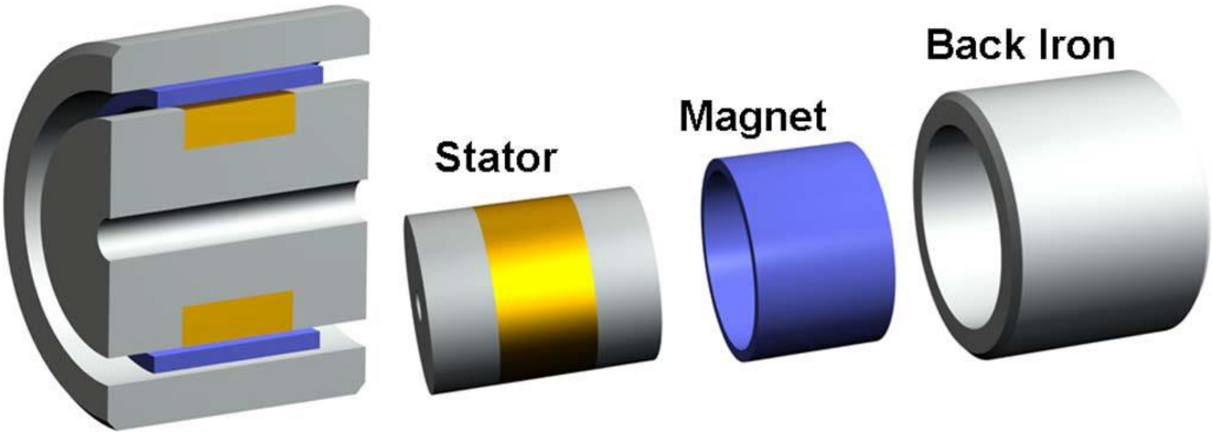

Figure 3.7: Small single-coil tubular moving-magnet linear oscillatory motor [31]

A single-pole coil design that incorporates a Halbach array permanent magnet configuration with radially and axially magnetized magnets stacked together is given in Figure 3.8. 10.5 mm stroke is achieved at 50 Hz in this configuration [32].

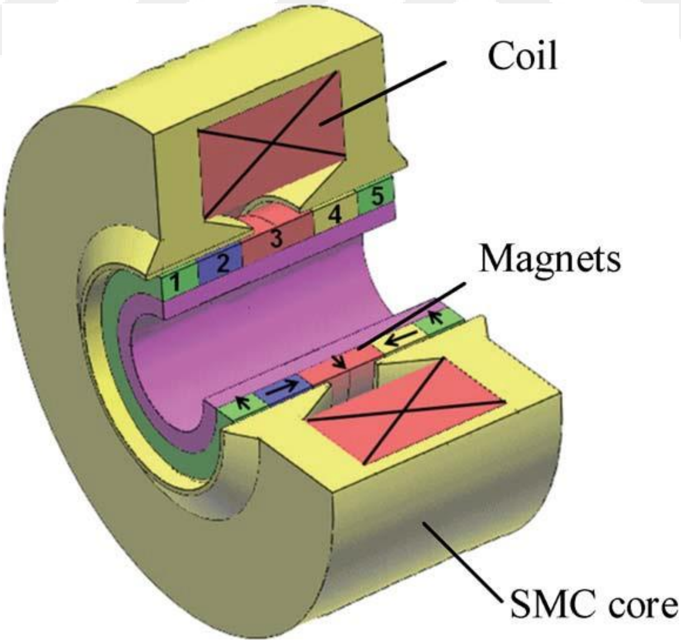

Figure 3.8: Tubular linear oscillating machine with single-pole coil stator and permanent magnet mover with the magnets in Halbach array configuration [32]

A tubular linear oscillatory motor used as a directly-driven hydraulic servo pump in electro-hydrostatic actuator (EHA) is presented by [33]. This design has a multi-pole configuration for both the stator coils and the permanent magnet mover. It has 8 stator poles and 3.5 permanent magnet pole pairs. The permanent magnets are again placed in Halbach configuration. A resonance frequency of 20.5 Hz and 10 mm stroke is achieved at a current density of 7 A/mm^2. The self-shielding capability of Halbach configuration enables for a hollow mover design which greatly reduces the mover weight, enabling higher operating frequency and easier attachment of resonant springs to the mover assembly.

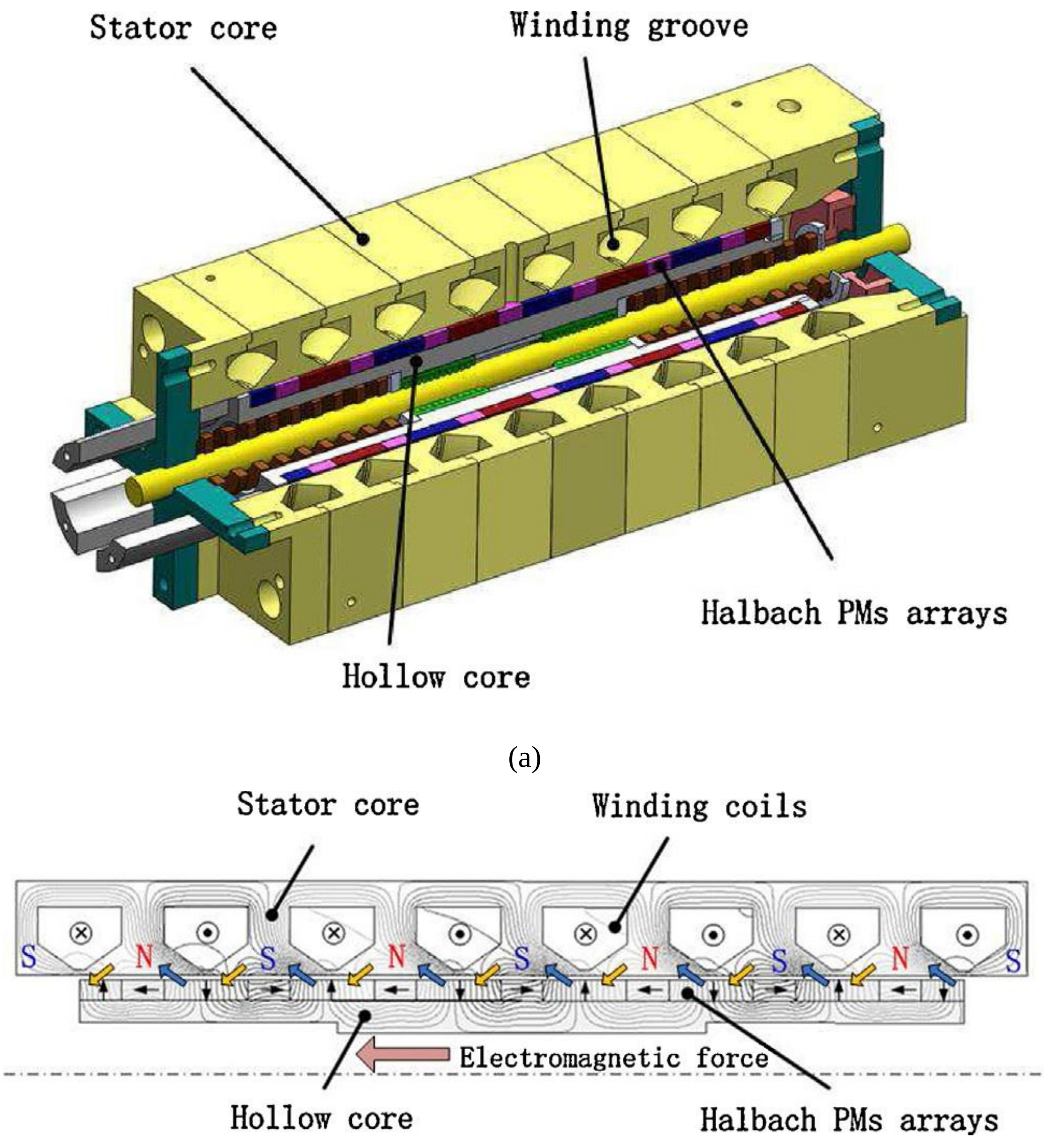

(a)

(b)

Figure 3.9: Tubular linear oscillatory motor used as a hydraulic servo pump (a) Overall pump assembly (b) Schematic for the stator and permanent magnet mover poles [33]

Among the peculiarities the moving-magnet machines show is the fringing and the permanent magnet leakage flux in single-pole solutions. These effects are lessened in multi-pole designs. Moving-magnet linear oscillatory motors offer a very good thrust density compared to the other types, but the stroke is rather limited. The maximum stroke that can be obtained is equal to the length at which the permanent magnet assembly changes the polarity, i.e. the pole pitch, which is also equal to the length of a coil. In practice, strokes nearing that value are achieved at oscillatory operation, with the highest achieved stroke being at resonance frequency.

Chapter 4

MINIATURE LINEAR COMPRESSOR DESIGN AND MAGNETIC CIRCUIT ANALYSIS

4.1 Introduction

In this chapter the components of the novel miniature linear compressor assembly are investigated in detail. The very first component that is investigated is the valve assembly. Every part of the miniature compressor is custom made with the exception of the valves used for the compression operation. The valve type that is considered for usage is the check valve, so a quick overview of commercially used check valve types is presented first. Then the commercially available miniature valve types are presented and the selection criteria for the valve type that is incorporated into the design is discussed. Once the selection is done, the chamber and valve housing assembly is manufactured according to the specifics of the selected valves. Next, the chamber and valve housing designs are presented. Basically, the linear compressor consists of this chamber-valve housing part and the linear oscillatory motor that is used to excite a piston that is directly connected to mover of the motor. The piston moves back and forth inside the chamber, with the valves at the end of the chamber providing suction and discharge at one cycle. In the section that follows, the linear oscillatory motor design with its individual components is presented.

Finally, a magnetic circuit analysis for the proposed motor is demonstrated to show the magnetic flux and the electromagnetic thrust force generated by the coil-magnet interaction. The geometric parameters of the back iron, permanent magnets and coils is demonstrated. The reluctances of each component is modeled and the corresponding equivalent magnetic circuit is generated according to the principles presented in Chapter 1. The calculated flux and thrust force values are compared to the FEM analysis results.

A more detailed analytical calculation for the motor will be presented in Chapter 5. There the analytical results will be compared with experiments carried out with the prototype motor.

4.2 Linear Compressor Concept

The linear compressor is a type of reciprocating compressor where the reciprocating action of the piston is provided by a linear actuator, which is usually a single-phase linear oscillatory motor. It can be divided into two major parts, namely the linear motor part and the compression chamber part, where the valve assembly is located.

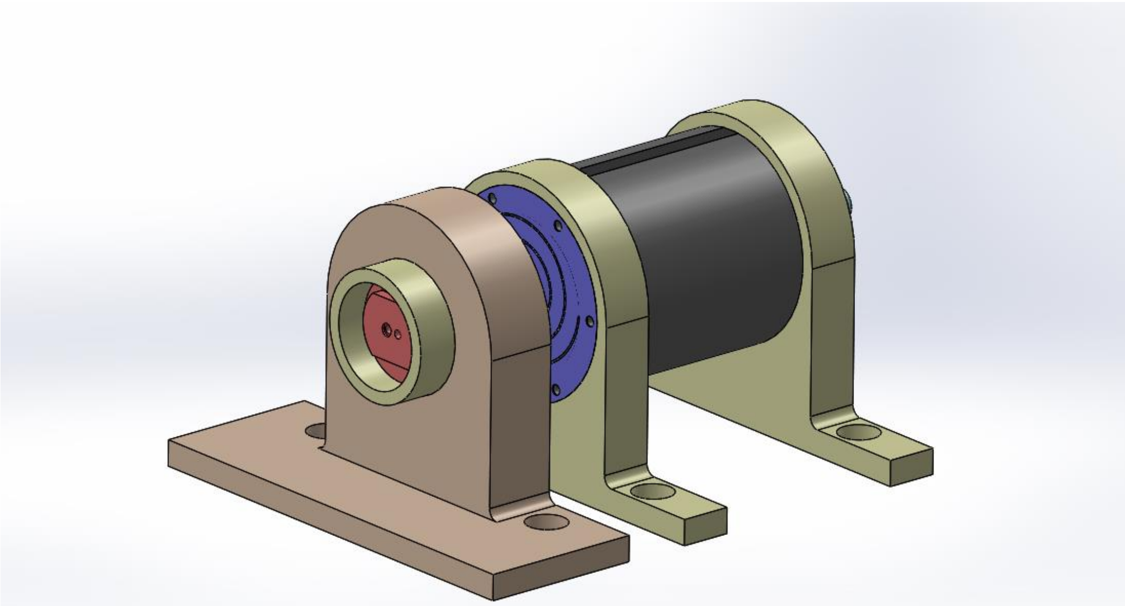

(a)

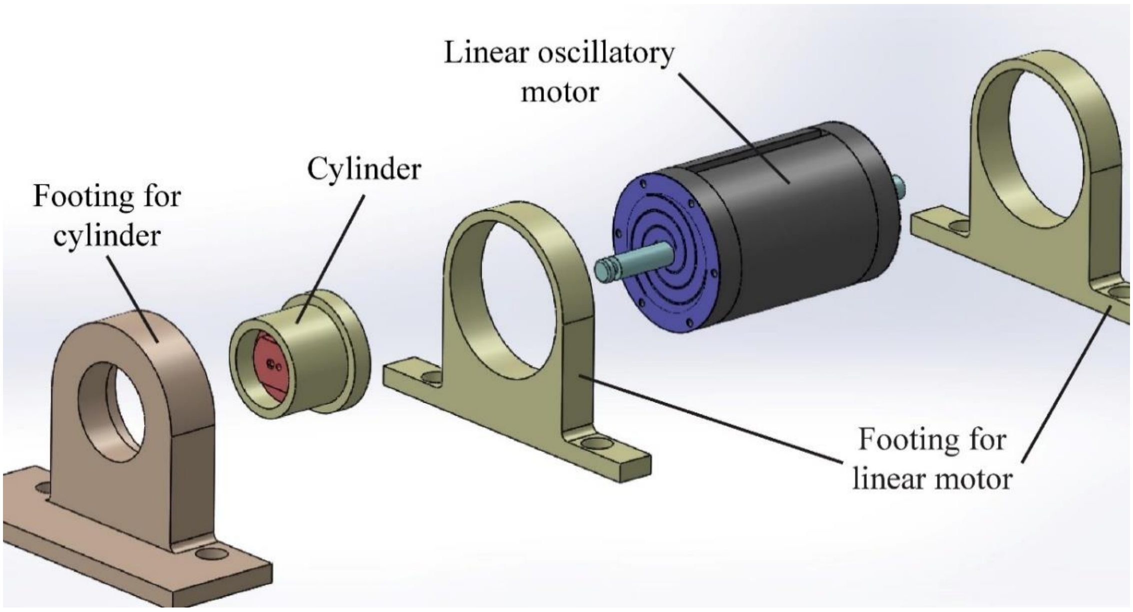

(b)

Figure 4.1: The proposed miniature linear compressor design (a) Overall CAD model (b) Exploded view

The oscillatory motion of the motor is backed up by mechanical springs, and the motor is excited at a frequency that matches the resonance frequency of the piston-spring system, which results in maximum electrical efficiency and largest stroke. This piston compresses the gas trapped in a cylinder, which at the other end is connected to a check valve duo, one being the intake valve and the other the outtake valve. Leakage through the piston-cylinder interaction can be prevented by using a clearance seal placed either on the piston or the cylinder.

The selection of suitable check valves is especially tricky in a miniaturized operation. In the next section, a review of check valve types is provided and the design steps which led to the selection of the appropriate valve type is demonstrated. Following sections will discuss the motor components.

4.3 Check Valve Types

Valves are used in hydraulic or pneumatic systems to regulate the flow and the pressure of the fluid. Starting and stopping, controlling flow rate, diverting or preventing flow, controlling or relieving pressure are among the functions of valves. All valves have a closure member inside which can be adjusted to get the desired effect. This can be done either manually or automatically. Manually controlled valves are used to control flow rate and start, stop and divert the flow, whereas automatically controlled valves are used to prevent backflow (check valve) and relieve pressure (relief valve) [34].

In pump and compressor applications the valve type that is used is the check valve. Check valves allow flow only in one direction, so they are used to prevent backflow in pump and compressor applications. The check mechanism can be accomplished with flap, disc, or ball configurations.

Swing type check valves (Figure 4.2) use a hinged plate. Tilting disc check valves (Figure 4.3) use a profiled disc that is counter weighted and tilts in one direction of the flow, allowing it, and preventing it altogether at the other direction. The disc is balanced in such a way that at low flow it tilts back to the closed position. Lift-type disc check valves (Figure 4.4) have a disc or plug that is lifted by flow in one direction and shutting back in its seat in reverse-flow. Piston check valves (Figure 4.5) have a dashpot included in the check mechanism in order to generate a damping effect during operation. Ball check valves (Figure 4.6) incorporate a ball as the check mechanism that is lifted with forward flow and pushed back to its seat with reverse flow, making this valve particularly suitable for viscous fluid flow. Metal, plastic, or ceramic balls can be used. Foot check valves (Figure 4.7) are pushed to the end of a suction pipe and prevent the total emptying of the pump. A flap or membrane can be used as well as ball-operating systems. Spring-loaded check valves (Figure 4.8) are lift type check valves where the check mechanism is connected to a spring for faster call-back. This enables closing of the valve even before the flow is fully stopped. One other advantage they offer is their ability to operate in any position. Wafer check valves (Figure 4.9) use a leaf that is connected to a torsion spring in one end. The leaf opens at forward flow and shut back by the spring when the flow stops [35].

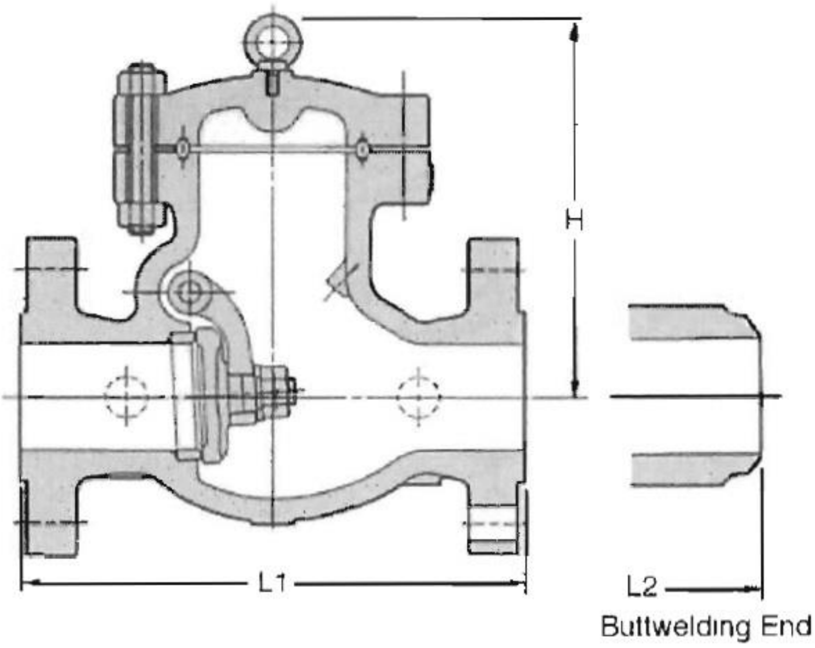

Figure 4.2: Swing check valve [35]

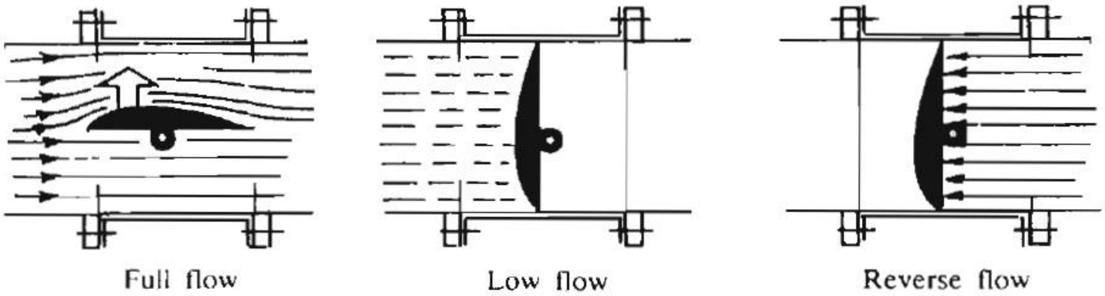

Figure 4.3: Tilting disc check valve [35]

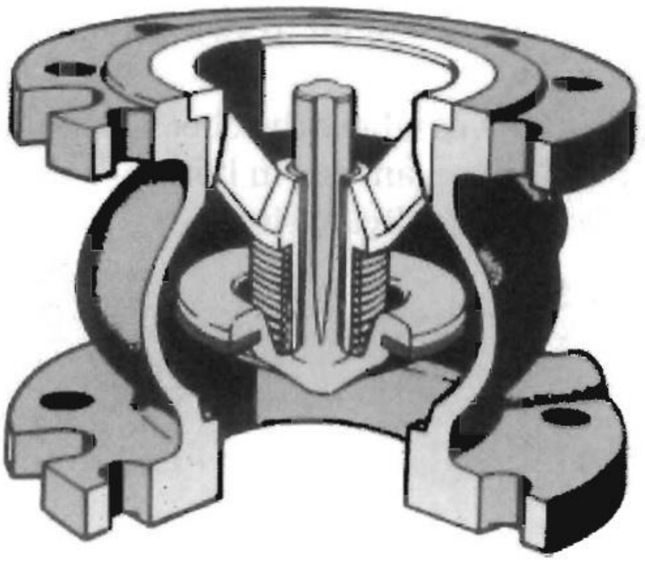

Figure 4.4: Lift-type check valve [35]

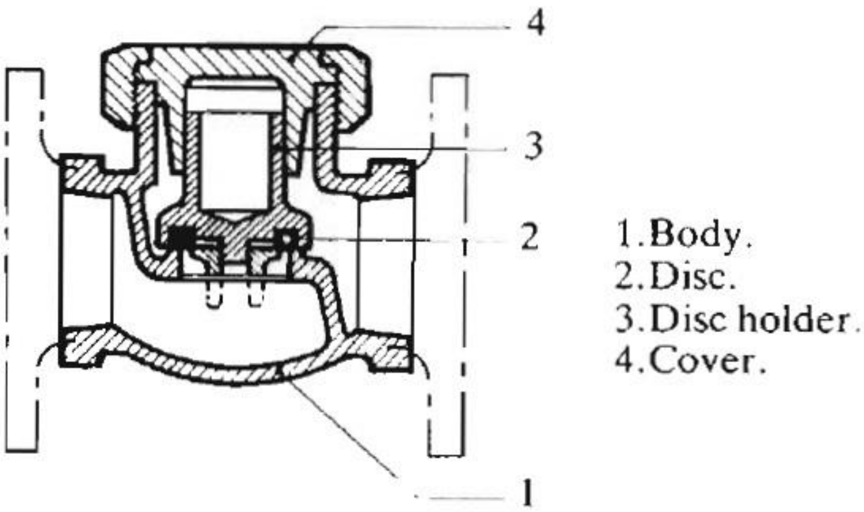

Figure 4.5: Piston check valve [35]

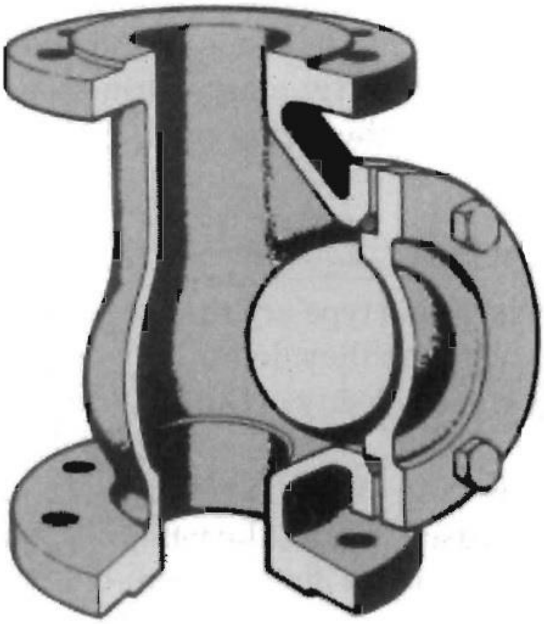

Figure 4.6: Ball check valve [35]

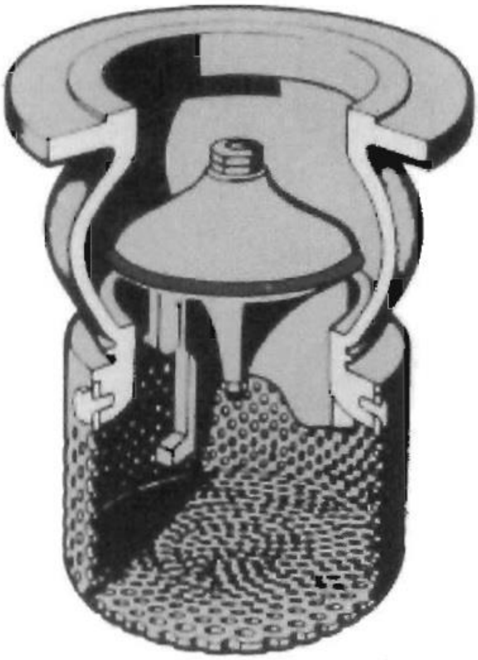

Figure 4.7: Foot check valve [35]

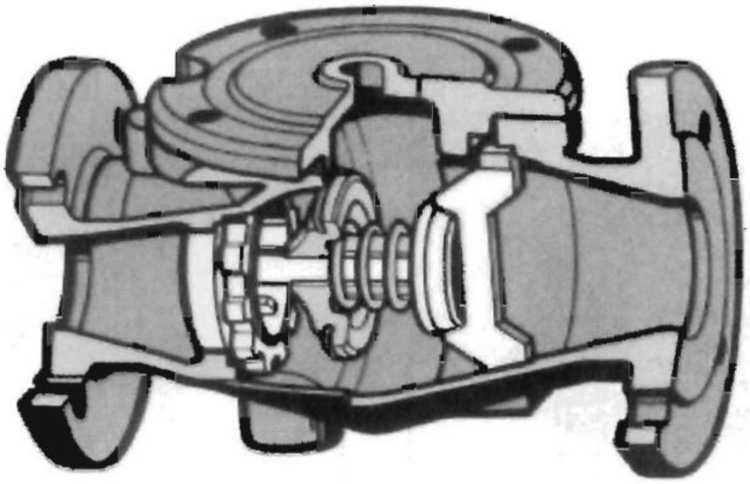

Figure 4.8: Spring loaded check valve [35]

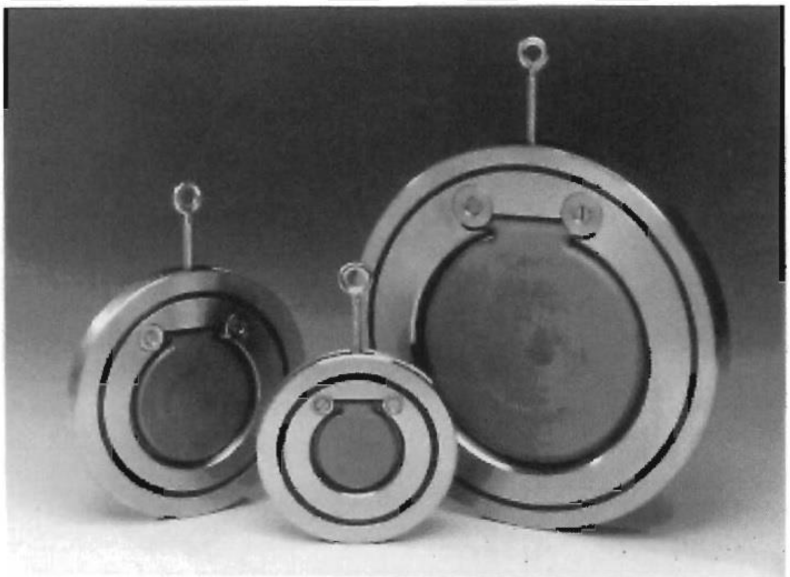

Figure 4.9: Wafer-type check valve [35]

Positive leak-tight sealing is typical for check valves that are used in hydraulic and pneumatic applications especially at high pressures. Ball-type and leaf type with spring action are among the most preferred types of check valves for these applications.

4.4 Valve Selection for the Miniature Compressor Application

Perhaps the only criterion for selecting the correct valve for the miniature compressor is the size. There are unfortunately not many valve types commercially available for miniature-size applications. The smallest check valves that are available have a diameter of 2.5 mm. These valves are generally designed for medical applications.

The most important miniature valve manufacturer is miniValve. Among the valves the company manufactures are duckbill valves (Figure 4.10(a)), umbrella valves (Figure 4.10(b)), duckbill-umbrella combination valves (Figure 4.10(c)), x-fragm valves (Figure 4.10(d)) and mini valve balls (Figure 4.10(e)).

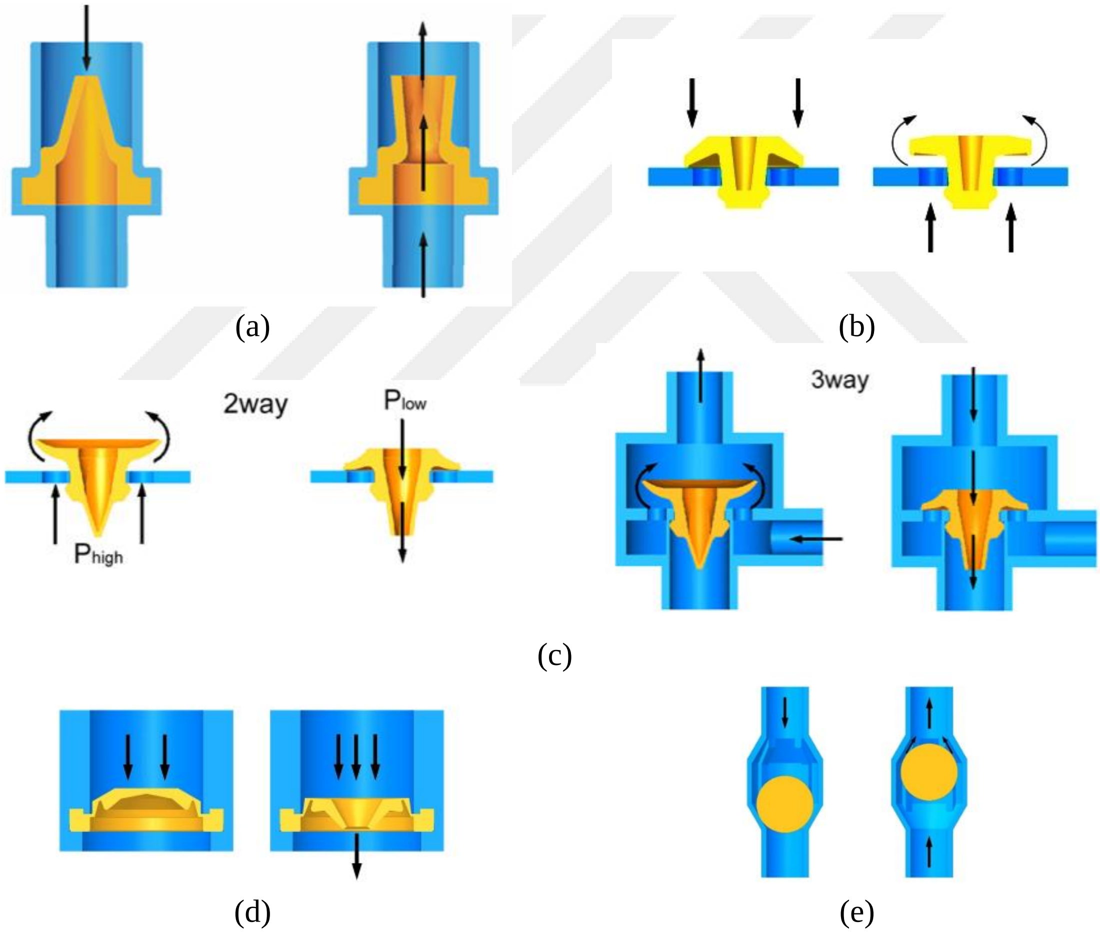

Figure 4.10: Valve types manufactured by miniValve (a) Duckbill valve (b) Umbrella valve (c) Duckbill-umbrella combination valve (d) X-fragm valve (e) Mini ball valve [36]

As seen from the schematics given in Figure 4.10, duckbill valves act as check valves where they prevent reverse flow but allow forward flow. These are cost effective valves which also allow easy installation. Umbrella valves are a type of lift valves discussed in Section 4.3, which also act as one way valves where the umbrella part allows forward flow after there is enough pressure to lift it. This means that they allow forward flow at a predetermined pressure and prevent reverse flow. Just like duckbill valves they are cost effective and easy to install. The duckbill-umbrella combination valves have the functionality of both duckbill and umbrella valves, and they can be used either in a 2-way or a 3-way configuration. In 2-way configuration they do not prevent back flow, but in one direction, the umbrella part ensures that flow occurs at a higher predetermined pressure than the other direction. In 3-way configuration they do the job of two check valves, i.e. in a compressor application they allow suction from one port that is opened by the umbrella at a certain pressure level, then close that port and guide discharge through the other port which is opened by the duckbill part almost immediately. X-fragm valves open at a certain pressure and close right after extracting the pressure surplus. They are thus used for dispensing purposes. Ball valves act like the ball check valves discussed in Section 4.3, with the company manufacturing valve balls as small as 3 mm in diameter. The materials used for these valves are various elastomeric material, such as medical and food-grade silicone and hydrocarbon-resistant fluorosilicone rubber [36].

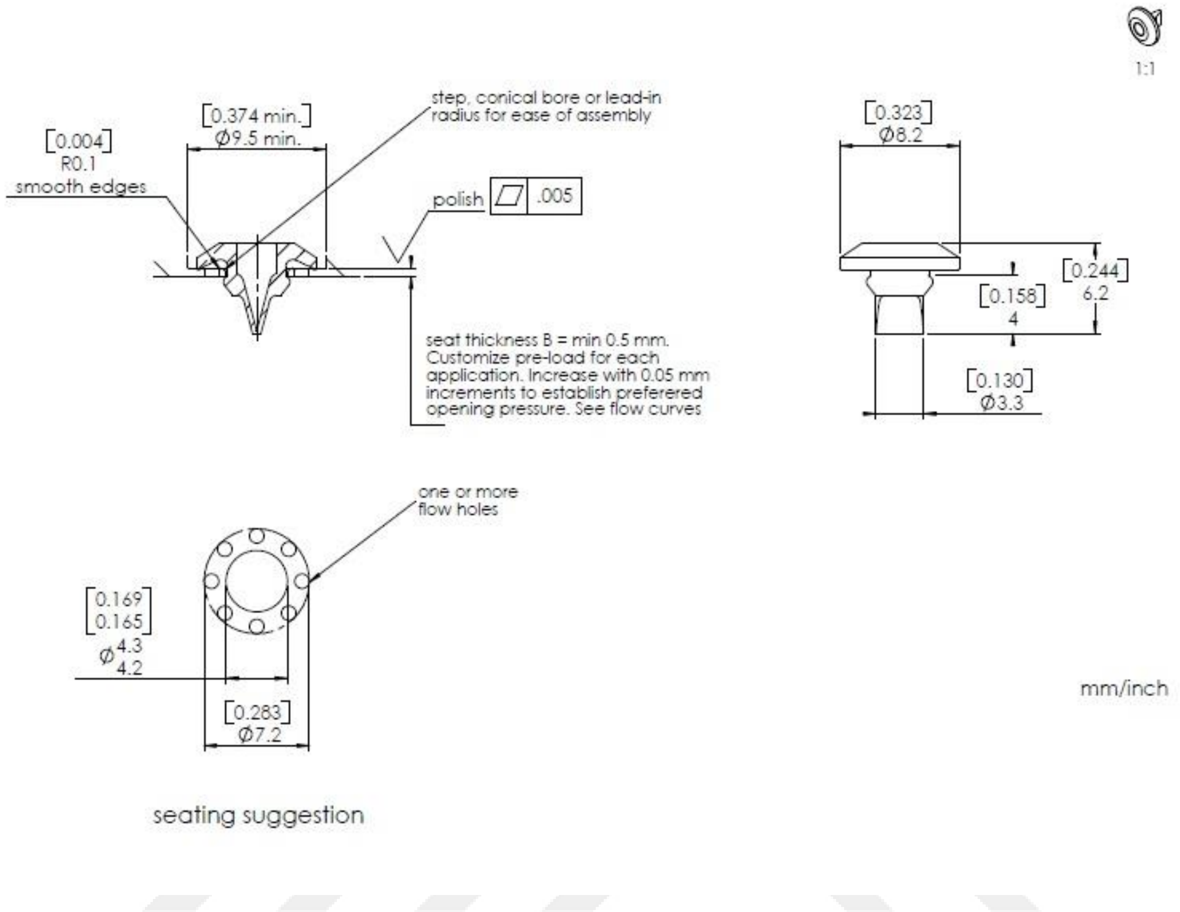

Figure 4.11: Technical drawing of the 8.2 mm duckbill-umbrella combination valve [36]

The very first considered valve type for the miniature linear compressor was the duckbill-umbrella combination valve. The smallest available size is the 8.2 mm valve which suggests a housing of at least 9.5 mm. The advantage this valve offers is naturally the combination behavior. When used as a 3-way valve, one single valve is capable of both regulating suction and discharge. However the housing that must be designed accordingly is somewhat complex and not easily achievable at miniature dimensions. For trial purposes this valve housing was produced.

The technical drawing of the 8.2 mm duckbill-umbrella combination valve is given in Figure 4.11. The manufactured valve housing on which this valve is placed on and its cross-sectional view is given in Figure 4.12.

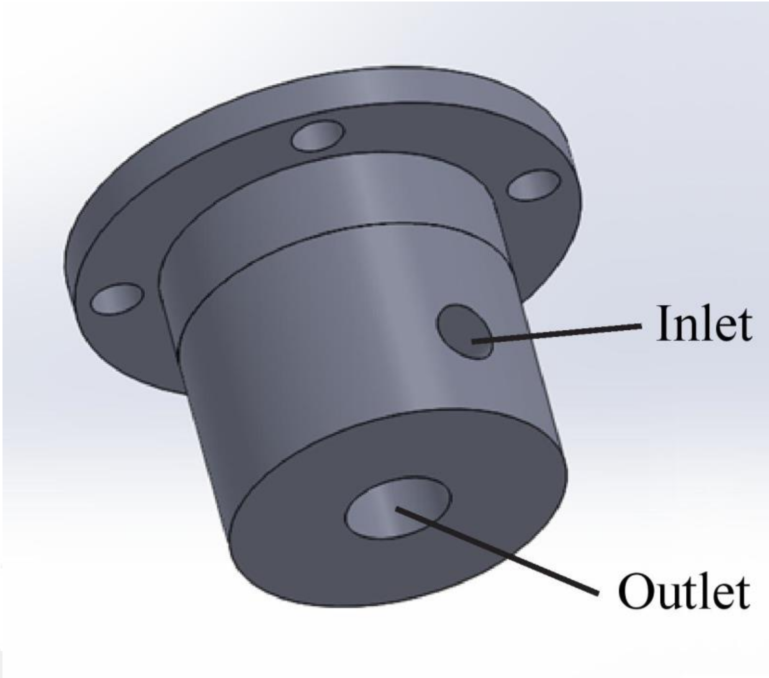

(a)

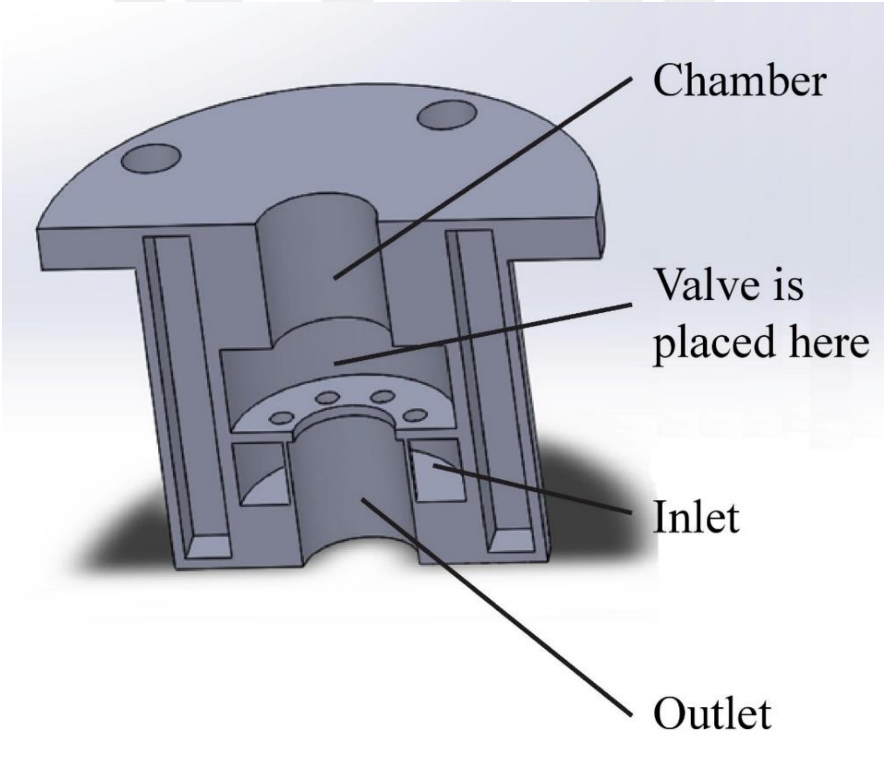

(b)

Figure 4.12: The manufactured valve housing for the duckbill-umbrella combination valve (a) CAD model (b) Cross-sectional view

This valve housing was manufactured using 3D printing and is made of ABS polymer. The piston of the motor was designed to reciprocate inside a chamber of 6 mm diameter (the reason for this dimension will be explained later) which opens up to an area of larger diameter, namely 9.5 mm on which the valve is placed (Figure 4.12 (b)). The major problem that is faced here is this sudden expansion of the diameter where naturally, a relatively large dead zone is introduced. Another problem is the surface quality of the valve housing. The surface on which the umbrella part of the combination valve sits must have very good quality which often is suggested to be achieved by polishing. Since the valve housing is a 3D printed part this is rather difficult to achieve.

Thus, this idea was abandoned in favor of check valve pairs, one responsible for suction, and the other for discharge. There are two candidates which are suitable for the job: the 1.5 mm duckbill valve by miniValve and the 2.5 mm check valve by The Lee Company. The latter is a spring assisted ball check valve that is available at several cracking pressures. This valve is designed for plastic housings and installation is accomplished simply by pushing the valve inside a groove of 2.5 mm diameter.

The schematic for 2.5 mm check valve is given in Figure 4.13 and the technical drawing for 1.5 mm duckbill valve is given in Figure 4.14.

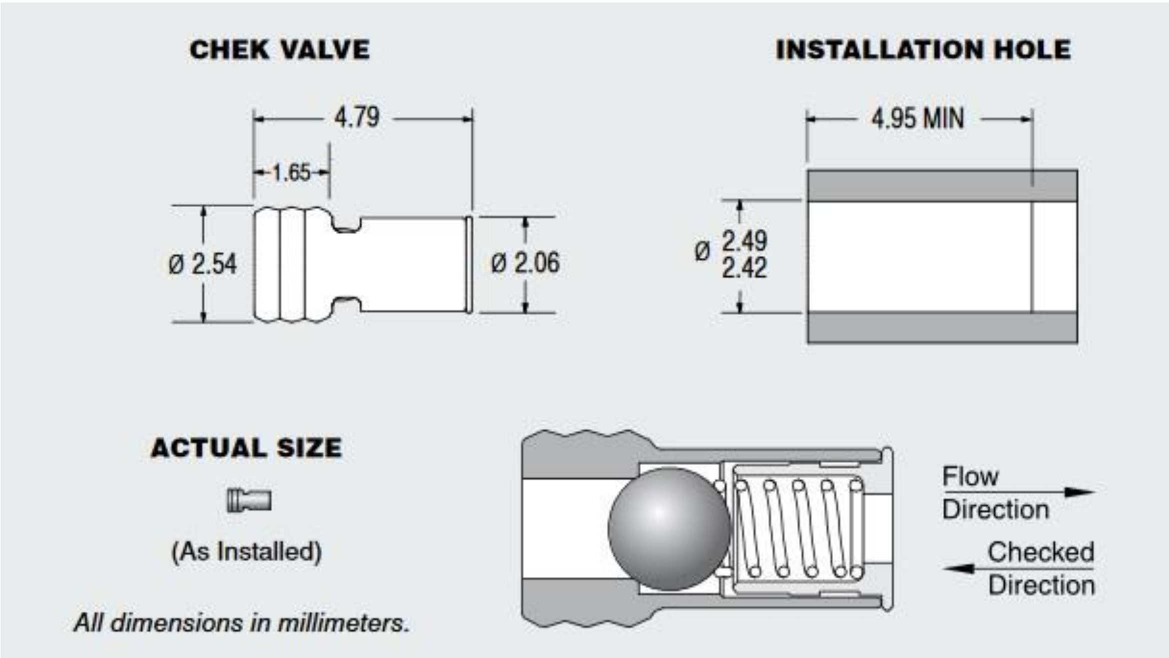

Figure 4.13: Schematic of the 2.5 mm check valve by The Lee Company [37]

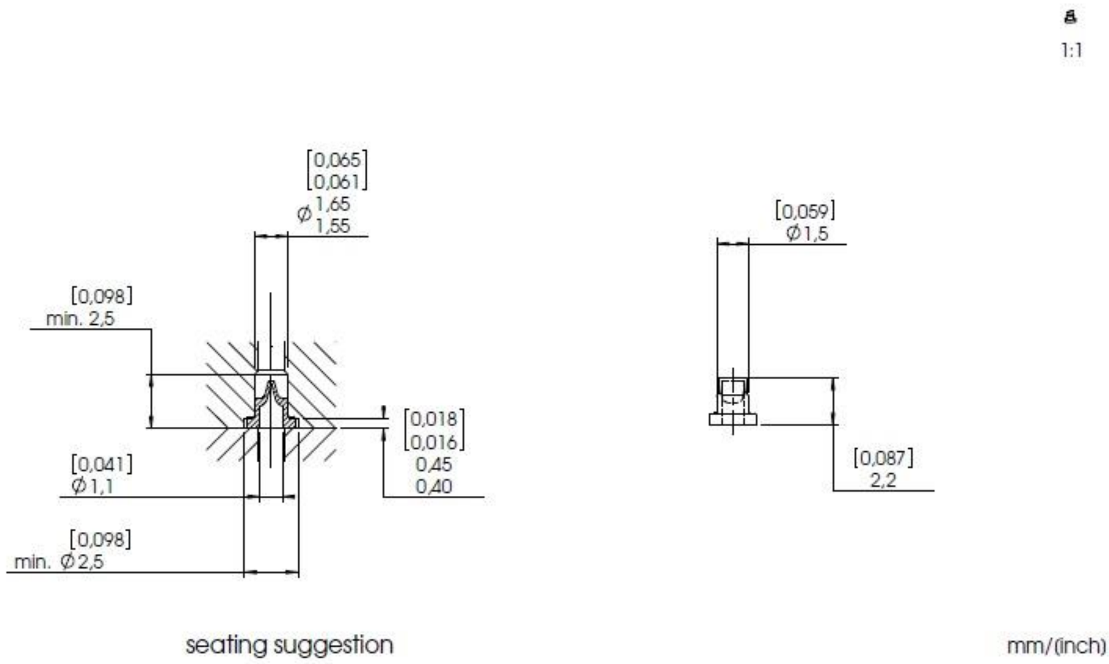

Figure 4.14: Technical drawing of the 1.5 mm duckbill valve by miniValve [36]

From Figure 4.14 it is seen that the 1.5 mm duckbill valve should be placed in a sealing of 2.5 mm diameter at minimum. This means that for both cases a groove of 2.5 mm must be made available for each member of the valve pair for both valve types. In order to face both suction and discharge valves directly along the axis of motion, a chamber diameter must be selected which covers both valves, and in this case the chamber diameter is 6 mm. Piston diameter is also selected to be of the same diameter.

The 2.5 mm check valves by The Lee Company are naturally more robust, however they are not leak tight at reverse flow direction and compared to duckbill valves by miniValve they have a relatively large cracking pressure. They are also more vulnerable to contamination than the duckbill valves. In the light of these reasons the duckbill valve was selected, however, measurements were also carried out with the check valve. The CAD model for the housing designed for the 2.5 mm check valves is given in Figure 4.15 and the CAD model for the housing designed for the 1.5 mm duckbill valves is given in Figure 4.16.

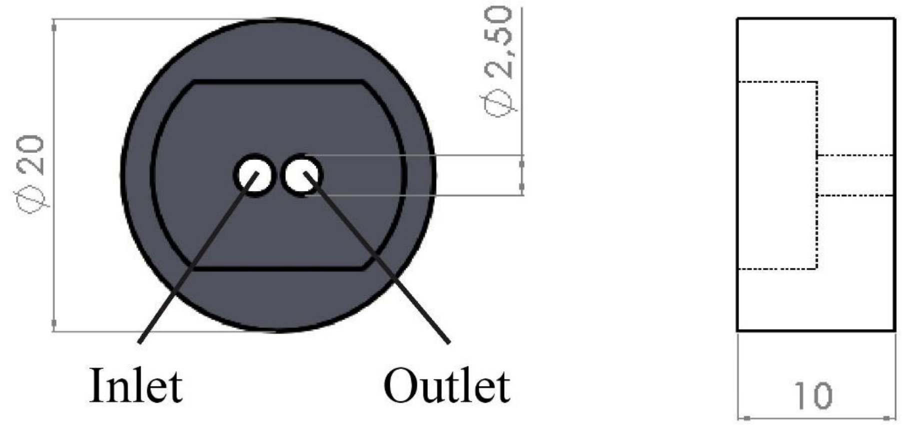

(a)

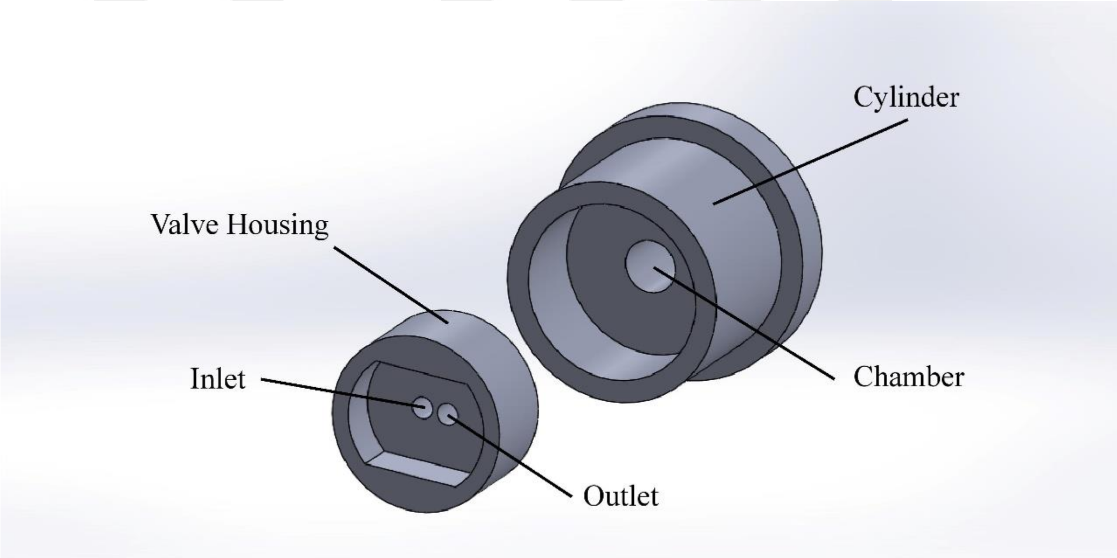

(b)

Figure 4.15: Valve housing CAD model for the 2.5 mm check valves by The Lee Company (a) Valve housing CAD model (b) Exploded view of the valve housing with the cylinder

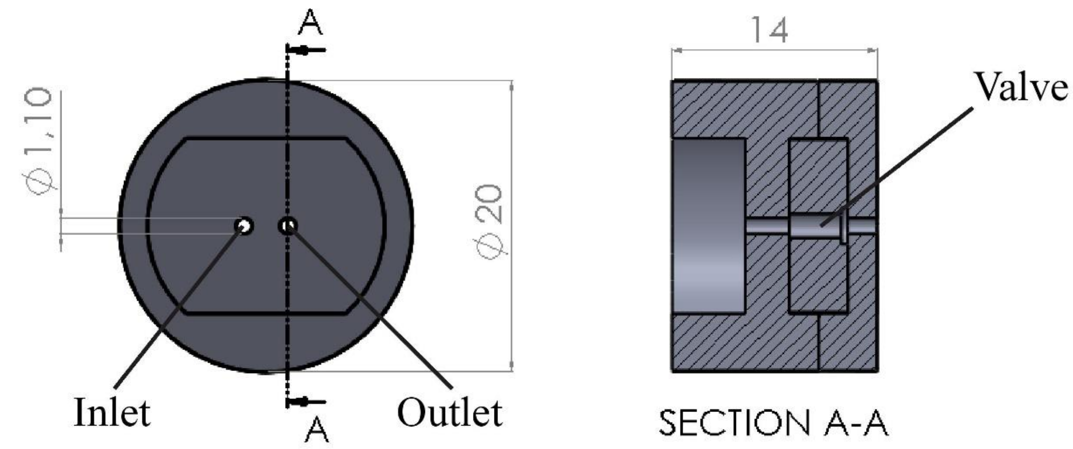

(a)

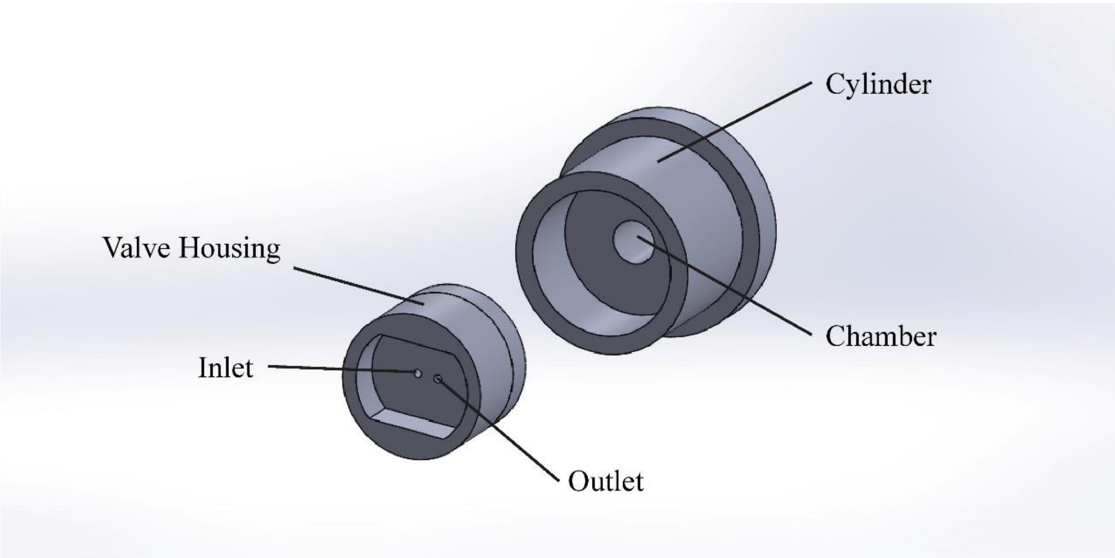

(b)

Figure 4.16: Valve housing CAD model for the 1.5 mm duckbill valves by miniValve (a) Valve housing CAD model (b) Exploded view of the valve housing with the cylinder

The dynamics associated with the gas compression will be investigated in Chapter 6, where the motor-chamber assembly will be revisited.

4.5 Linear Oscillatory Motor Components

Next, the components that make up the linear oscillatory motor are presented. The motor is a moving-magnet type with multi-pole coils placed in the stator and the permanent magnets placed on the mover in Halbach configuration. The reason for selecting multi-pole configuration is that the multi-pole configuration reduces fringing and flux leakage losses and enables higher thrust at the cost of increased mover weight.

4.5.1 Coil Housing

First a tube that holds the coils is manufactured. This tube does not take any part in the magnetic circuit, it only serves as a guidance for the coils holding them in place. Aluminum is used as a material for this part because of it having a relative permeability close to air. The part has an inner diameter of 15 mm and an outer diameter of 30 mm. It has 5 slots of 6 mm length and the coils are placed inside these slots up to the outer diameter of 30 mm. The CAD model is shown in Figure 4.17.

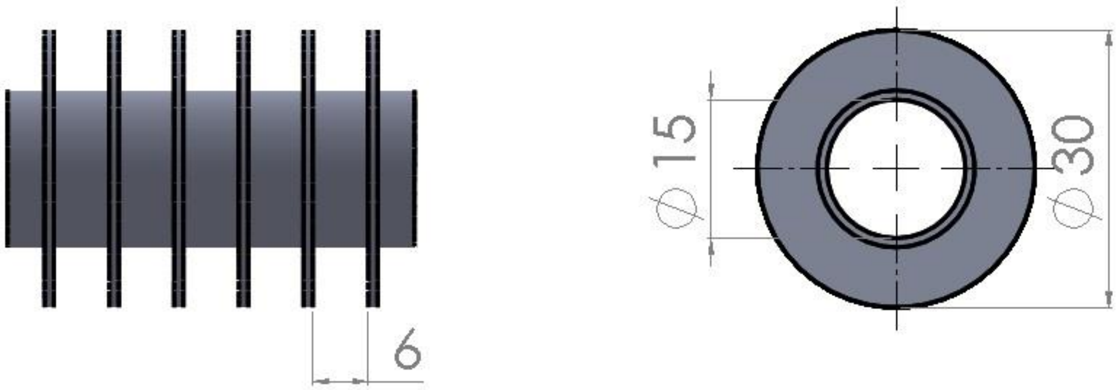

Figure 4.17: Coil housing made of aluminum

4.5.2 Stator Back Iron

The stator back iron is the outer cover the coil housing is put inside. It provides a return path to the flux, closing the magnetic circuit. For this reason a highly permeable material must be selected, which in this case, is 430F steel. The outer diameter of the back iron is 40 mm. Six holes at 60^0 distance from each other are opened to hold the side plates. The CAD model for the back iron is given in Figure 4.18.

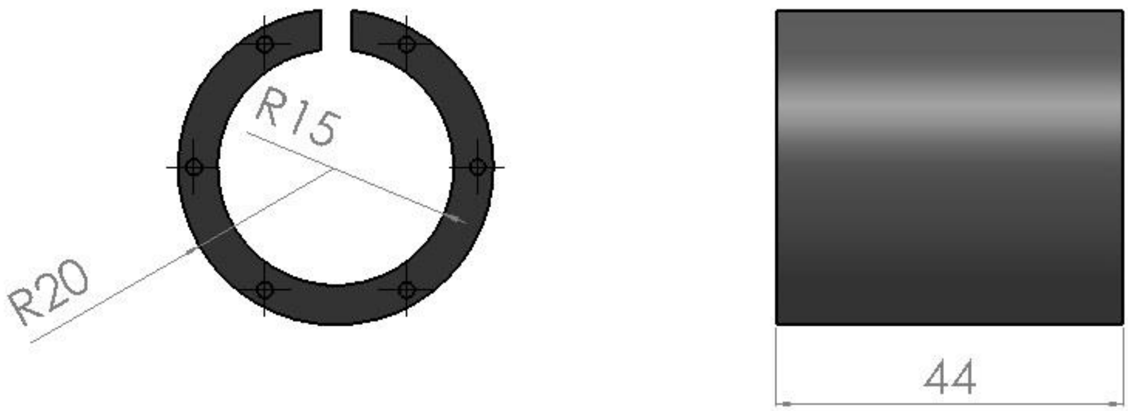

Figure 4.18: CAD model for the stator back iron

4.5.3 Side Plates

The side plates close the magnetic circuit from the sides. Therefore 430F steel is again selected as raw material for them. The plates are of 40 mm outer diameter with six M2 holes opened on them at 60^0 distance from each other. These holes serve as the connection with the back iron and also the flexures are screwed to the side plates through these holes. The CAD model for the side plates is given in Figure 4.19.

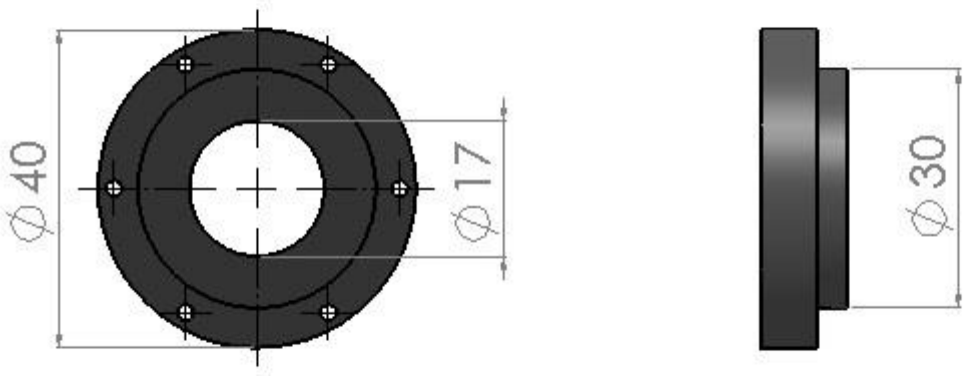

Figure 4.19: CAD model of the side plates

4.5.4 Mover Assembly

The mover is made up of four separate parts. The largest one is a hollow tube-like part which serves as a housing for the permanent magnets (Figure 4.20(a)). The long cylindrical part goes inside this tube-like part through the holes of the permanent magnets, and gets connected to the bottom (Figure 4.20(b)). The other two parts are the end parts to which the flexures are attached at the center (Figure 4.20(c)). One of the two serves as the piston (Figure 4.20(d)). A groove is placed on it where the gasket is put on. The exploded view of the mover is given in Figure 4.21.

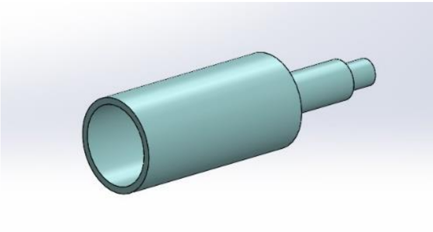

(a)

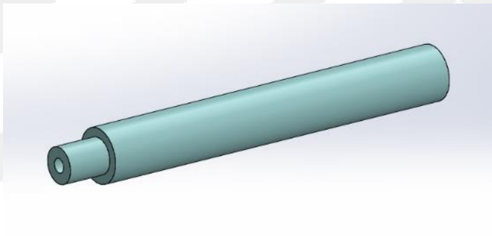

(b)

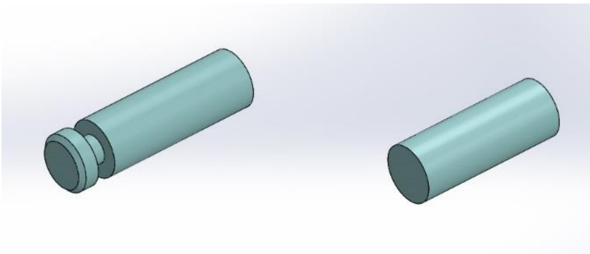

(c)

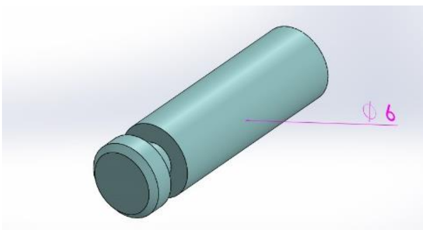

(d)

Figure 4.20: Mover parts (a) Magnet housing (b) The in-connector (c) End parts (d) Piston

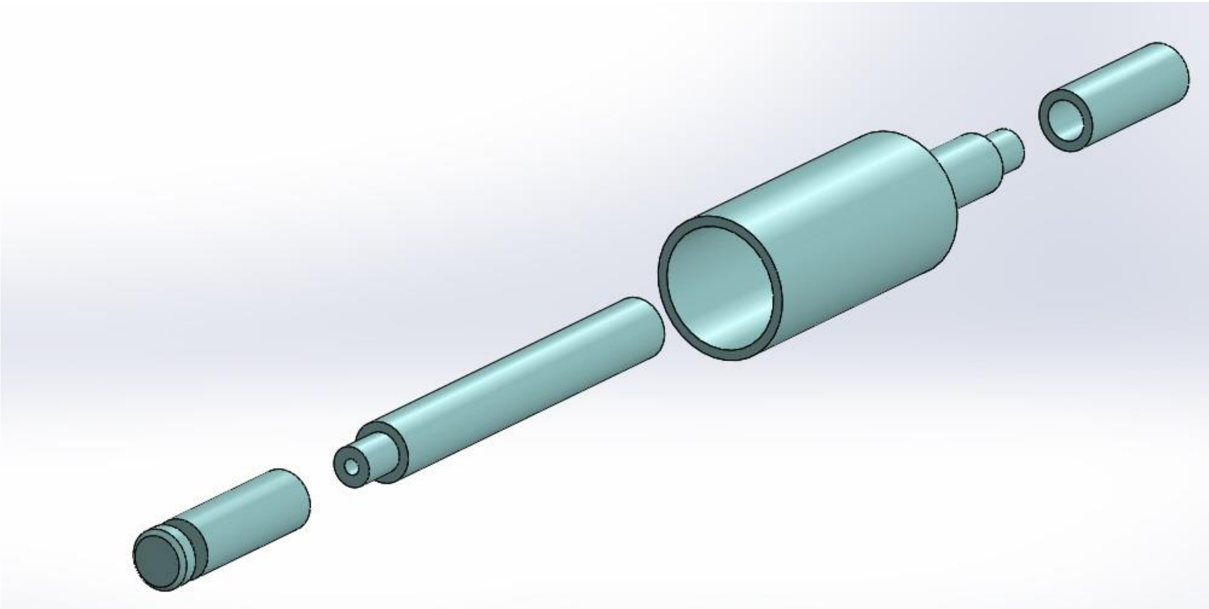

Figure 4.21: Mover assembly

4.5.5 Permanent Magnets

The permanent magnets that are put inside the tube part of the mover are arranged in Halbach array configuration. This configuration results in the magnetic field strengthening on one side and almost elimination on the other, and for a cylindrical configuration this means strengthening on the outer side and weakening in the other. Resulting effect corresponds to a stronger linkage with the coil magnetic field and almost no magnetic flux through the mover, enabling design flexibility such as hollow or non-magnetic movers.

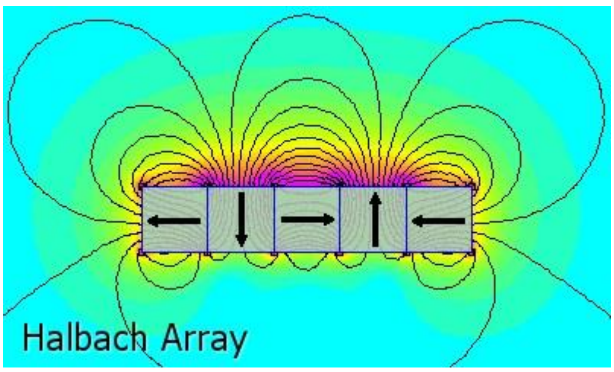

Figure 4.22: Halbach array schematic [38]

In order to generate a Halbach array effect, axially as well as radially magnetized permanent magnets should be utilized. In a tubular topology, the permanent magnets used are ring magnets. As explained in Chapter 2, axial magnetization of ring magnets is a relatively easier endeavor, and in order to obtain a ring magnet that is radially magnetized, the ring magnet is built up from arc shaped magnets that are individually magnetized through their diameter. The axially magnetized ring magnets have an inner diameter of 6 mm, and outer diameter of 12 mm, with a thickness of 3 mm. The radially magnetized arc magnets are 60^0 arcs with the same inner diameter, outer diameter and thickness, so six of them make up a complete ring. The schematic of the permanent magnet assembly is given in Figure 4.23.

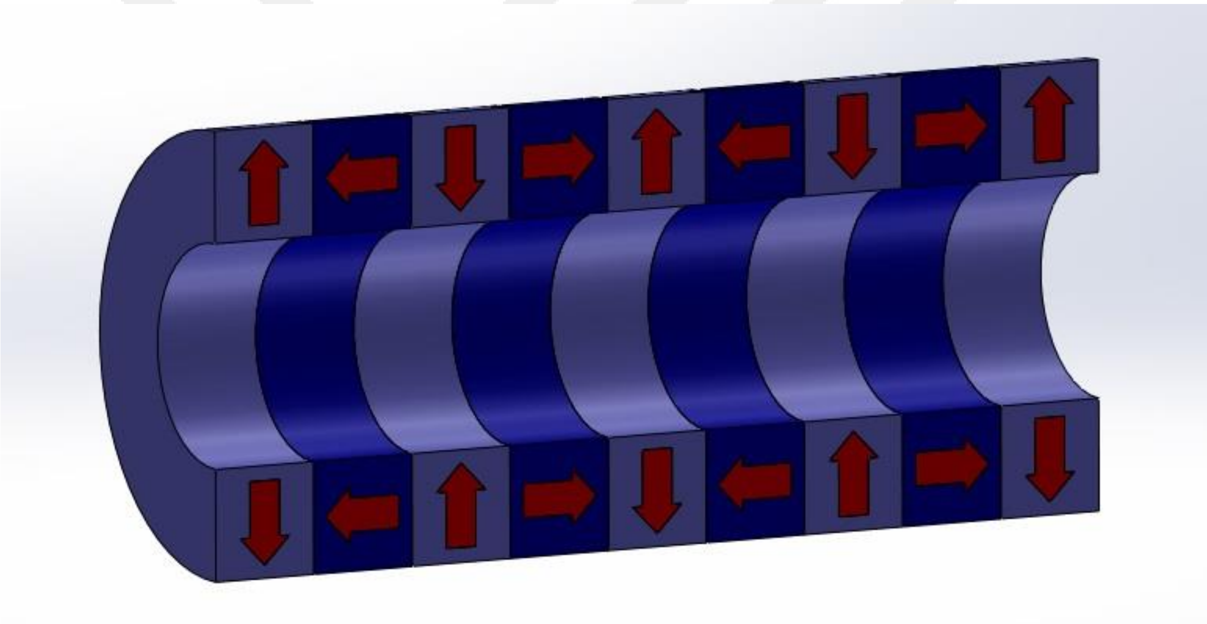

Figure 4.23: Permanent magnets placed on the mover in Halbach array configuration

4.5.6 Flexures

Disc shaped flexures serve as both resonant springs and linear bearing for the mover. The idea behind this arrangement is that a thin disc shaped metal is given grooves of certain shapes to produce flexure spring action. The deformation is within the elastic limits of the flexure, so such bearings are suitable only for operations of low load and displacement.

For the selection of accurate flexure type, [39] was used as a reference. Here various flexure bearing geometries were investigated in terms of maximum stresses appearing at the same loading conditions. The investigated geometries were,

- Helical arm,
- 6 legs Archimedes spiral,
- Tangential 3 legs,
- Staggered arm,
- 3 legs Archimedes spiral.

Each geometry has a thickness of 0.3 mm, an outer diameter of 69 mm, and twelve 6 mm holes for clamping along the periphery. The performed ANSYS analysis suggests helical arm geometry to be superior to the others in terms of stress under the same load conditions. The results are compared in Figure 4.24 to 4.28.

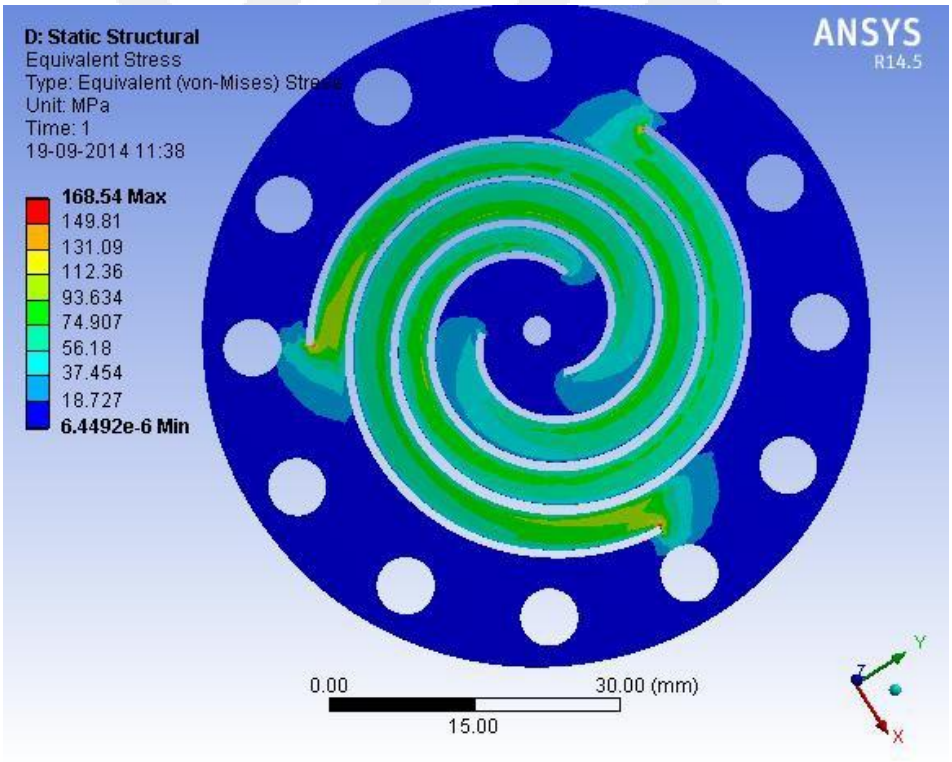

Figure 4.24: Helical arm geometry results [39]

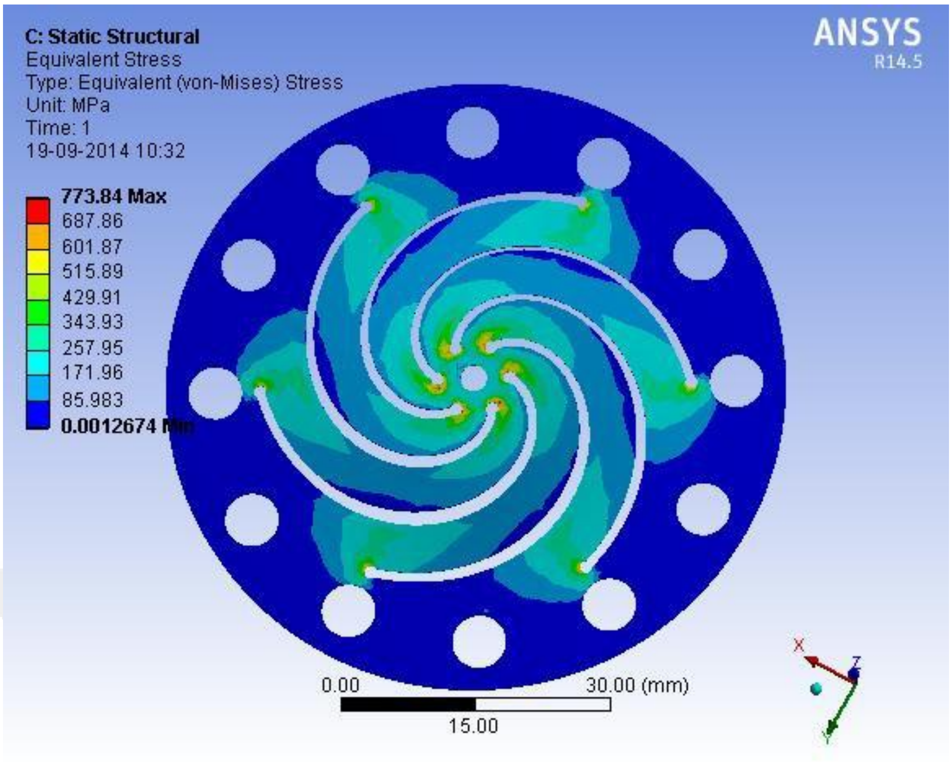

Figure 4.25: 6 legs Archimedes spiral geometry results [39]

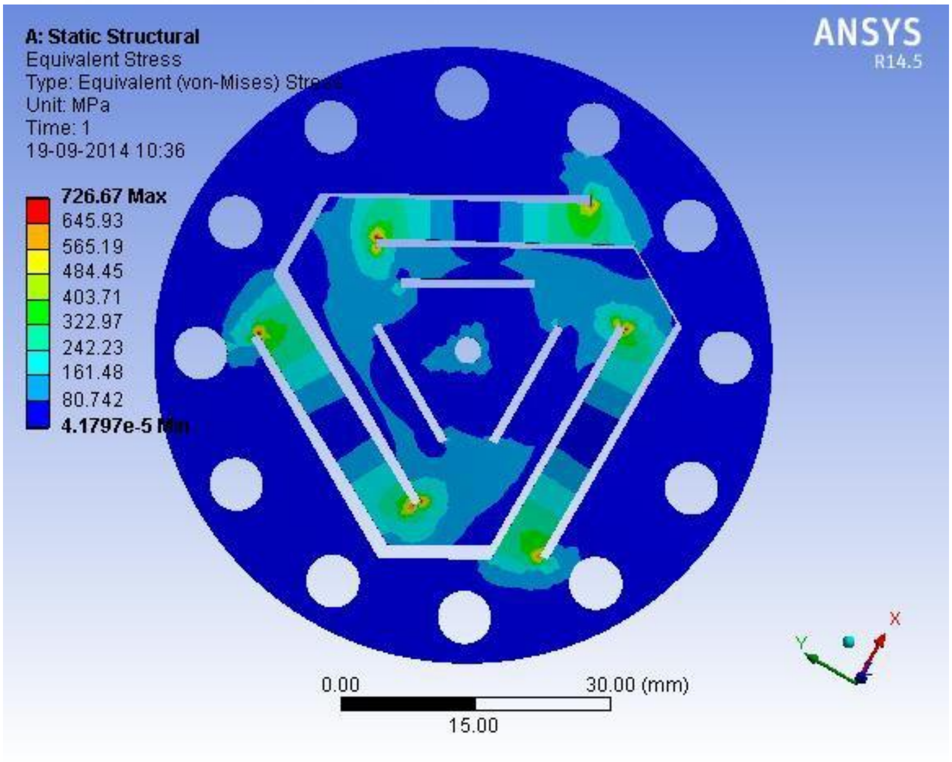

Figure 4.26: Tangential 3 legs geometry results [39]

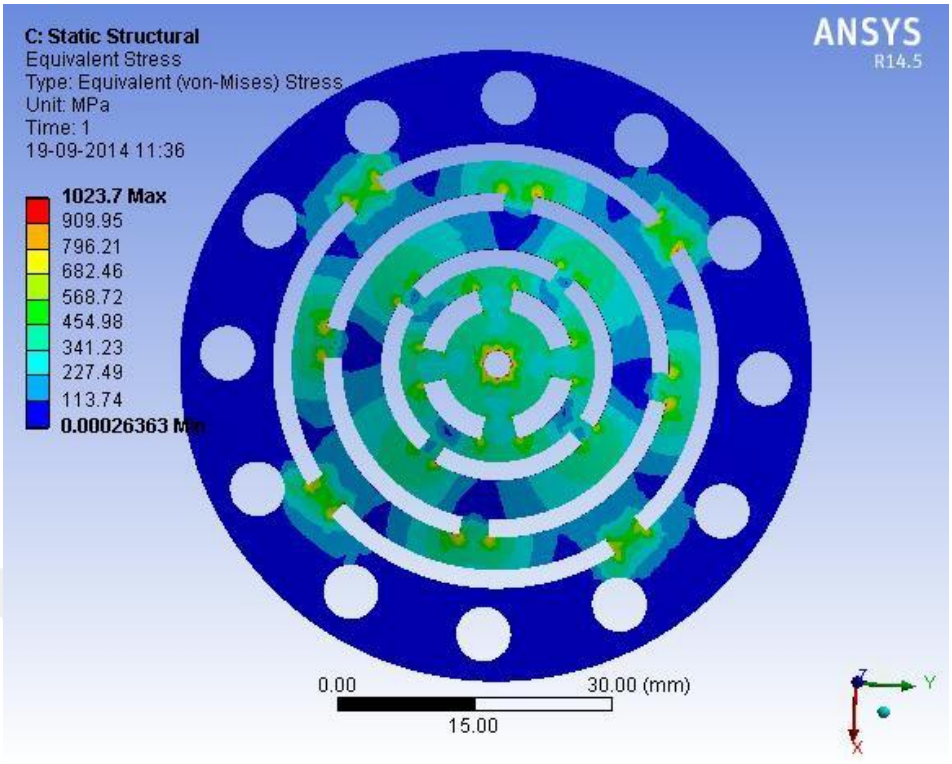

Figure 4.27: Staggered arm geometry results [39]

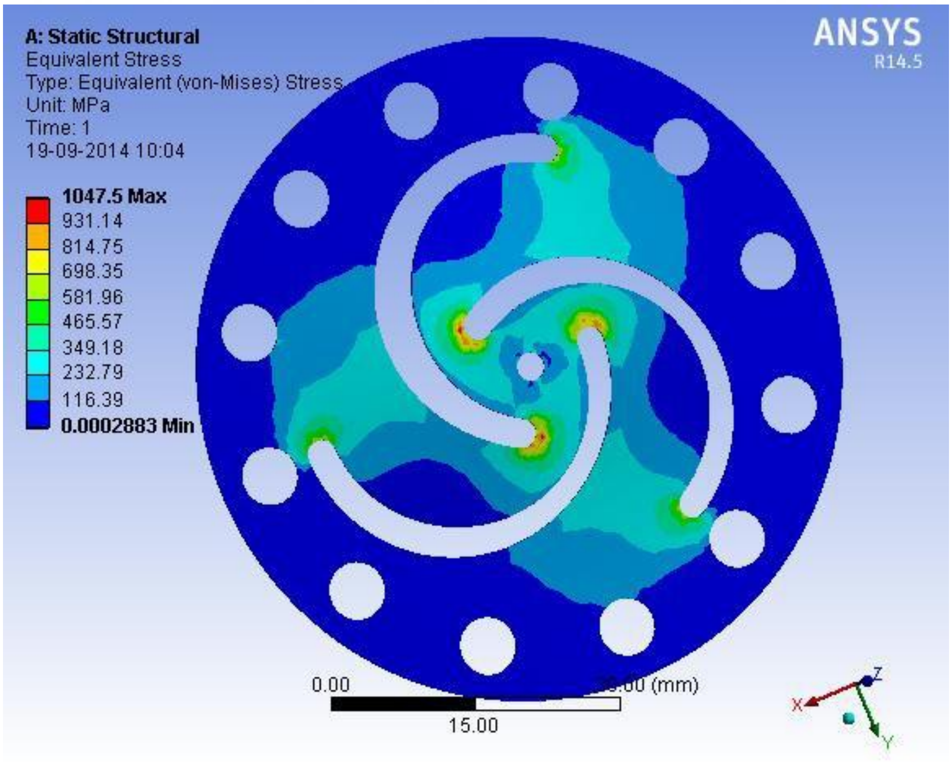

Figure 4.28: 3 legs Archimedes spiral geometry results [39]

Thus, for the miniature linear oscillatory motor a helical arm geometry was selected. The thickness of each flexure is 0.2 mm with the outer diameter of 40 mm and six 2 mm holes along the periphery for clamping. Laser engraving on stainless steel plates of 0.2 mm thickness is applied in order to produce the grooves. The CAD model is given in Figure 4.29.

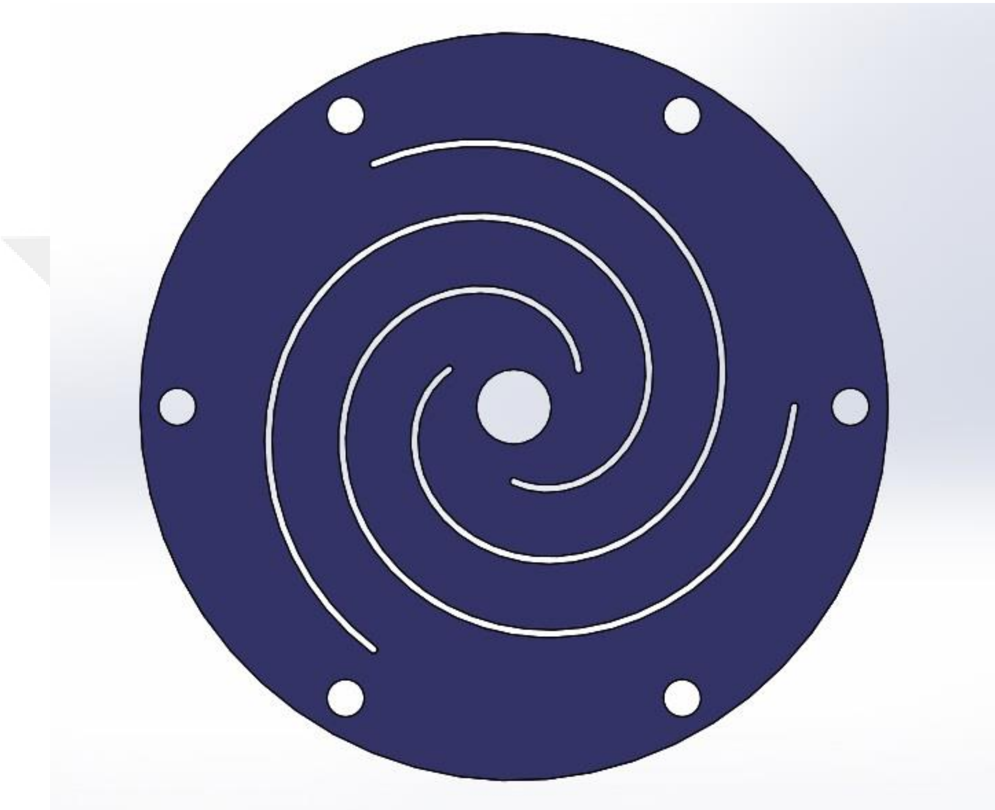

Figure 4.29: Flexure geometry used for the motor

The theoretical stiffness of the flexure geometry was determined using FEA simulation in COMSOL by applying a load in the center and calculating the displacement. The force vs displacement curve given in Figure 4.30 was obtained. The curve suggests an almost linear behavior and by calculating its slope an estimate for the flexure stiffness was obtained, which turns out to be 1.076 N/mm. A stress analysis similar to the one in [39] was conducted to the flexure geometry in COMSOL. The results suggest stress on the flexure to be at acceptable levels (Figure 4.31).

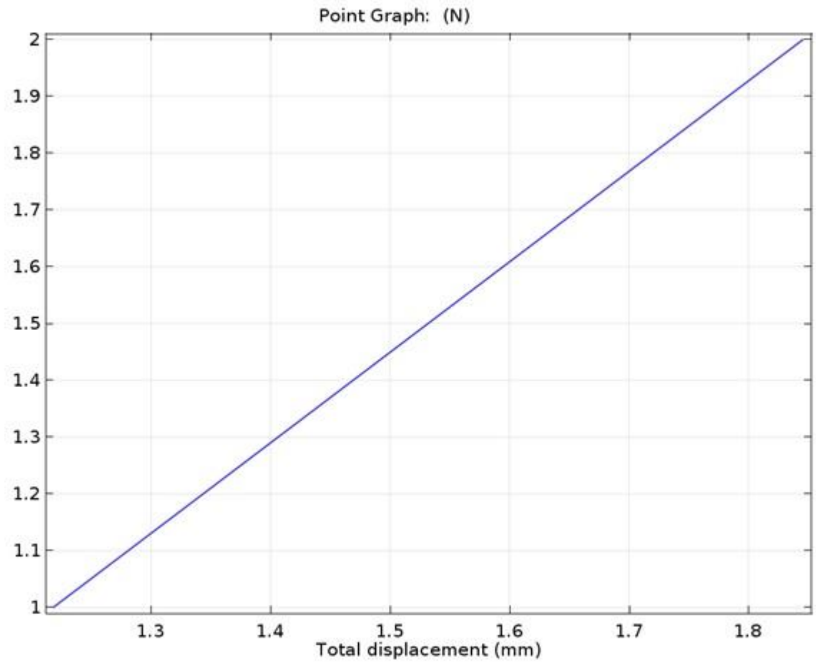

Figure 4.30: Force vs. displacement curve for the flexure obtained in COMSOL

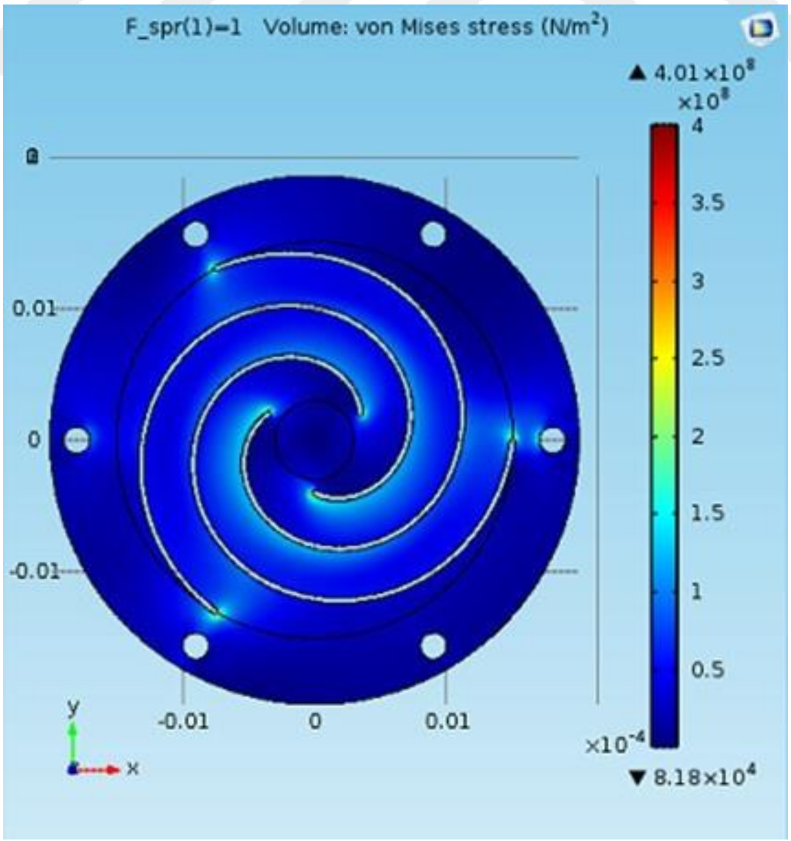

Figure 4.31: Stress analysis for the flexure conducted in COMSOL

The exploded view of the linear oscillatory motor assembly is given in Figure 4.32. There are four flexures in total, two at each side, and by knowing the total mover mass the resonance frequency can be calculated. A detailed analysis of the motor is provided in Chapter 5.

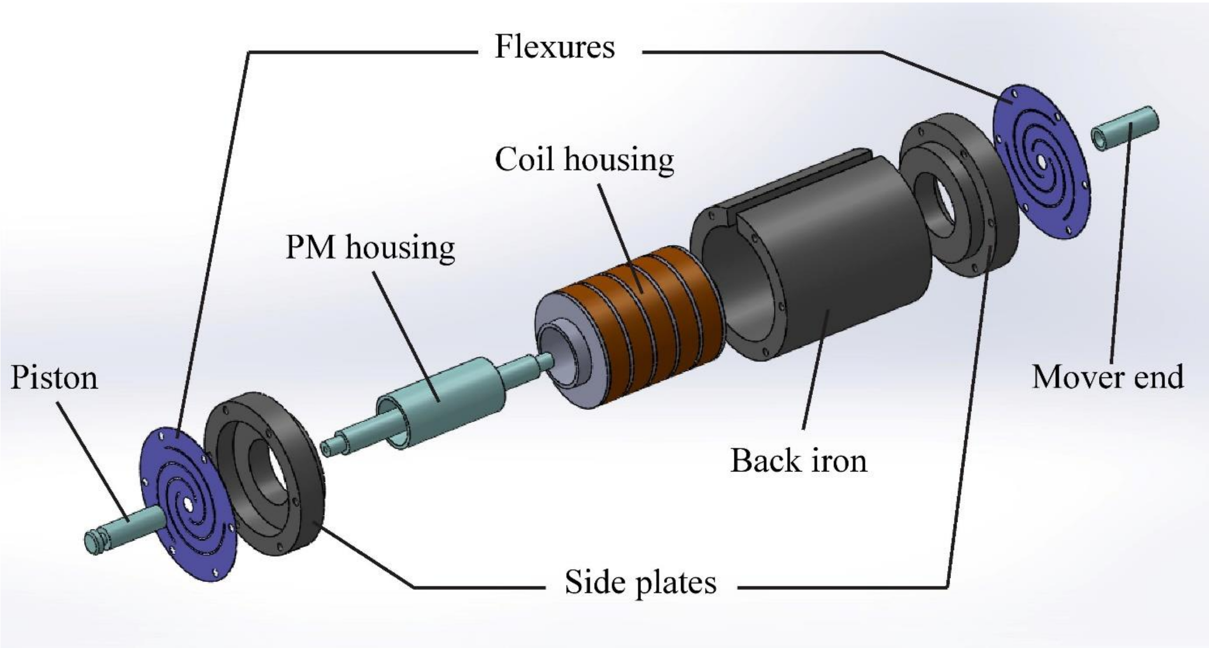

Figure 4.32: Exploded view of the linear oscillatory motor assembly

4.6 Magnetic Circuit Analysis of the Linear Oscillatory Motor

As discussed in the previous section, this kind of actuator operates under the principle of electrodynamic actuation, which means the thrust force and the back-emf generated are the result of the flux appearing in the air gap between the coils and the magnets. In order to define this relationship, a magnetic field analysis is needed, which will be shown next.

The back-emf and the thrust force are both a function of the magnetic flux density generated in the air gap between the coils and the permanent magnets (B_g). In order to come up with an expression for it, the magnetic circuit model will be investigated according to the actuator parameters. The geometric parameters are shown in Figure 4.33.

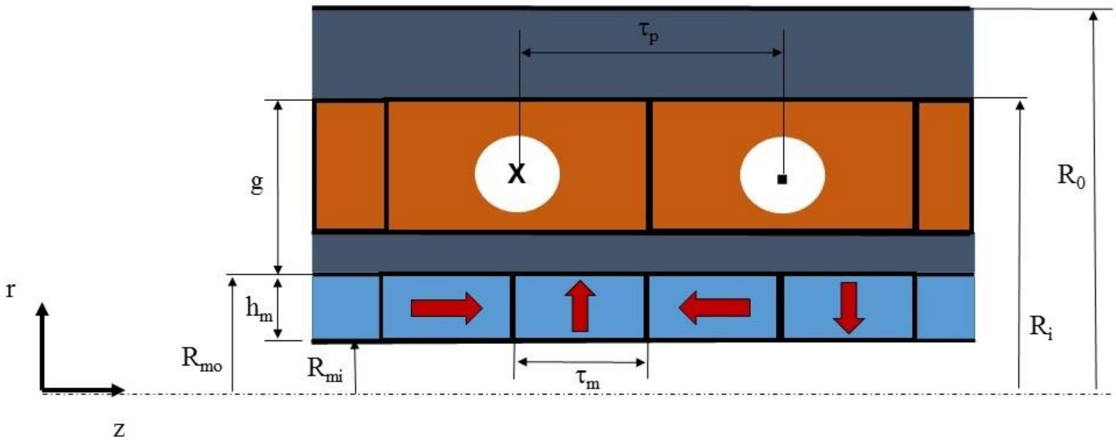

Figure 4.33: Geometric parameters of the linear oscillatory motor

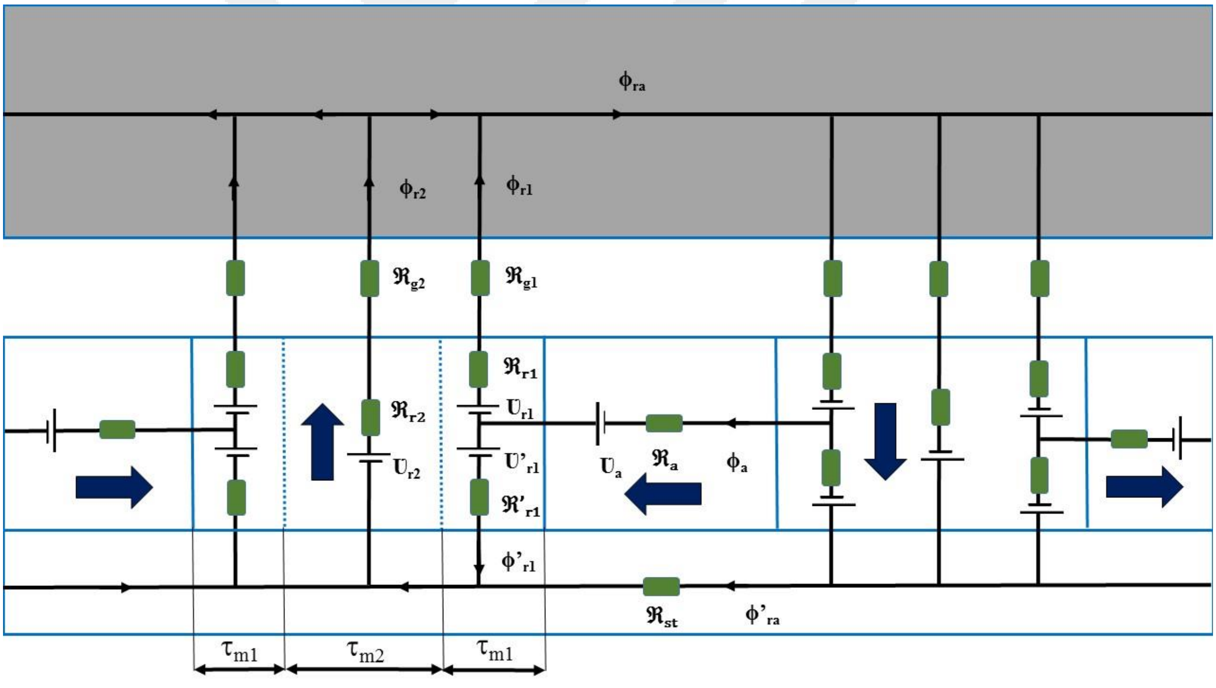

Figure 4.34: Lumped magnetic circuit model

The magnetic circuit for the actuator assembly is given in Figure 4.34. Here the reluctance of the stator back-iron is considered zero. For the magnetic circuit in a Halbach configuration, the approach presented in [40] and [33] will be used. The contribution of the axially magnetized magnets on the radially magnetized ones can be shown as an axial penetration which is calculated by:

$$\tau_{m1} = \frac{{R_{mo}}^2 - (R_{mo} - \alpha h_m)^2}{2R_{mo}} = \frac{(R_{mo} - \alpha h_m)^2 - (R_{mo} - h_m)^2}{2(R_{mo} - h_m)}$$
$$\tau_{m2} = \tau_m - 2\tau_{m1} \tag{4-1}$$

Here, α is the correction factor.

From the circuit, the following relationships can be written:

$$2\mho_{r1} + \mho_a - \Phi_{r1}\left(2\Re_{g1} + 2\Re_{r1}\right) - \Phi_a\Re_a = 0$$
$$2\mho_{r2} - \Phi_{r2}\left(2\Re_{g2} + 2\Re_{r2}\right) - \Phi'_{ra}\Re_{st} = 0$$
$$\mho_a - 2\mho'_{r1} - \Phi_a\Re_a - \Phi'_{r1}2\Re'_{r1} + \Phi'_{ra}\Re_{st} = 0$$
$$\Phi_a = \Phi_{r1} + \Phi'_{r1}$$
$$\Phi'_{ra} = \frac{\Phi_{r2}}{2} - \Phi'_{r1} \tag{4-2}$$

The axial and radial magnet magneto-motive forces are given by

$$\mho_{r1} = H_c\alpha h_m$$
$$\mho_{r2} = H_c h_m$$
$$\mho'_{r1} = H_c(1-\alpha)h_m \tag{4-3}$$
$$\mho_a = H_c\tau_m$$

with $H_c$being the permanent magnet coercivity. The reluctances are given by

$$\Re_{g1} = \frac{g}{\mu_0 2\pi(R_i - g/2)\tau_{m1}}$$
$$\Re_{g2} = \frac{g}{\mu_0 2\pi(R_i - g/2)\tau_{m2}}$$

$$
\begin{aligned}
\Re_{r1} &= \frac{\alpha h_m}{\mu_0 \mu_r 2\pi (R_i - g - \alpha h_m/2)\tau_{m1}} \\
\Re_{r2} &= \frac{h_m}{\mu_0 \mu_r 2\pi (R_i - g - h_m/2)\tau_{m2}} \\
\Re'_{r1} &= \frac{(1-\alpha) h_m}{\mu_0 \mu_r 2\pi (R_i - g - (1-\alpha) h_m/2)\tau_{m1}} \\
\Re_a &= \frac{\tau_m}{\mu_0 \mu_r \pi ({R_{mo}}^2 - (R_{mo} - \alpha h_m)^2)} \\
\Re_{st} &= \frac{\tau_m + 2\tau_{m1}}{\mu_0 \mu_r \pi {R_{mi}}^2}
\end{aligned}
\tag{4-4}
$$

Using these relationships, the fluxes Φ_{r1} and Φ_{r2} can be calculated which in turn will be used for the calculation of air-gap flux densities B_{g1} and B_{g2} at the axial widths τ_{m1} and τ_{m2} :

$$
\begin{aligned}
B_{g1} &= \frac{\Phi_{r1}}{2\pi \tau_{m1} (R_s - g/2)} \\
B_{g2} &= \frac{\Phi_{r2}}{2\pi \tau_{m2} (R_s - g/2)}
\end{aligned}
\tag{4-5}
$$

Using the air-gap flux density the back-emf and thrust force can be calculated. For a very small displacement Δx the flux linkage is given as

$$\Lambda_{|\Delta x} = 4NB_g 2\pi R_s \Delta x \tag{4-6}$$

where N is the number of turns for each coil. Using the flux linkage the back-emf coefficient is calculated as

$$K = \frac{\Lambda_{|\Delta x}}{\Delta x} = 8\pi N B_g R_s \tag{4-7}$$

Therefore, the back-emf is given as

$$V_{back} = Ku(t) = 8\pi N B_g R_s u(t) \tag{4-8}$$

where $u(t)$ is the velocity. Finally, the thrust force is given as

$$F_{th} = Ki = 8\pi N B_g R_s i \tag{4-9}$$

where i is the current.

The air gap flux density B_g calculated using the reluctance method approach is calculated as 0.47 T, which, at 0.5 A applied current corresponds to a thrust force (F_{th}) of 10.44 N. The thrust force vs applied current graph is given in Figure 4.35.

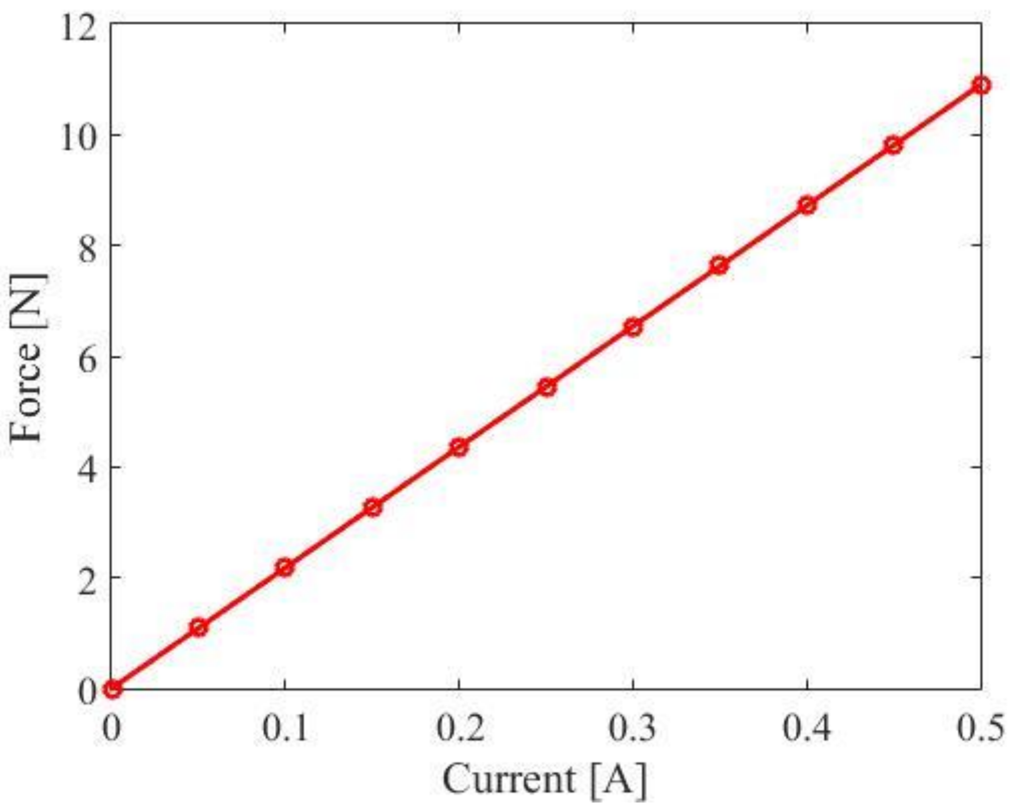

Figure 4.35: Force vs. applied current curve obtained from the reluctance method

4.7 Conclusion

In this chapter, the design parameters of the miniature size linear compressor with its slotless tubular moving magnet linear actuator and the chamber-valve topology were presented. The piston diameter is miniaturized down to 6 mm and not further, because the smallest commercially available valves have a housing diameter of 2.5 mm. After considering other miniature valve types, duckbill valves that serve as check valves are chosen as a pair with one serving as the inlet valve and the other as the outlet valve. The valves provided by miniValve company have a very low cracking pressure at the level of some minibars and leak-tight against reverse flow. This enables fast response.

A slotless multi-pole tubular moving magnet linear motor is selected as the actuator because a slotless configuration eliminates cogging which can be detrimental at miniature sizes. As mentioned in the previous chapter a multi-pole configuration helps with the reduction of leakage flux and fringing effects and produces a good thrust density, for that reason a five pole coil configuration in the stator is selected. The permanent magnets placed in the mover are arranged in a Halbach array configuration in order to increase the flux in the air gap and decrease the flux that is on the mover itself. This self-shielding capability of Halbach magnets enables selection of non-magnetic or hollow mover designs, reducing mover weight for high frequency operations and offering design flexibility.

As mentioned in the previous chapter, the linear oscillatory motor operates at resonance frequency for enhanced efficiency. The most common member utilized to produce a mechanical resonance effect is the mechanical spring. In linear oscillatory motor applications several types of springs, such as compression or extension springs can be employed. One other type is the flexure spring, which also serves as a bearing for the motor. There are many flexure geometries encountered in the literature such as Archimedes spirals, triangular arms, staggered arms or helical arms. For the miniature linear oscillatory motor flexures possessing a helical arm geometry were selected because of their relatively low operating stress behavior. 0.2 mm thick stainless steel sheets were given grooves using laser cutting to produce the desired geometry. Six holes of 2 mm diameter were also cut into the sheet through which the flexures are clamped to the side plates of the stator. Another hole, again of 2 mm diameter was opened at their center where the mover is fastened with the piston and the back-end part, and this way the flexures serve as linear bearings for the mover. Using COMSOL, a finite element analysis was conducted on the flexure geometry to find out the stresses acting and to produce the applied force vs. flexure displacement behavior in order to find an estimate for the stiffness coefficient. A nearly linear behavior was obtained from the curve with a calculated slope of 1.076 N/mm taken as the estimate for the coefficient.

As it will be discussed in the next chapters, the spring coefficient of the flexure is important for the determination of mechanical resonance frequency at which the coils are excited to produce resonant oscillation, producing the same thrust with less pulled current, which in turn increases efficiency.

The next chapter will deal with a detailed analytical and experimental analysis of the miniature linear oscillatory motor that is used as the actuator in the miniature linear compressor prototype. Its design parameters will be revisited and for no load condition the resonance behavior will be demonstrated. In the following chapter the dynamic analysis of the entire compressor with the electromagnetic excitation and the resulting gas compression will be presented. The efficiency of the prototype will be discussed.

Chapter 5

DETAILED ANALYSIS OF THE MINIATURE TUBULAR LINEAR ACTUATOR EXCITED AT RESONANCE FREQUENCY

5.1 Introduction

In this section a detailed analysis for the magnetic flux and thrust generation along with the resonance behavior of the miniature-size resonant moving-magnet linear actuator design to be used in miniature linear compressor applications is demonstrated. The miniature linear actuator has a slotless stator and a tubular topology. It utilizes moving magnets in which the magnets are lined up in the Halbach array structure. Finite element and analytical analyses of the actuator are performed to determine the flux density and thrust force. Experimental thrust force behavior at the resonant frequency is determined. It is shown that the FEM simulation, analytical and experimental results agree with each other.

5.2 Literature Review

Linear actuators are very attractive components to be used for compressor applications where they provide better efficiency, better dynamic performance, and smoother operation. These devices may operate under two different mechanisms [41]. The first one is electromagnetic actuation, i.e. the principle of magnetic field alignment, where the magnetic field generated by the stator makes the iron translator move to the position where the flux lines are aligned. The second mechanism is electrodynamic actuation where the magnetic field in one component interacts with the other under Ampere’s force law. Here there might be three configurations; in the first one both the stator and the mover have coils, so they have both their fields generated electromagnetically, in the second one there are coils on the stator and permanent magnets on the mover, and in the third one the magnets are on the stator and the coils on the mover. The moving magnet type is superior to the others in terms of low inertia, thrust density, fast response and loss in energy [41].

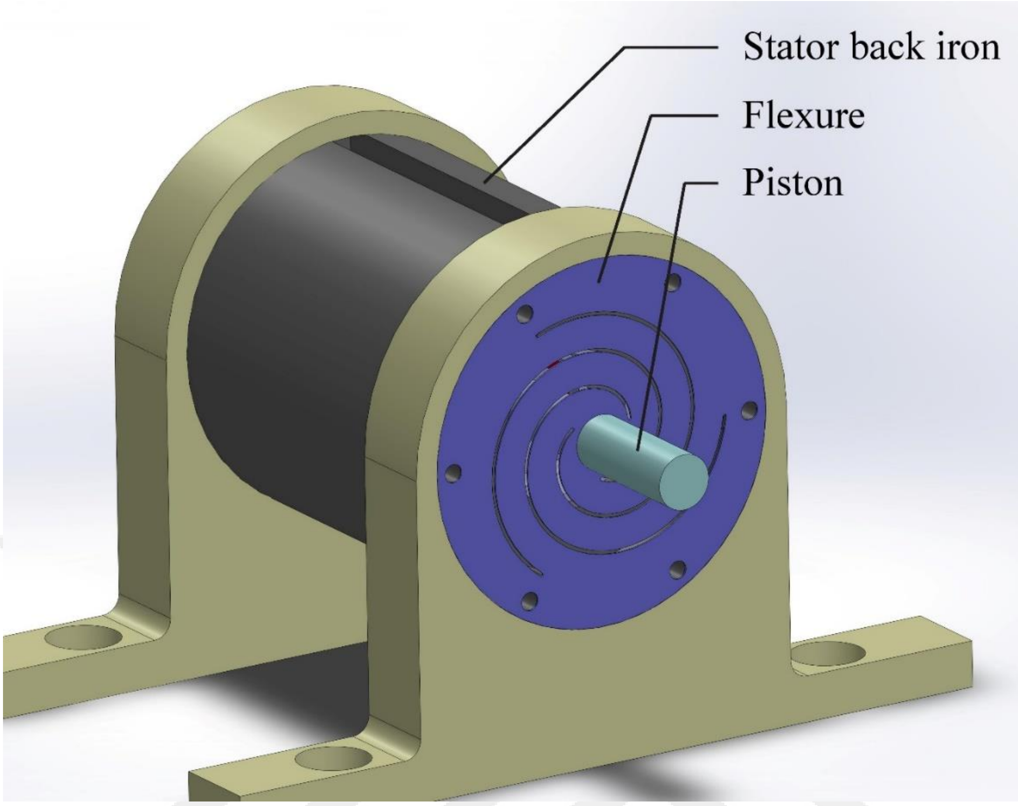

(a)

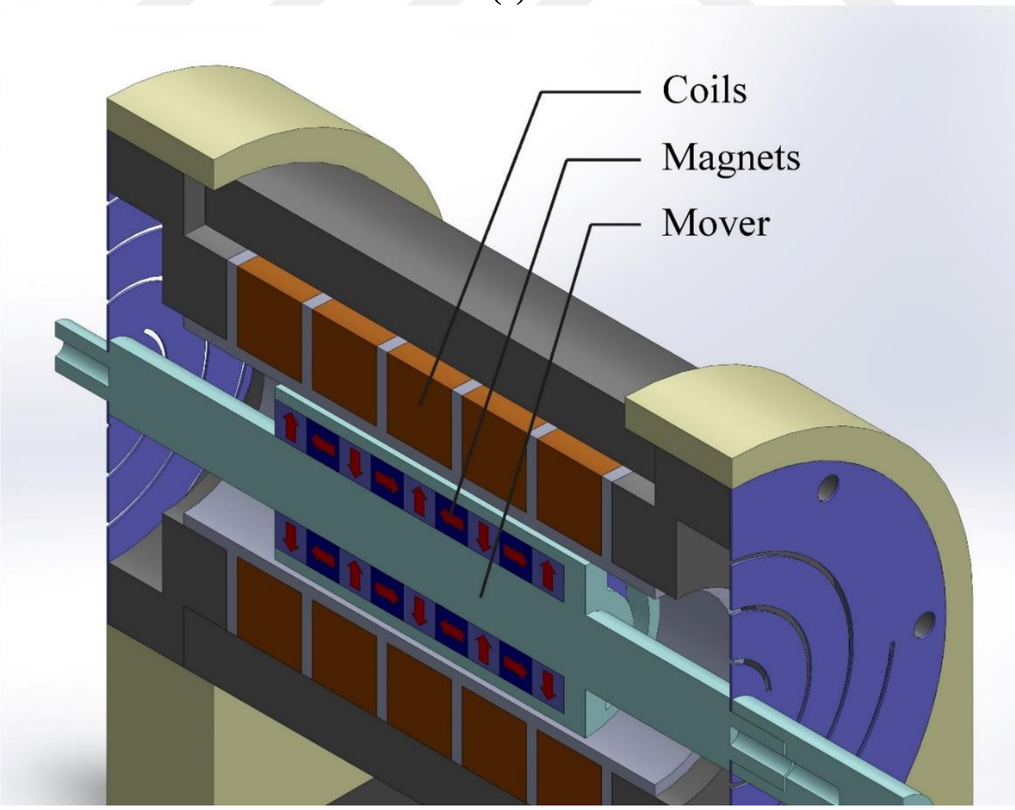

(b)

Figure 5.1: (a) Assembly of the proposed actuator (b) The cross-sectional view of the actuator

In this study, the actuators investigated are moving magnet type, i.e. they have permanent magnets in their mover. For its compactness and ease of assembly, the tubular configuration is selected. It is of oscillating nature because it is to be used for miniature linear compressor applications. In the literature, there have been several tubular linear oscillating permanent magnet actuator designs. [42] developed a six phase linear pulse motor as linear oscillatory actuator where the six phase operation is reported to provide thrust regulation and therefore a stable operation. This actuator was proposed for the assisting of an artificial heart. [43] designed a single winding oscillatory actuator with a large stroke and low-frequency operation and made an improvement on its starting thrust characteristics for artificial heart application in [44]. [45] laid out a design methodology for moving-magnet actuators and investigated selection criteria for a cryocooler with given parameters. [46] applied a design similar to [43] to a liquid hydrogen pump with a slightly larger operating frequency. [47] developed another single winding moving magnet linear actuator and investigated its dynamic performance for gas compression. [48] laid out a general framework for the design and analysis of linear permanent magnet machines, where analytical and simulation analyses were performed for different slotted and slotless topologies. [49] investigates the influence of magnetization pattern on a linear actuator with two-pole coils and radially magnetized moving magnets where the employment of radially magnetized magnets composed of arc segments are compared to a full circle magnet in terms of performance, demonstrating almost full performance for the segmented magnets. [50] did an analytical field and thrust force computation for a slotless multi-pole actuator where radially magnetized magnets are placed on the mover. [51] proposed a Redlich type linear motor for a linear compressor which has 95% efficiency. [52] designed a slotless linear actuator with multiple stator poles, which uses a Halbach array on the mover. Here, arc segments were employed for the radially magnetized magnets. They also investigated the addition of mechanical resonance in the system [54]. [53] developed a single coil, slotted type linear actuator and applied lumped magnetic circuit model to define the motor constant and investigated its effect on actuator performance. [55] developed a linear oscillatory actuator which employs gas springs and is designed for drilling applications. Thanks to the gas springs high-frequency oscillations and large strokes can be obtained even with a heavy piston. [56] presented a two-pole, slotted type actuator where the performance of two topologies, one being radially magnetized moving magnets and the other quasi-Halbach magnetized are compared.

Here it is reported that the quasi-Halbach magnetized topology shows better performance. Then, [57] did analysis on an E-core interior permanent magnet linear oscillating actuator and in [40] they made an analytical determination of the optimal split ratio of surface mounted, Halbach surface mounted and interior permanent magnet configurations. Apparently, the salient mover structure of the interior magnet actuator greatly contributes to the oscillation by generating a reluctance force. [32] investigated a short-stroke, single phase motor for refrigeration applications. This is a slotted design with Halbach array magnets on the piston and a single pole coil on the stator. Here it is stated that the compressed gas greatly changes the input impedance and is an important design parameter. [58] developed another magnetically-driven actuator for linear compressor application. This is a slotless design with a Halbach array magnet structure which employs active magnetic bearings. [59] starts from a design which uses interior permanent magnets and employs Halbach magnetized magnets instead to report the improvement on the previous design. They employ three arc segments for the radially magnetized magnets with silicon steel placed in-between. Then they use a genetic algorithm to optimize the Halbach array parameters to increase the thrust force while obtaining a lesser volume for the yoke. [60] developed a novel permanent magnet transverse flux machine. Laminations in this actuator are unlike conventional linear actuators and similar to a rotating motor, enabling easy stacking. [64] integrated this actuator in a linear compressor where mechanical springs are used. [33] developed a tubular motor for EHA pump. This is a slotted type actuator with Halbach array magnets on the piston. The employment of Halbach array magnets enables the usage of a hollow piston which reduces mover mass and facilitates the installation of resonant springs. [61] developed a high efficiency 3-phase linear motor for compressor applications which introduced magnetic springs to the design, enabling a more compact design and larger strokes. [62] did an improved design over their previous work in [33], where an improved Halbach array, a nonmagnetic mover and different connection types for stator slots are tried for improved performance. [63] again proposed an improved Halbach structure with dual array and investigated its performance analytically.

The linear actuator presented in this study is a single-phase, tubular, moving magnet actuator intended for miniature size compressor applications. In the next sections, the design will be presented with geometric parameters. Then, a theoretical analysis will be shown for this particular topology from the perspective of generated magnetic field and thrust force. Finally, FEM simulations for the flux density and experimental results for the no load resonance condition will be presented.

5.3 The Actuator Design Revisited

The actuator is a moving magnet type, i.e. the magnets are placed in the mover and coil windings are placed in the stator. The CAD model of the proposed actuator and its cross-sectional view is given in Figure 5.1. In order to counter the radial and cogging forces, especially disturbing at miniature sized configurations, a slotless structure is selected. The coils are wound around an aluminum casing with 5 EM poles present. In order to remedy the diminished thrust force capability due to the slotless stator, N52 grade NdFeB magnets are placed in Halbach configuration on the mover. Each consequent coil is wound in opposite directions to each other so that when a DC current to alternating direction is employed, the coils push and pull the magnetic piston and an oscillatory motion is achieved. There are four flexures in total, two on each side, and they act as bearings as well as springs. Using the spring action the actuator operates at a frequency which matches the mechanical resonant frequency, so that desired displacements can be achieved at lower currents, thereby increasing the efficiency. The geometric parameters of the actuator assembly are given in Table 5.1.

Table 5.1: Linear actuator parameters

Symbol	Quantity	Value
N	Number of turns per coil	200
r_{out}	Stator outer radius	20 mm
r_{in}	Stator inner radius	15 mm
τ_p	EM pole pitch	6 mm
τ_m	PM pole pitch	3 mm
h_m	PM height	3 mm
r_m	PM outer radius	6 mm
r_0	Mover inner radius	3 mm
r_s	Gap outer radius	7 mm

For the piston diameter size, the selected value did not go below 6 mm because this actuator is used for linear compressor application and the smallest commercially available valves have a seating diameter of 2.5 mm. The Halbach configured magnet assembly consists of axially and radially magnetized magnets with 12 mm outer and 6 mm inner diameter with 3 mm thickness. Since it is very difficult to manufacture a full circle radially magnetized magnet, 6 arc-shaped magnets are used in its place. The coil housing is placed inside a steel cover which serves as stator back iron and the flexures are fixed on it. The flexures serve as bearings for the mover which facilitates the assembly of the components and a lot of space in the axial direction is saved, allowing for a more compact design.

As discussed in the previous section, this kind of actuator operates under the principle of electrodynamic actuation, which means the thrust force and the back-emf generated are both due to the flux appearing in the air gap between the coils and the magnets. In order to define this relationship, a magnetic field analysis is needed, which will be shown in the next section.

5.4 Analytical Modeling of Magnetic Fields and Thrust Force

The magnetic field analysis will be done in two parts: the first part will deal with the magnetic field analysis due to the permanent magnets, and the second part will deal with the magnetic fields due to the currents. For the analysis, the approach presented by [50] will be used as the basis. The geometric parameters are shown in Figure 5.2.

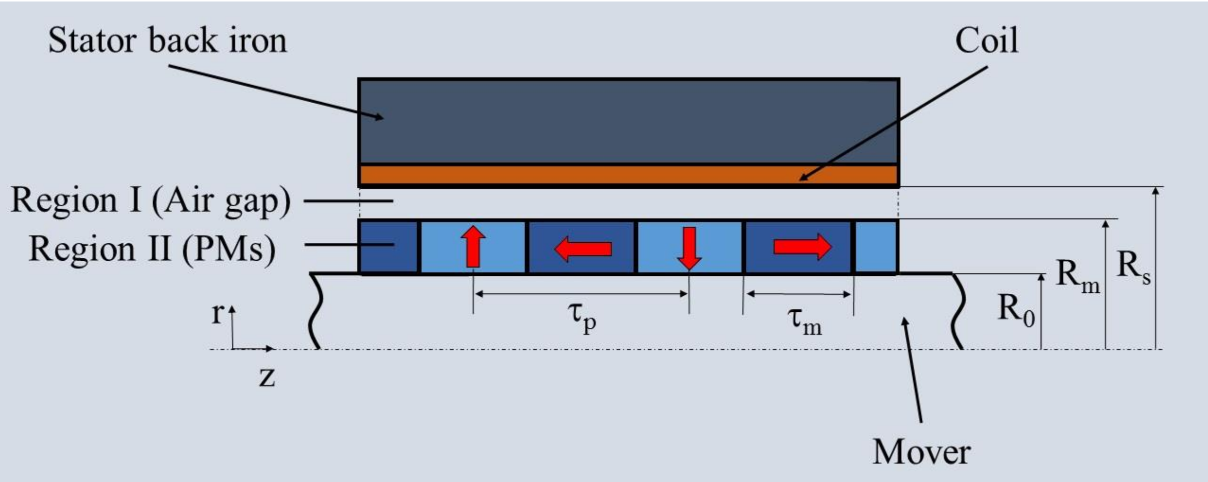

Figure 5.2: Schematic structure of the linear actuator for the analytical model

For the permanent magnet field analysis, infinite iron permeability and infinite motor length will be assumed. As seen from the figure, there are two regions, region I which is comprised of the air gap and region II which is comprised of the permanent magnets. For these two regions the magnetic field equations can be written as:

$$\nabla^2 \boldsymbol{A} = 0 \qquad \text{(Region I)}$$
$$\nabla^2 \boldsymbol{A} = -\mu_0 \nabla \times \boldsymbol{M} \qquad \text{(Region II)} \qquad (5\text{-}1)$$

Here, $\boldsymbol{A}$ is the magnetic potential defined as $\nabla \times \boldsymbol{A} = \boldsymbol{B}$, and $\boldsymbol{M}$ is the magnetization which is null in region I and in region II it can be expressed in terms of radial and axial components as:

$$\boldsymbol{M} = \boldsymbol{M_r} + \boldsymbol{M_z} \qquad (5\text{-}2)$$

The radial and axial components can be expressed by Fourier series:

$$M_r(z) = \sum_{n=1,3,5,\dots}^{\infty} M_{nr} \sin(k_n z)$$
$$M_z(z) = \sum_{n=1,3,5,\dots}^{\infty} M_{nz} \cos(k_n z) \qquad (5\text{-}3)$$

where

$$M_{nr} = \frac{4B_{rem}}{n\pi\mu_0} \sin(\frac{n\pi}{2}) \sin(\frac{n\pi}{4})$$
$$M_{nz} = \frac{4B_{rem}}{n\pi\mu_0} \sin(\frac{n\pi}{4}) \qquad (5\text{-}4)$$

with B_{rem}being the remanent flux density and $k_n = n\pi/\tau_p$ with τ_p being the pole pitch.

The equations given in (1) are Poisson’s equations which have both the same type of homogenous solution of the form

$$A_h^I(r,z) = \sum_{n=1,3,5,\dots}^{\infty} [a_n^I I_o(k_n r) + b_n^I K_o(k_n r)] \cdot [c_n^I sin(k_n z) + d_n^I cos(k_n z)]$$
$$A_h^{II}(r,z) = \sum_{n=1,3,5,\dots}^{\infty} [a_n^{II} I_o(k_n r) + b_n^{II} K_o(k_n r)] \cdot [c_n^{II} sin(k_n z) + d_n^{II} cos(k_n z)] \tag{5-5}$$

Here, I_0 and K_0 are the modified Bessel functions of zero order, of the first and second kind, respectively. The coefficients a_n^I, b_n^I, c_n^I, d_n^I, a_n^{II}, b_n^{II}, c_n^{II}, d_n^{II} are determined from the boundary conditions.

In addition to the homogeneous solution, region II should have a particular solution A_p^{II}, however this does not exist in explicit form. Using the approximation approach presented in [10], the following expression is found for the particular solution:

$$A_p^{II}(z) = -2c_2 \sum_{n=1,3,5,\dots}^{\infty} M_{nr} \frac{{\tau_p}^2}{n^2\pi^2} \sin(k_n z) \tag{5-6}$$

and the following boundary conditions

$$\begin{aligned} H_z^{II}(r_0,z) &= 0 \\ H_z^{II}(r_m,z) &= H_z^I(r_m,z) \\ B_r^{II}(r_m,z) &= B_r^I(r_m,z) \\ H_z^I(r_s,z) &= 0 \end{aligned} \tag{5-7}$$

lead to the following solutions for flux density in both regions:

$$H_z^I(r,z) = \sum_{n=1,3,5,\dots}^{\infty} k_n[-A_n^I I_0(k_n r) - B_n^I K_0(k_n r)]\cos(k_n z)$$

$$H_z^{II}(r,z) = \sum_{n=1,3,5,\dots}^{\infty} k_n[-A_n^{II} I_0(k_n r) - B_n^{II} K_0(k_n r) + \frac{2c_2 M_{nr}}{{k_n}^2}]\cos(k_n z)$$

$$B_r^I(r,z) = \mu_0 \sum_{n=1,3,5,\dots}^{\infty} k_n[-A_n^I I_1(k_n r) + B_n^I K_1(k_n r)]\sin(k_n z)$$

$$B_r^{II}(r,z) = \mu_0\mu_r \sum_{n=1,3,5,\dots}^{\infty} k_n \left[-A_n^{II} I_1(k_n r) - B_n^{II} K_1(k_n r) + (\frac{c_1}{r} + c_2 r)\frac{M_{nr}}{k_n}\right] \sin(k_n z) \tag{5-8}$$

Here I_1 and K_1 are the modified Bessel functions of first order, of first and second kind respectively. The coefficients c_1 and c_2 are given as

$$c_1 = \frac{r_0 r_m}{r_0 + r_m}$$
$$c_2 = \frac{1}{r_0 + r_m} \tag{5-9}$$

The coefficients $A_n^I = a_n^I c_n^I$, $B_n^I = b_n^I c_n^I$, $A_n^{II} = a_n^{II} c_n^{II}$, $B_n^{II} = b_n^{II} c_n^{II}$ are given as

$$A_n^I = a_n^I c_n^I = \alpha_n^I B_n^I$$
$$B_n^I = b_n^I c_n^I = \frac{SX_{01}P + U[K_0(\omega_n r_m) - TI_0(\omega_n r_m)]}{PX_{01}(T + \alpha_n^I)} - \frac{2c_2\widehat{M}_n}{P{\omega_n}^2}$$
$$A_n^{II} = a_n^{II} c_n^{II} = \frac{\alpha_n^I SX_{01} - TU}{X_{01}(T + \alpha_n^I)} \tag{5-11}$$
$$B_n^{II} = b_n^{II} c_n^{II} = \frac{SX_{01} + U}{X_{01}(T + \alpha_n^I)}$$

where

$$\alpha_n^I = \frac{K_0(\omega_n r_s)}{I_0(\omega_n r_s)}$$
$$P = \alpha_n^I I_0(\omega_n r_m) + K_0(\omega_n r_m)$$
$$Q = \alpha_n^I I_1(\omega_n r_m) - K_1(\omega_n r_m)$$
$$S = \frac{2c_2\widehat{M}_n}{{\omega_n}^2 I_0(\omega_n r_0)} \tag{5-12}$$
$$T = \frac{K_0(\omega_n r_0)}{I_0(\omega_n r_0)}$$

$$U = \frac{\widehat{M}_n}{\omega_n}\left(\frac{2c_2Q}{\omega_n} - P\right)$$

$$X_{01} = K_0(\omega_n r_m)I_1(\omega_n r_m) + K_1(\omega_n r_m)I_0(\omega_n r_m)$$

For the analysis of the magnetic fields due to the currents, the electric current at the EM poles is assumed to be on an infinitesimally thin surface on the interior surface at $r = r_s$. The current density $\boldsymbol{J}$ has only the azimuthal component $J_\theta(z)$ which can be expressed as

$$J_\theta(z) = \sum_{n=1,3,5,\dots}^{\infty} J_n sin(k_n z) \tag{5-13}$$

with $J_n = 4N_s i/n\pi\tau_p$, N_s being the number of conductors per pole and i the flowing current. The following boundary condition holds:

$$H_z^I(r_s, z) = J_\theta(z) \tag{5-14}$$

Since the current is assumed to be on an infinitesimally thin surface and the PMs are considered inert, i.e. $\boldsymbol{M} = 0$, region I and II can be considered together and the following solution for magnetic fields are:

$$\begin{aligned} H_z(r,z) &= \sum_{n=1,3,5,\dots}^{\infty} k_n\,[I_o(k_n r) + \beta_n K_0(k_n r)]\gamma_n J_n \sin(k_n z) \\ B_r(r,z) &= \mu_0 \sum_{n=1,3,5,\dots}^{\infty} k_n\,[-I_1(k_n r) + \beta_n K_1(k_n r)]\gamma_n J_n \cos(k_n z) \end{aligned} \tag{5-15}$$

with the coefficients β_n and γ_n given as

$$\begin{aligned} \beta_n &= -\frac{I_o(k_n r_0)}{K_o(k_n r_0)} \\ \gamma_n &= \frac{1}{k_n[I_0(k_n r_s) + \beta_n K_0(k_n r_s)]} \end{aligned} \tag{5-16}$$

The axial thrust force appears due to the interaction of PMs' magnetic flux and the current density and is calculated as

$$dF_z(z) = -2\pi r_s J_\theta(z) B_r^I(r_s, z) dz \tag{5-17}$$

Integrating this along the motor length F_z is obtained which is on the current sheet. The thrust per pole on the mover F_m is opposite to this. So, for F_m the following solution is obtained:

$$F_m = \sum_{n=1,3,5,\dots}^{\infty} 8\pi r_s \frac{N_s}{\tau_p} \mu_0 [-A_n^I I_1(k_n r_s) + B_n^I K_1(k_n r_s)] \cos(k_n z_c) i \tag{5-18}$$

5.5 FEM Simulation

Using FEM analysis, a simulation was conducted in order to find the flux density distribution and thrust force for the given assembly parameters. The FEM analysis was conducted as a 2D axisymmetric model using Comsol Multiphysics. After applying material properties to each respective zone, each permanent magnet is defined as a separate zone assigning them a remanent flux density of 1.43 T in their respective axial and radial magnetization directions. The corresponding B-H curves for NdFeB magnets are also applied under material properties. Once the material assigning is done, a user-controlled mesh is applied where zones with lesser sharp corners and larger dimensions coarser meshes and zones with smaller dimensions finer meshes are assigned.

The radial flux densities due to the PMs are compared in Figure 5.3 to 5.5 for both analytical and FEM results.

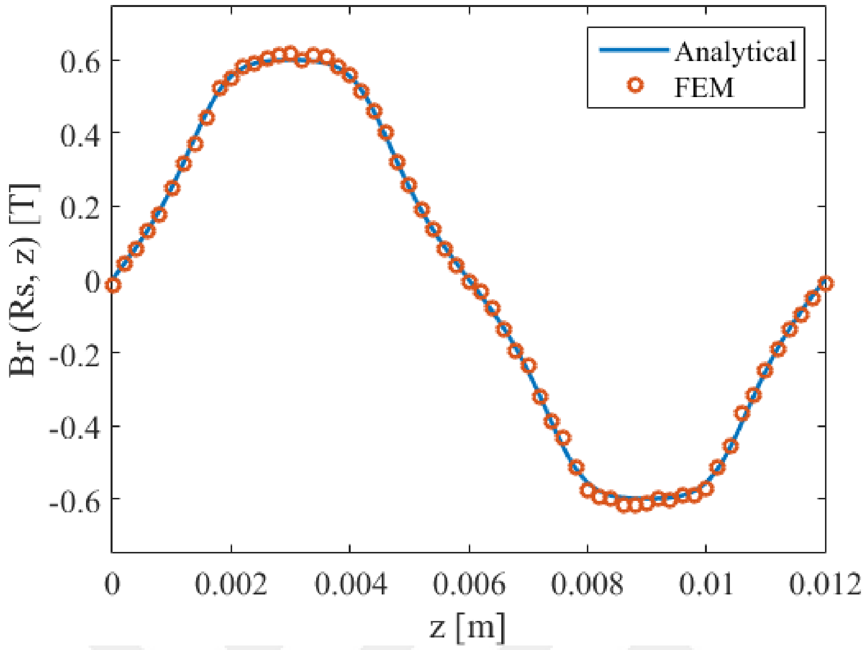

Figure 5.3: Radial flux densities due to the PMs at the gap outer radius ($r = R_s$)

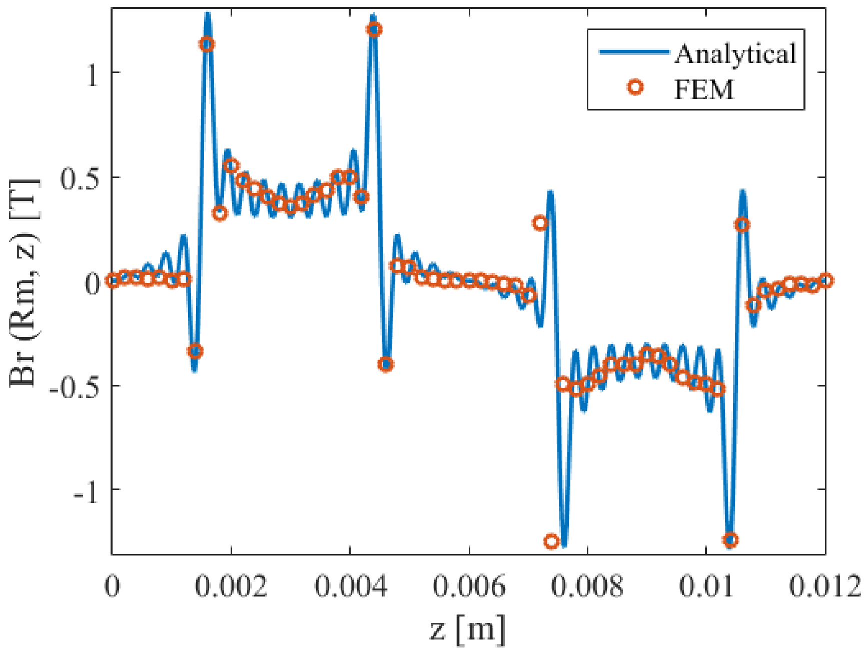

Figure 5.4: Radial flux densities due to the PMs at the PM outer radius ($r = R_m$)

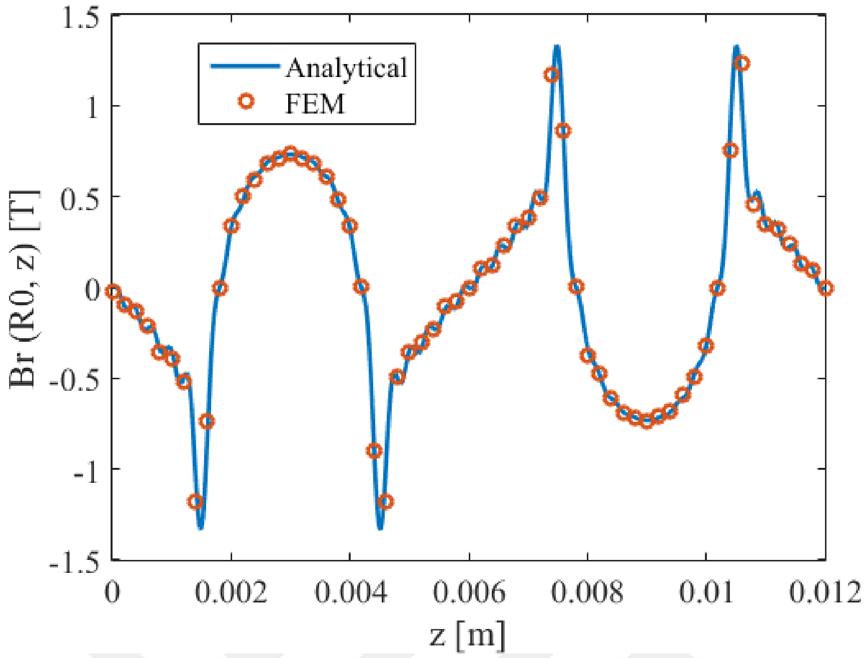

Figure 5.5: Radial flux densities due to the PMs at the mover inner radius ($r = R_0$)

For an applied current of 0.5 A, the thrust force per pole is compared in Figure 5.6 for analytical and FEM cases.

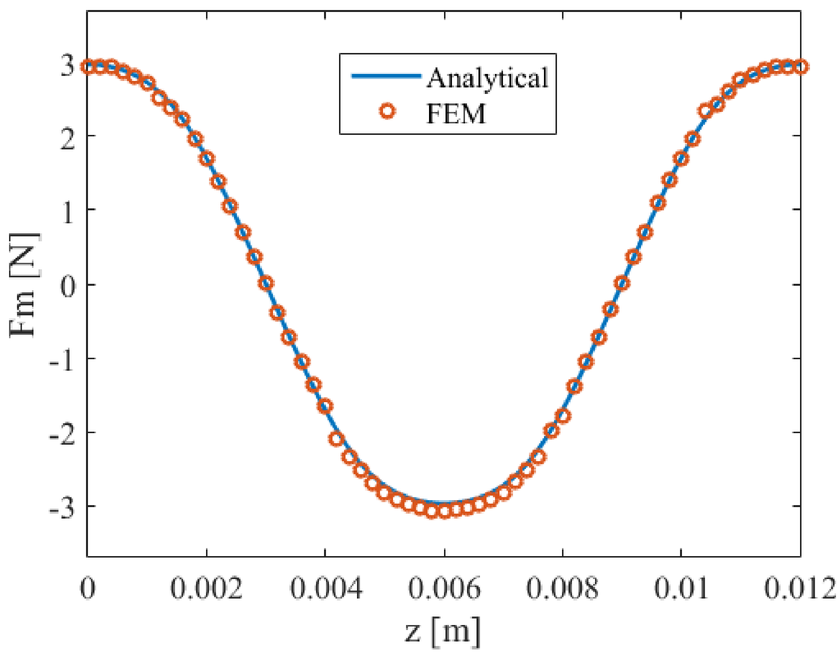

Figure 5.6: Thrust force on the mover for 0.5 A

5.6 Experimental Setup

According to the geometric parameters given in Section 5.3, a prototype moving magnet linear actuator was manufactured.

The 6 mm piston size was a limiting factor for the miniaturization due to the valve sizes used in the compressor. In order to use a current output ranging around and not exceeding 0.5 A, a 26 AWG wire is employed with 200 windings at each pole (5 poles in total). The total length of the actuator is 58 mm with an overall diameter of 40 mm. The actuator is driven with an H-bridge driver using DC current. A mini-dynamometer is used to measure the force output and a laser displacement sensor is used to measure the displacement generated by the oscillatory motion. The entire test setup can be seen in Figure 5.7.

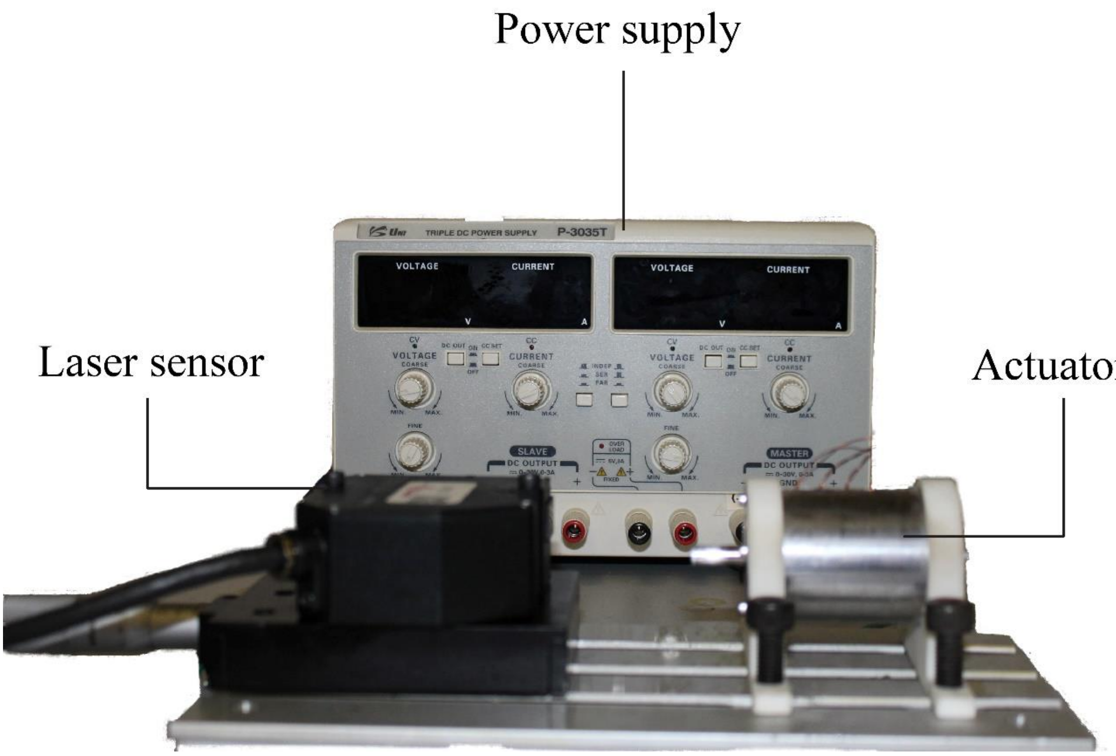

Figure 5.7: Test setup for the miniature linear actuator

In this study, the force output and resonant characteristics are shown for the actuator only.

When considering the entire compressor, the pressure force should also be investigated and the gas has a spring constant, becoming a part of resonance behavior.

The measured average thrust output for given current values is shown in Figure 5.8.

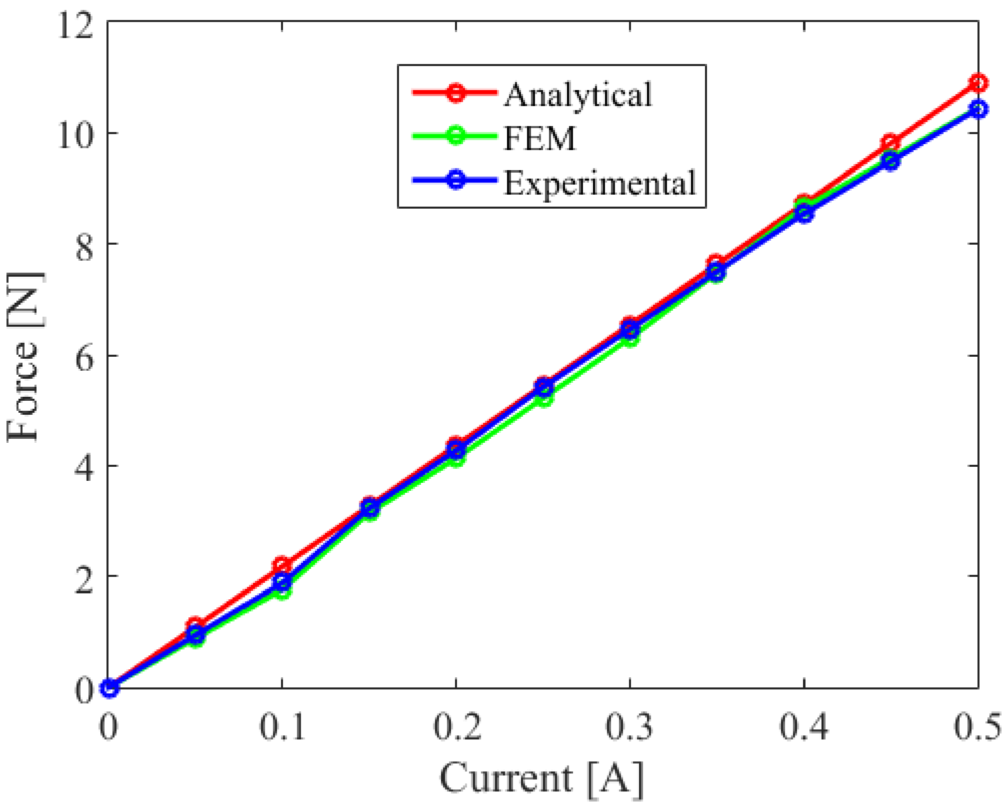

Figure 5.8: Thrust force vs. rated current

Finally, the resonant frequency was investigated in order to operate at a lower current to improve the efficiency. For this matter, the stiffness constant for the flexures were calculated using both simulation and experimentation. The found stiffness for a single flexure (there are four in total) is 1.076 N/mm. The resonant frequency for the no-load condition is given as

$$f_n = (1/2\pi)\sqrt{k/m} \tag{5-19}$$

The piston mass is 54.52 g, therefore the resonant frequency is at around 45 Hz. The actuator is driven at frequencies around these values and the currents generated are plotted against their respective frequencies, which is shown in Figure 5.9. It can be seen that the lowest current value appears at 45 Hz. The measured displacement is the highest at that frequency with $\pm$2mm.

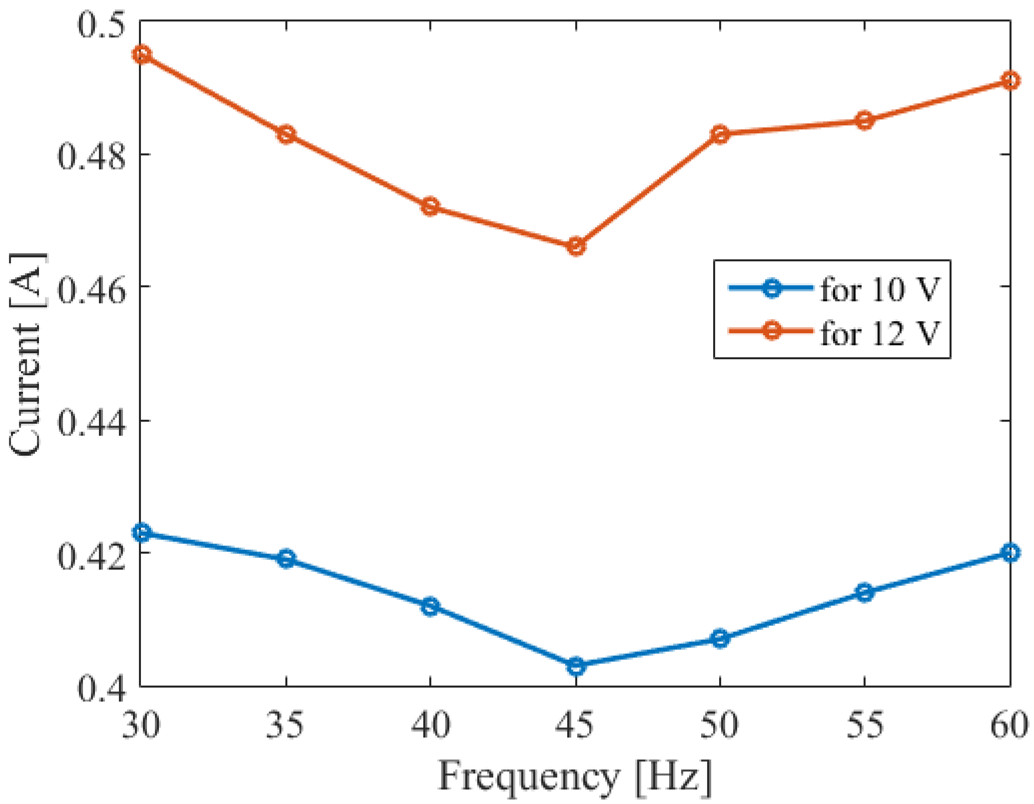

Figure 5.9: Variation of current with frequency for two different voltages

5.7 Conclusion

In this chapter, the miniature size slotless tubular moving magnet linear actuator design was analyzed for miniature linear compressor applications. The configuration is selected to be tubular for increased power factor and compactness. A slotless stator is selected to eliminate cogging forces. Flexure bearings were proposed to enhance the compactness of the design even further. N52 grade NdFeB magnets are employed to cover for the reduced force capabilities associated with slotless designs. The magnets were placed in Halbach array configuration, for self-shielding capability. Using this property, low density, nonmagnetic or hollow mover structures can also be selected to enable design flexibility and the utilization of movers with lower mass. Analytical calculations were presented to find expressions for the back-emf and thrust force. FEM simulation is performed to find the magnetic flux density and thrust force. Finally, the prototype actuator is driven at different frequencies to view the current used up by it, and the force and displacement measurements were conducted. It was shown that at the resonant frequency which is calculated to be 45 Hz the current value is at its lowest. The measured force output is in good agreement with the analytical and FEM simulation results.

Chapter 6

DYNAMIC ANALYSIS OF THE MINIATURE LINEAR COMPRESSOR

6.1 Introduction

In this chapter the components of the novel miniature linear compressor are presented. It consists of a moving-magnet linear actuator which uses flexure springs and a mini chamber and valve assembly. The analytical model for the system dynamics for such an actuator is presented and this model is compared with the experimental results. It is shown that the best efficiency for the compressor is achieved at the natural frequency, which is investigated through experimental means. Also shown is that, at resonance, 80.4% electrical efficiency is achieved.

6.2 Literature Review

Linear compressors offer many advantages over conventional compressors, where for the conventional case the crank mechanism that is usually employed to convert rotational motion to reciprocating motion introduces additional friction to the system, thereby reducing the efficiency. Linear compressors are not subject to this problem because the motion generated by the actuator is already a reciprocating one, thus the need for a conversion mechanism is eliminated. This also means that the entire assembly consists of less parts in total, which in turn leads to a more compact design. Moreover, the employment of linear actuators leads the way to efficient stroke control methods.

While linear compressor technology is not new, the miniature linear compressor is a recent favorite. The aforementioned compactness in linear compressor design combined with the smallness in scale makes this type of compressor a very interesting candidate for many practical applications, for example in the cooling of electronic equipment or in building mini refrigerators.

Linear actuators can come as several types. The most commonly used type for linear compressor applications is the electromagnetic actuator. However, different types such as electrostatically actuated ones can also be encountered. For example, the compressor introduced by [10] employed one such actuator, which is intended for miniature-scale use like the one presented in this article. [65] performed a resonant frequency analysis for the Stirling cryocooler, which is a very commonly encountered type with a moving magnet actuator. Here simulation and experiment results were presented to show that the resonant frequency for moving magnet case depends on the spring coefficient of the mechanical springs, the gas and the magnets, and the mover mass, whereas for the moving coil case it depends on the spring coefficient of the mechanical spring and gas and the mover mass. [11] introduced a miniature linear compressor intended for electronics cooling applications. Aside from the linear motor and the mechanical springs the compressor is custom made with an appropriate valve assembly. Then they improved on their model using a sensitivity analysis for leakage gap and overall friction [66]. [67] utilized capacity modulation for their moving magnet linear compressor for a guaranteed efficient operation instead of active stroke control. They compared the capacity modulated compressor to the electrical resonance compressor and claim the potential energy saving capabilities for the capacity modulated version [68]. Then they investigated the dynamic response of the compressor to supply voltage disturbances [69]. [70] presented a moving-magnet linear compressor with clearance seals and flexure springs. They applied a test loop to determine the compressor efficiency and coefficient of performance using R134a. In another study [5] they compared the linear compressor to a conventional crank-drive compressor and showed that the linear compressor has a much higher motor efficiency, however, the volumetric efficiency of the linear compressor is yet to surpass the conventional one. In a further study, they employed a search coil for piston position sensing [71] and compared the operation of the compressor with a fixed clearance to zero DC offset operation [72]. [73] used linearization for the non-linear gas spring model and utilized this for a moving-magnet linear compressor, analyzing the system as a linear time varying one. [74] investigated the dynamic and thermodynamic characteristics of a moving coil Stirling-type cryocooler. [9] used a solenoid actuator for their linear compressor and investigated the system dynamics and natural frequency of their system. [75] introduced a moving-magnet Stirling-type with a cold compression capability, which improves the effectiveness in reaching lower temperatures. [76] divided a linear compressor to control volumes and performed heat transfer analysis for each control volume. Then they used calorimetric test and defined thermal network and introduced a software tool for its analysis.

In this study, the dynamic analysis will be shown for a miniature-scale, moving-magnet type linear compressor. The force model and the natural frequency analysis will be presented and the model will be compared with the output from the experimental setup. The entire assembly is custom-made with the exception of off-the-shelf miniature valves.

6.3 Linear Compressor Design

The proposed linear compressor is comprised of two parts: the linear actuator and the chamber assembly. The linear actuator is a moving-magnet type and it uses multiple poles in the stator. The magnets are placed inside the piston in a Halbach configuration in order to increase the magnetic force output. At the two ends of the piston, four flexure springs are attached which were manufactured from stainless steel. The employment of springs helps with the resonant behavior of the actuator. The coils at the stator are energized at a forward-backward sequence using DC current and the piston moves back-and-forth accordingly in order to align the magnetic fields of the coils and the magnets. If the excitation frequency matches the natural frequency of the actuator, which is determined by the total mover mass and the spring constant of the flexure springs, the used-up current decreases and large piston displacements are obtained.

The chamber assembly consists of a stainless steel cylinder with a bore diameter of 6 mm and an inlet-outlet valve pair placed at the end. Using 3-D printing, a housing for the valves was manufactured and this was attached at the end of the cylinder. The valves are commercially available mini-valves used usually for medical applications. They have an outer diameter of 2.5 mm. The schematic diagram of the entire assembly is presented in Figure 6.1.

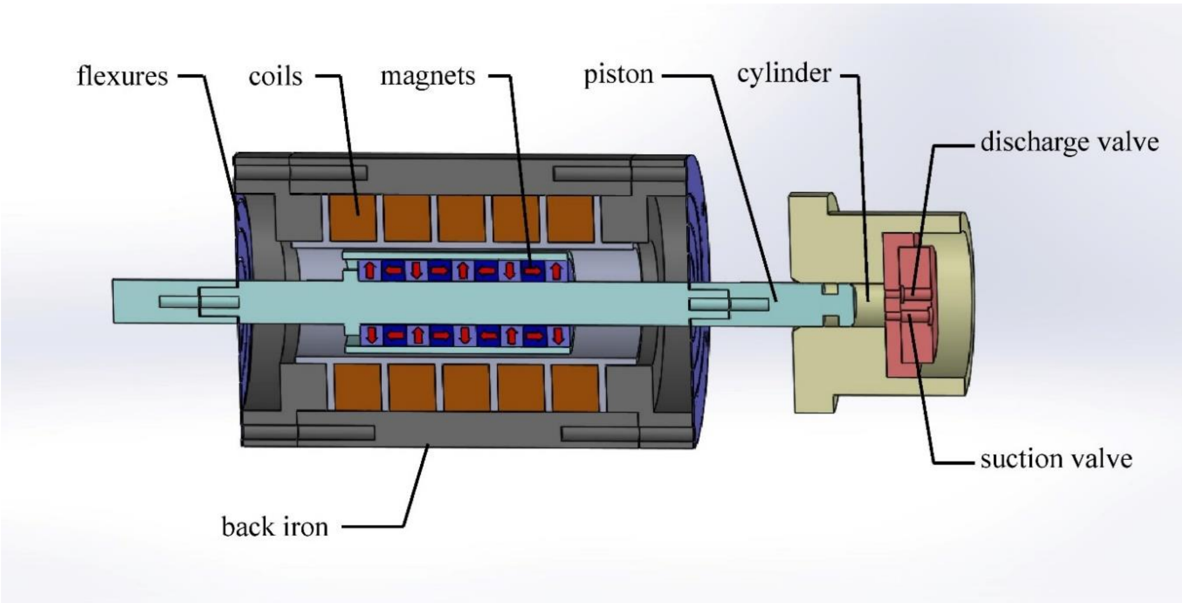

Figure 6.1: Schematic view of the linear compressor

In a linear compressor, the forces acting on the moving body are the inertia, the electromagnetic force, the mechanical spring force, the friction force and the gas force. In Figure 6.2, the free body diagram for the mover is presented. The dynamic equation is given as

$$m_{mover}\ddot{z} + k_{spr}z + c_{fr}\dot{z} + f_{gas}(t) = f_{em}(t) \tag{6-1}$$

where m_{mover} is the mover mass, z is the displacement, k_{spr} is the spring coefficient of flexures, c_{fr} is the viscous damping coefficient of friction.

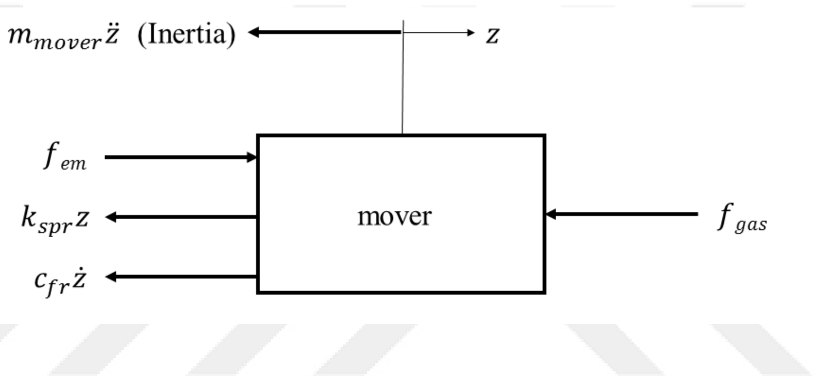

Figure 6.2: Free body diagram for the mover

The gas force $f_{gas}(t)$ can be determined using the cylinder pressure $P_{cylinder}(t)$ and the suction pressure $P_{suction}$:

$$f_{gas}(t) = (P_{cylinder}(t) - P_{suction})A_{cp} \tag{6-2}$$

where A_{cp} is the cross-sectional area of the piston.

In order to accurately model the system dynamics, the nonlinear model of the electromagnetic force and the gas force must be realized.

6.3.1 Electromagnetic Force Model

6.3.1.1 Analytical Model

The magnetic force provided by the actuator is generated by the interaction between magnetic fields of the permanent magnets inside the piston and the coils in the stator. The schematic structure of the actuator is given in Figure 6.3. Assuming infinite iron permeability and motor length, two regions can be observed from the figure, the first being the air gap, and the second the permanent magnets. Writing the magnetic field equations for these regions:

$$\nabla^2 \boldsymbol{A} = 0 \qquad \text{(Region I)}$$
$$\nabla^2 \boldsymbol{A} = -\mu_0 \nabla \times \boldsymbol{M} \qquad \text{(Region II)} \qquad (6\text{-}3)$$

with $\boldsymbol{A}$ the magnetic potential defined as $\nabla \times \boldsymbol{A} = \boldsymbol{B}$. $\boldsymbol{M}$ is the magnetization which is null in region I and in region II it is given in terms of radial and axial components as:

$$\boldsymbol{M} = \boldsymbol{M_r} + \boldsymbol{M_z} \qquad (6\text{-}4)$$

The radial and axial components can be expressed by Fourier series:

$$M_r(z) = \sum_{n=1,3,5,\dots}^{\infty} M_{nr} \sin(k_n z)$$
$$M_z(z) = \sum_{n=1,3,5,\dots}^{\infty} M_{nz} \cos(k_n z) \qquad (6\text{-}5)$$

where

$$M_{nr} = \frac{4B_{rem}}{n\pi\mu_0} \sin(\frac{n\pi}{2}) \sin(\frac{n\pi}{4}) \qquad (6\text{-}6)$$

$$M_{nz}=\frac{4B_{rem}}{n\pi\mu_0}\sin(\frac{n\pi}{4})$$

with B_{rem} being the remanent flux density and $k_n=n\pi/\tau_p$ with τ_p being the pole pitch.

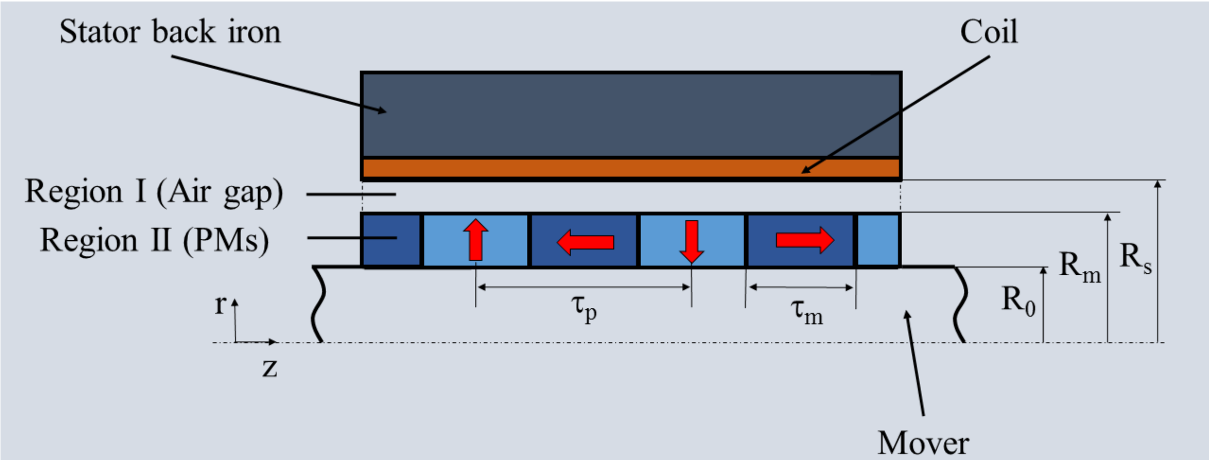

Figure 6.3: Schematic view of the moving magnet linear actuator

Solving the equations given in (6-3), the axial and radial magnetic flux densities for both regions are given as

$$H_z^I(r,z)=\sum_{n=1,3,5,\dots}^{\infty}k_n[-A_n^I I_0(k_nr)-B_n^I K_0(k_nr)]\cos(k_nz)$$

$$H_z^{II}(r,z)=\sum_{n=1,3,5,\dots}^{\infty}k_n[-A_n^{II} I_0(k_nr)-B_n^{II} K_0(k_nr)+\frac{2c_2M_{nr}}{{k_n}^2}]\cos(k_nz)$$

$$B_r^I(r,z)=\mu_0\sum_{n=1,3,5,\dots}^{\infty}k_n[-A_n^I I_1(k_nr)+B_n^I K_1(k_nr)]\sin(k_nz)$$

$$B_r^{II}(r,z)=\mu_0\mu_r\sum_{n=1,3,5,\dots}^{\infty}k_n\left[-A_n^{II} I_1(k_nr)-B_n^{II} K_1(k_nr)+(\frac{c_1}{r}+c_2r)\frac{M_{nr}}{k_n}\right]\sin(k_nz) \quad (6\text{-}7)$$

with I_0 and K_0 the modified Bessel functions of zeroth order, of first and second kind respectively, and I_1 and K_1 the modified Bessel functions of first order, of first and second kind respectively. The coefficients c_1 and c_2 are correction coefficients appropriately selected to reduce the modification of radial component M_r and are given as

$$c_1 = \frac{r_0 r_m}{r_0 + r_m}$$
$$c_2 = \frac{1}{r_0 + r_m} \tag{6-8}$$

Magnetic fields due to the currents are modeled by assuming the electric current at the EM poles to be on an infinitesimally thin surface on the interior surface at $r = r_s$. The current density $\boldsymbol{J}$ has only the azimuthal component $J_\theta(z)$:

$$J_\theta(z) = \sum_{n=1,3,5,\dots}^{\infty} J_n sin(k_n z) \tag{6-9}$$

with $J_n = 4N_s i/n\pi\tau_p$, N_s being the number of turns per pole and i the current. The current density appears according to the boundary condition:

$$H_z^I(r_s, z) = J_\theta(z) \tag{6-10}$$

Thus,

$$H_z(r,z) = \sum_{n=1,3,5,\dots}^{\infty} k_n \left[I_o(k_n r) + \beta_n K_0(k_n r)\right]\gamma_n J_n \sin(k_n z)$$
$$B_r(r,z) = \mu_0 \sum_{n=1,3,5,\dots}^{\infty} k_n \left[-I_1(k_n r) + \beta_n K_1(k_n r)\right]\gamma_n J_n \cos(k_n z) \tag{6-11}$$

with the coefficients β_n and γ_n given as

$$\beta_n = -\frac{I_o(k_n r_0)}{K_o(k_n r_0)}$$
$$\gamma_n = \frac{1}{k_n[I_0(k_n r_s) + \beta_n K_0(k_n r_s)]} \tag{6-12}$$

The axial thrust force is the result of the interaction of the magnetic flux of the PMs and the current density:

$$dF_z(z) = -2\pi r_s J_\theta(z) B_r^I(r_s, z) dz \tag{6-13}$$

F_z is obtained by integrating this along the motor length. The thrust per pole on the mover F_m is opposite to this, thus:

$$F_{mover} = \sum_{n=1,3,5,\dots}^{\infty} 8\pi r_s \frac{N_s}{\tau_p} \mu_0 [-A_n^I I_1(k_n r_s) + B_n^I K_1(k_n r_s)] \cos(k_n z_c) i \tag{6-14}$$

6.3.1.2 FEM Simulation

The flux density distribution and thrust force was also investigated via FEM simulation. A 2D axisymmetric model using Comsol software is considered for this matter. The metallic parts of the actuator are taken as stainless steel, with 430F used as the back iron. NdFeB is assigned to the permanent magnets with a remanent flux density of 1.43 T. The magnetic material naturally has a specific B-H curve, which is also assigned accordingly.

A user controlled mesh is used with finer meshes assigned to sharp corners and coarser meshes assigned to areas with larger dimensions.

The FEM results for magnetic flux density is given in Figure 6.4 and the thrust force per pole is compared in Figure 6.5 for analytical and FEM cases for an applied current of 0.5 A.

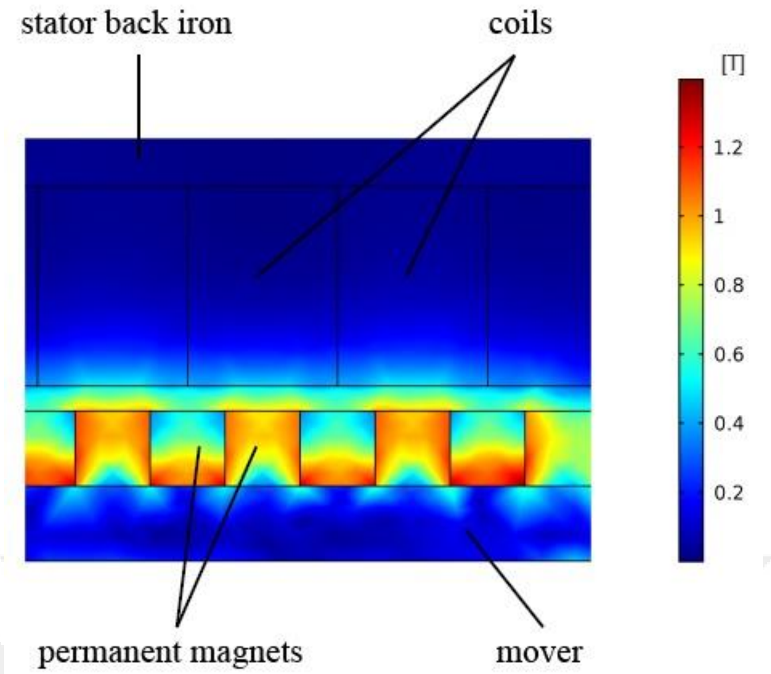

Figure 6.4: Magnetic flux density distribution for 0.5 A

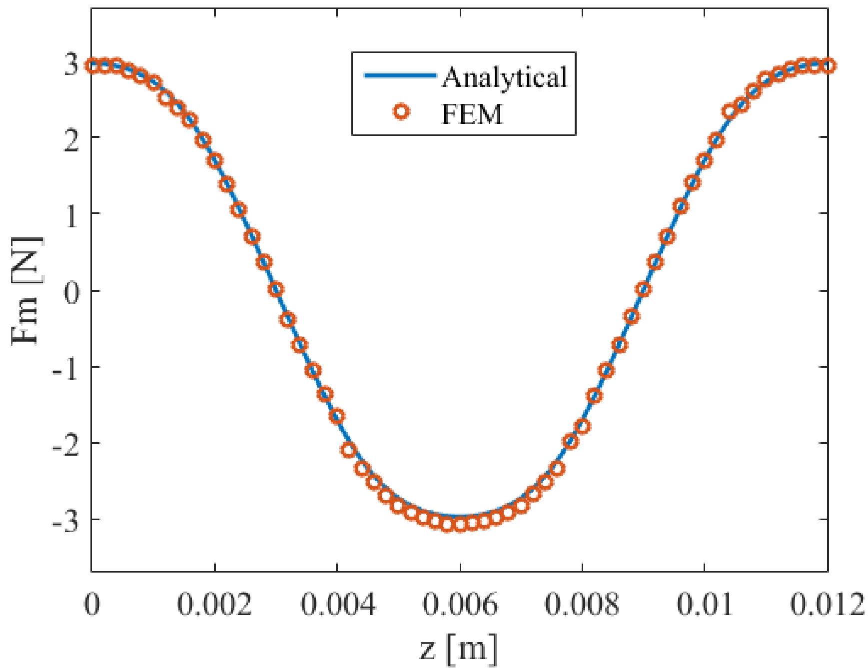

Figure 6.5: Thrust force on the mover for one coil at 0.5 A

6.3.2 Gas Force Model

The gas force is the force generated by the compressed gas and acts on the piston in the opposing direction. It can be modeled in terms of the following nonlinear relationship:

$$f_{gas}(t) = k_{gas}z + c_{gas}\dot{z} \tag{6-15}$$

Here, k_{gas} is the gas stiffness and c_{gas} is the gas damping coefficient. These coefficients can be estimated by interpolation. In this case, a Fourier interpolation is suitable with its parameters given as

$$f_{gas} = a_0 + a_1 \sin(\omega t) + a_2 \cos(\omega t) \tag{6-16}$$

$$\begin{aligned} a_1 &= k_{gas}Z \\ a_2 &= c_{gas}Z\omega^2 \end{aligned} \tag{6-17}$$

where Z is the peak stroke, a_0 is the gas force at the point where the suction valve is closed.

6.3.3 Resonance Model

The linear compressor operates most efficiently at its resonant frequency, so a resonance model is required in order to find that particular operating point. Starting with the governing dynamic equation,

$$m_{mover}\ddot{z} + \left(k_{spr} + k_{gas}\right)z + \left(c_{fr} + c_{gas}\right)\dot{z} = F_0 \sin(\omega t + \phi) \tag{6-18}$$

where F_0 is the amplitude of the electromagnetic force. Dividing by m_{mover}:

$$\ddot{z} + 2\zeta\omega_n\dot{z} + {\omega_n}^2 z = \frac{F_0}{m_{mover}}\cos(\omega t) \tag{6-19}$$

with $\zeta = \frac{(c_{fr}+c_{gas})}{2\sqrt{(k_{spr}+k_{gas})m_{mover}}}$ the damping ratio, and $\omega_n = \sqrt{\frac{k_{spr}+k_{gas}}{m_{mover}}}$ the natural frequency of the system. The solution to (6-16) and (6-17) is given as

$$z = Zsin(\omega t) \tag{6-20}$$

with

$$Z = \frac{\frac{F_0}{(k_{spr}+k_{gas})}}{\left\{\left[1-\left(\frac{\omega}{\omega_n}\right)^2\right]^2 + 4\zeta^2\left(\frac{\omega}{\omega_n}\right)^2\right\}^{\frac{1}{2}}}$$
$$\phi = tan^{-1}\frac{2\zeta\left(\frac{\omega}{\omega_n}\right)}{1-\left(\frac{\omega}{\omega_n}\right)^2} \tag{6-21}$$

where ω is the operating frequency. From (6-19) it can be seen that the maximum stroke amplitude is obtained at $\omega = \omega_n$ and and substituting (6-18) for (6-16) again for $\omega = \omega_n$ it can be seen that the inertial and stiffness forces cancel each other out, leaving only the damping forces as the effective contributors to power loss at resonance.

6.4 Experimental Setup

According to the geometric parameters given in Section 2, a prototype moving magnet linear compressor was manufactured.

The 6 mm piston size was a limiting factor for the miniaturization due to the valve sizes used in the compressor. In order to use a current output ranging around and not exceeding 0.5 A, a 26 AWG wire is employed with 200 windings at each pole (5 poles in total). The total length of the compressor is 75 mm with an overall diameter of 40 mm. The actuator is driven with an H-bridge driver using DC current. A mini-dynamometer is used to measure the force output and a laser displacement sensor is used to measure the displacement generated by the oscillatory motion. A miniature pressure sensor is employed inside the gas chamber for real-time pressure sensing. The compressor absorbs the ambient atmospheric air during suction and the compressed air is transferred via the discharge valve to the higher pressure medium. The entire test setup can be seen in Figure 6.6 and the prototype specifications are given in Table 6.1.

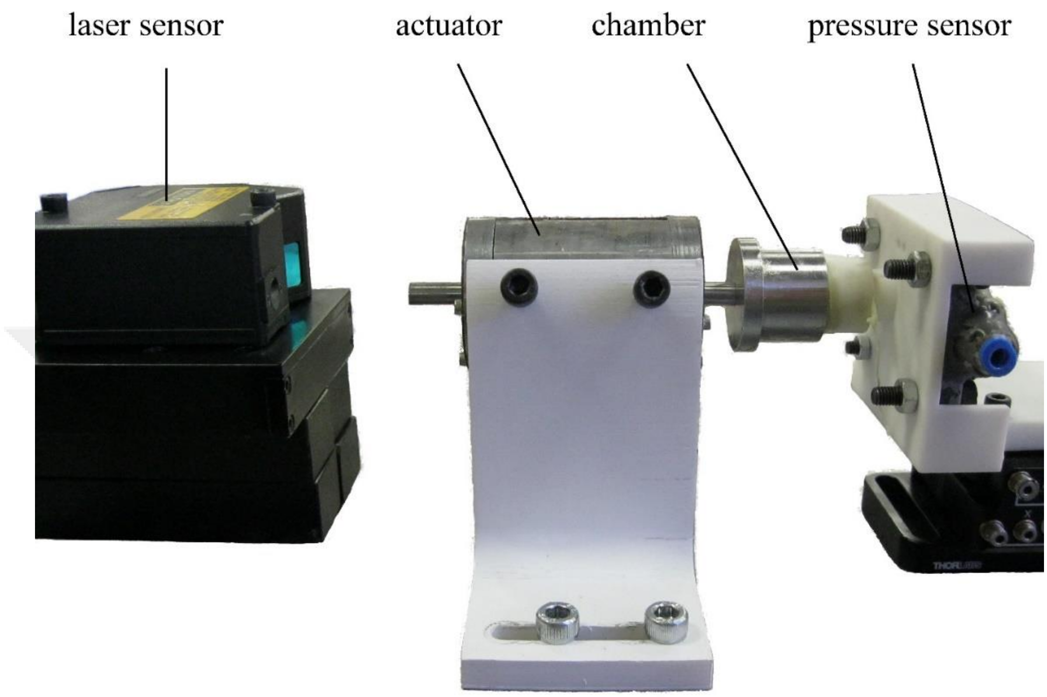

Figure 6.6: Experimental setup

Table 6.1: Prototype specifications

Total length of the compressor [mm]	75
Overall diameter of the compressor [mm]	40
Piston diameter [mm]	6
Mover mass [g]	54.52
Number of turns per coil	200
Stroke [mm]	4
Applied current [A]	0.502
Input power [W]	7.53
Max. discharge pressure [bar]	3.3

Two tests were performed to validate the dynamic characteristics of the system. First an impact hammer test was performed to identify the system characteristics. Figure 6.7 shows the modal analysis results of the test. The mode at 50.05 Hz has a comparably higher magnitude of 1.923 mN^{-1} with a damping ratio of 0.0142, system modal stiffness of 3.3708E+002 Nm^{-1} and system mass of 3.4087E-003 kg.

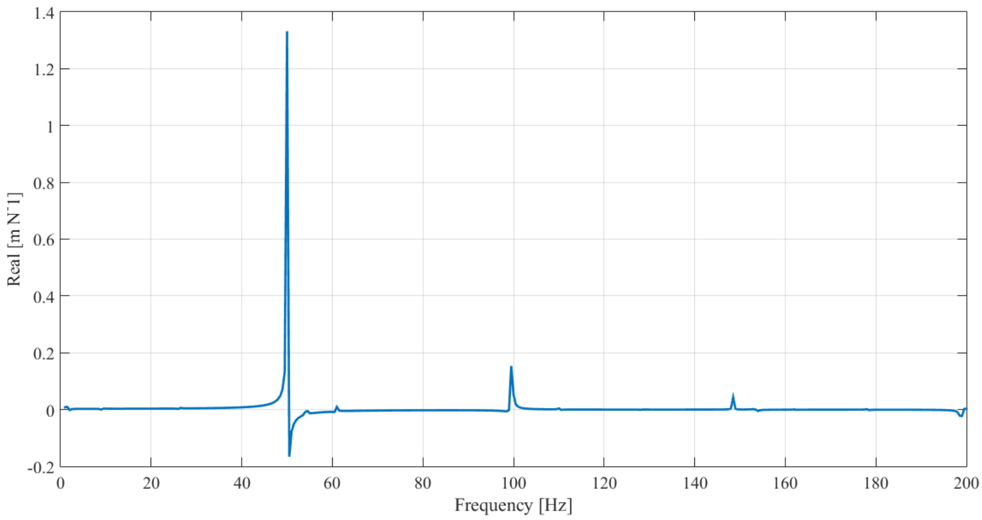

(a)

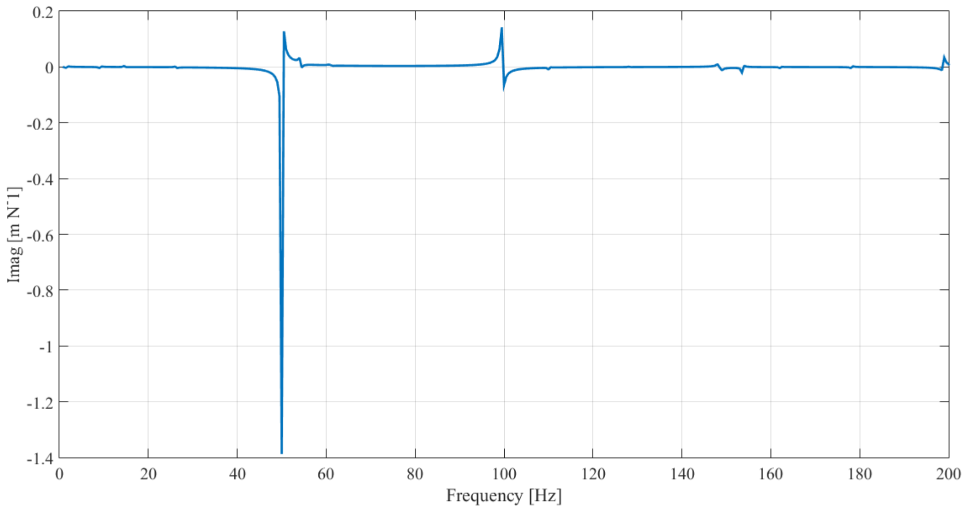

(b)

Figure 6.7: Real and imaginary parts of the frequency response function

In the second test a frequency sweep was performed in order to see the stroke to current ratio, starting from 30 Hz to 60 Hz. The obtained graph in Figure 6.8 shows that the maximum value is achieved at 45 Hz.

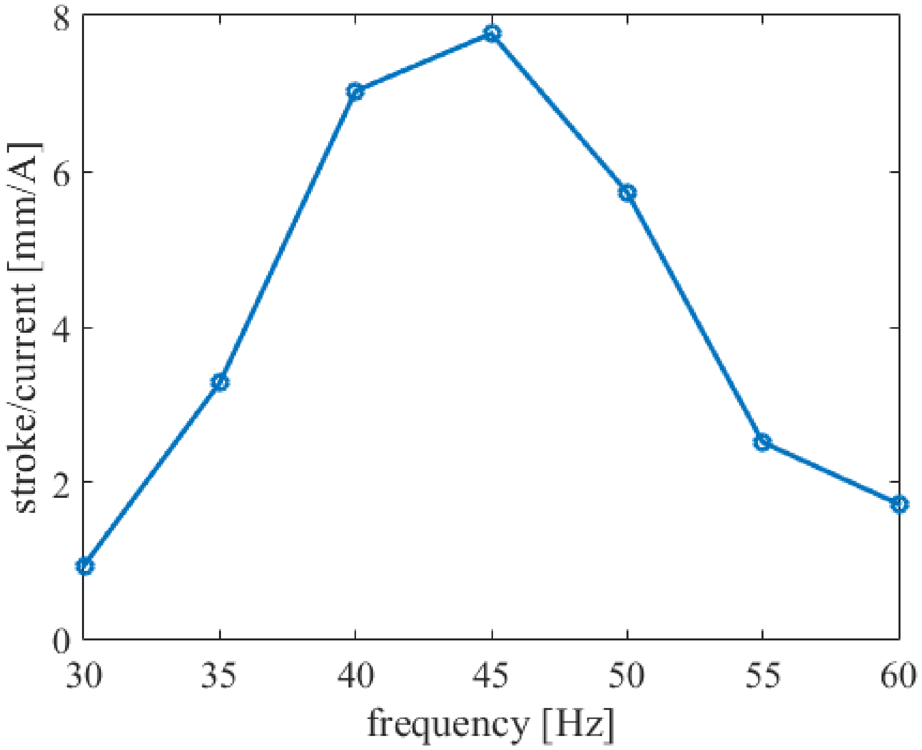

Figure 6.8: Stroke to current ratios shown from 30 Hz to 60 Hz

The gas force is experimentally validated for one cycle and it is compared with the Fourier interpolation, which can be seen in Figure 6.9. Using this interpolation a resonance frequency of 43.17 Hz is obtained.

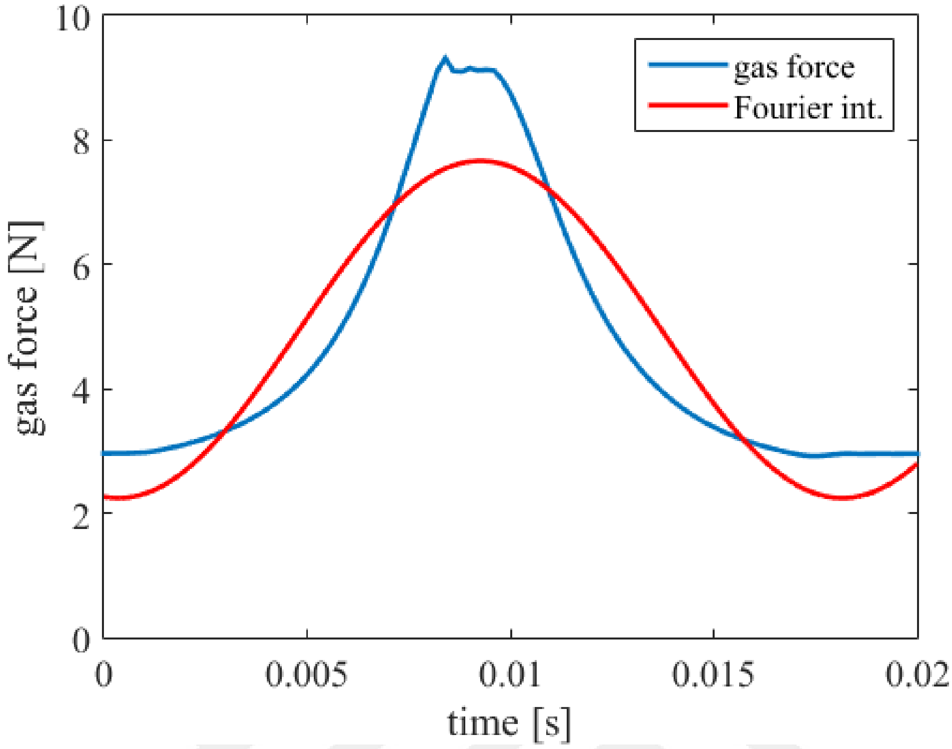

Figure 6.9: The measured gas force for one cycle and its Fourier interpolation

The generated P-V diagram for the compressor is given in Figure 6.10. There is a dead volume of 15 mm^3 which contributes negatively to the work done by the gas, which is calculated to be 8.6 mJ. The input power is 7.53 W, and at resonance frequency an electrical efficiency of 80.4% is achieved.

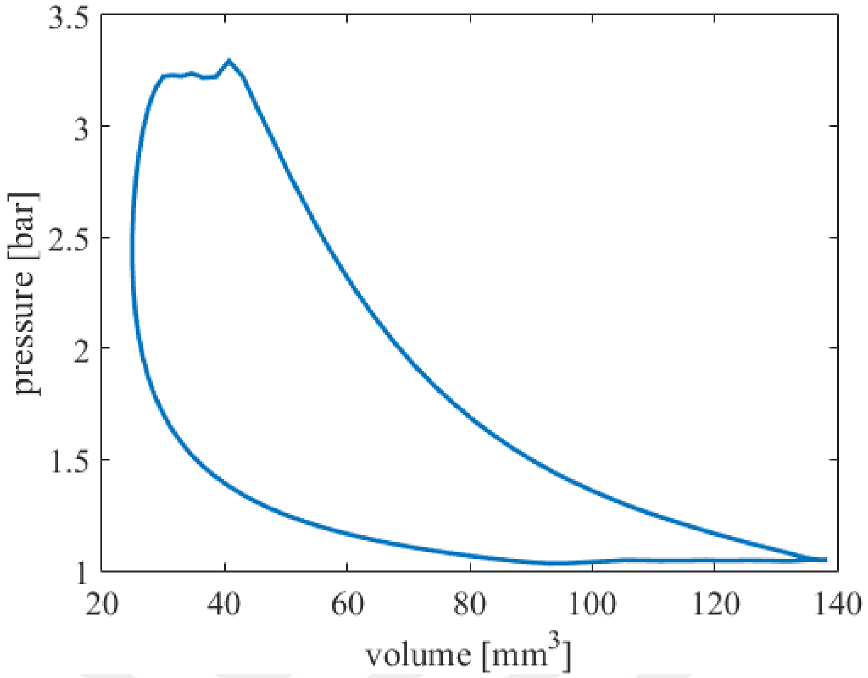

Figure 6.10: The generated P-V diagram for one cycle

6.5 Conclusion

In this chapter, the miniature size linear compressor design was analyzed in its entirety along with the linear actuator and the gas compression mechanism in the chamber-valve assembly. As mentioned in the previous chapter, the compressor owes its compactness to its tubular configuration and the employment of flexure bearings which serve as both resonant springs and linear bearings for the mover. One other contributor to the compactness is the employment of N52 grade NdFeB magnets in order to cover for the reduced force capabilities associated with slotless designs, where the magnets are placed in Halbach array configuration, for self-shielding capability and using this property, low density, nonmagnetic or hollow mover structures can also be selected to enable design flexibility and the utilization of movers with lower mass. The governing dynamic equation during compressor operation is introduced and each force contributor to this equation is demonstrated. Analytical calculations and a FEM simulation are performed to find the magnetic flux density and the thrust force generated by the linear actuator. The gas force model was introduced with a Fourier approximation for the calculation of nonlinear gas parameters. Finally, the prototype compressor is driven at different frequencies to view the stroke to current ratio, and the efficiency of the system. At the resonant frequency which is found to be 45 Hz the stroke to current ratio and the system efficiency is at the highest. At this frequency, an electrical efficiency of 80.4% is achieved.

Chapter 7

CONCLUSION

Linear compressors are a very good alternative to conventional rotary compressors where the rotary-to-linear motion conversion mechanisms, which in the case of the rotary compressor, usually are the crank mechanisms, are eliminated, which in turn enables noise reduction and force losses such as friction and radial forces, and paves the way for a lot more compact designs. While this greatly enhances the overall efficiency of the compressor, it is further improved by the manipulation of the actuator mechanism that is employed for this operation, i.e. the linear oscillatory motor. This member of the compressor is excited at its resonance frequency where the mechanical resonance effect is usually realized by the employment of resonant springs. At resonance the pulled current by the motor at the same input voltage is reduced, thus the input power is reduced, which in turn means an increase on the efficiency.

A linear compressor consists of two main members: the aforementioned linear oscillatory motor which serves as the actuator for the compressor, and the chamber-valve assembly where the gas compression occurs. In a compressor, gas compression is accomplished by the piston-chamber interaction and in the case of a linear compressor the piston is directly connected to the moving part of the linear motor, which only generates motion in the axial direction. As with the conventional compressors, the piston-chamber interaction is important; an efficient sealing between those components must be accomplished all the while trying to eliminate the occurring friction during operation as much as possible. The valves used at the end of the chamber should be selected as quickly responsive and leak-tight to reverse flow.

Just like the conventional rotary motor, motion in a linear motor is generated by the interaction of the magnetic fields between that of the stationary part, i.e. the stator, and of the moving part, i.e. the mover or the armature. The magnetic fields can be generated by either electromagnets, i.e. coils, or permanent magnets. The motors can be induction motors, synchronous motors, plunger solenoids, or oscillatory motors. The linear motor type that is used for linear compressor application is the linear oscillatory motor. While many linear motor types are three phase motors, linear oscillatory motors are single phase motors which oscillate back and forth at relatively smaller displacements, which in the case of linear compressor application can be called the stroke. There are mainly three types of linear oscillatory motors: moving-coil, moving-iron and moving-magnet. In a moving-coil linear oscillatory motor the coils are placed on the moving part and the permanent magnets are placed in the stator. Moving-iron linear oscillatory motors are basically plunger solenoids operated at a fixed frequency continuously. In this configuration the coils are placed in the stator and the mover is a magnetic iron. Permanent magnets can also be put on the stator to further enhance the magnetic fields. In a moving-magnet linear oscillatory motor the coils are placed in the stator and the mover includes permanent magnets in it. While the linear oscillatory motors are single phase, especially for the moving-coil and moving-magnet type motors multiple-pole configurations are available both for the coils and the permanent magnets. Such configurations are preferred to remedy the low coil inductance problems and leakage flux and fringing losses, however one downside to this is that the mover weight might significantly increase, and the mechanical spring cost must go higher in order to generate resonance at the same frequency. As with the other types of linear motors, tubular and flat-type configurations are available for linear oscillatory motors, however, tubular types have the advantage of more surface area between stator and mover, which leads to higher thrust and enhanced heat dissipation and better dealing with radial forces due to circularity. Of the three linear oscillatory motor types, the moving-magnet linear oscillatory motor offers the best thrust density with a relatively limited stroke.

For the miniature linear compressor application, the moving-magnet type linear oscillatory motor is selected as the actuator due to the thrust advantage and compactness it offers. Multiple-coil and permanent magnet configuration is selected to further improve the thrust capability and deal better with electromagnetic losses. NdFeB permanent magnets are selected as permanent magnets for their superior remanent flux density and on the mover they are placed in Halbach array configuration to further enhance the flux density in the air gap between the coils in the stator and the permanent magnets. The axially magnetized magnets in the Halbach array are selected as ring magnets. Since it is very difficult to produce radially magnetized ring magnets, arc magnets are employed which are used to form a complete ring of radially magnetized magnet in the Halbach array. As resonant springs, flexure bearings are proposed which are produced by opening grooves on thin steel plates, and they also have the functionality of serving as linear bearings for the mover. The employment of such members as resonant springs helps with the ease of assembly as well as the reduction of the overall length of the motor, which enhances the compactness even further. In order to come up with an estimation for the stiffness coefficient of the flexures, an FEM simulation is conducted to find out the applied force vs. displacement curve, from which the coefficient is extracted. The simulation also gives an idea on the stresses generated on the flexure under axial load. The estimation of the stiffness coefficient helps with the analytical determination of the resonance frequency of the linear oscillatory motor.

On the chamber-valve assembly side, duckbill valves by miniValve company are chosen as check valves to be put at the end of the chamber. These are the smallest commercially available valves with a housing diameter of 2.5 mm. The piston and chamber diameter miniaturization is thus kept at 6 mm and not further down in order to house both the inlet and the outlet valve. These valves have the advantage of having a very low cracking pressure and being leak-tight to backward flow, enabling very fast response during gas compression.

The moving-magnet linear oscillatory motor is a slotless configuration, selected this way in order to eliminate cogging forces. For the motor, a magnetic circuit analysis is presented to come up with an estimation of magnetic flux generated and the thrust force acting on the mover. Then, a detailed analysis using Maxwell's equations is conducted for these quantities and an FEM simulation is carried out for comparison. For no load condition, i.e. only considering the excitation of the motor and not the gas compression part, the motor is operated at several frequencies and current inputs, to show that the motor is most efficient at its resonance frequency, pulling the least amount of current at that frequency, and the thrust force measurements agree with the analytical and the FEM simulation results. The force and stroke measurements are carried out using a mini-dynamometer and a laser displacement sensor suitable for this kind of application.

The actuator is then connected with the chamber-valve assembly to build the linear compressor. The chamber is a stainless steel cylinder with a bore diameter of 6 mm. The valve housing for the valves is manufactured using 3D printing and attached at the end of this cylinder. A dynamic analysis is then presented for the entire assembly at resonance excitation. The governing equations of motion have this time the component of gas force where the components of this force contain the stiffness of the gas and the damping coefficient of the gas. This means that there is a nonlinearity for the total stiffness and damping of the system. The gas coefficients can be estimated by interpolation. There are several approaches for this matter including the linearization method. For this study a Fourier interpolation is selected. Two tests are performed to find out the system dynamics. The first one is an impact hammer test to identify the system characteristics. The second one is a frequency sweep test where the compressor operates at several frequencies to determine the stroke to current ratio corresponding to each frequency. Using these two tests, an estimate for the resonance behavior of the system is obtained. The resonance frequency values obtained from these two analyses are then compared with the one calculated from the Fourier interpolation of the gas force. The resonance frequency values obtained from these three approaches are in close proximity with each other. Next, the P-V diagram is generated for one cycle of the compressor. There is some dead volume contributing negatively to the work generated by the gas, despite this a very good efficiency is achieved at resonance frequency for a considerably low input power. This shows that linear compressors are very suitable for miniaturization and become very suitable candidates for applications such as electronics cooling and miniature scale refrigerator prototypes.

BIBLIOGRAPHY

[1] J. Rees, *Refrigeration Nation: A History of Ice, Appliances, and Enterprise in America,* The Johns Hopkins University Press, Baltimore, p. 2, 2014.

[2] "Production – household refrigerators — Country and Region Comparisons," [Online]. Available: http://statinfo.biz/Data.aspx?act=6132&lang=2. [Accessed: 01-Jul-2017].

[3] Y. Cengel, M. Boles, *Thermodynamics: An Engineering Approach, 8th Ed.*, McGraw-Hill Education, pp. 609-610, New York, 2015.

[4] "Technical Information: Compressors," [Online]. Available: http://www.ref-wiki.com/en/technical-information/145-compressors/31773-hermetic-compressors.html. [Accessed: 01-Jul-2017].

[5] K. Liang, R. Stone, W. Hancock, M. Dadd, P. Bailey, "Comparison between a crank drive reciprocating compressor and a novel oil-free linear compressor," *International Journal of Refrigeration*, vol. 45, pp. 25-34, 2014.

[6] H. Lee, G. Song, J. Park, and E. Hong, "Development of the linear compressor for a household refrigerator," *International Compressor Engineering Conference*, Purdue University, 2000.

[7] Z. Lin, J. Wang, J. Park, and D. Howe, "A Resonant Frequency Tracking Technique for Linear Vapor Compressors," *Electric Machines & Drives Conference*, 2007. IEMDC '07. IEEE International, Antalya, Turkey, 2007.

[8] J. Tan, H. Dang, "Effects of the driving voltage waveform on the performance of the Stirling-type pulse tube cryocooler driven by the moving-coil linear compressor," *International Journal of Refrigeration*, vol. 75, pp. 239-249, 2017.

[9] A. Bijanzad, A. Hassan, I. Lazoglu, "Analysis of solenoid based linear compressor for household refrigerator," *International Journal of Refrigeration*, vol. 74, pp. 116-128, 2017.

[10] A. A. Sathe, E. A. Groll, S. V. Garimella, "Optimization of electrostatically actuated miniature compressors for electronics cooling," *International Journal of Refrigeration*, vol. 32, pp. 1517-1525, 2009.

[11] C. R. Bradshaw, E. A. Groll, S. V. Garimella, "A comprehensive model of a miniature-scale linear compressor for electronics cooling," *International Journal of Refrigeration*, vol. 34, pp. 63-73, 2011.

[12] I. Boldea, Syed A. Nasar, *Linear Electric Actuators and Generators.* Cambridge University Press, pp. 8-10, New York, 1997.

[13] R. Groessinger, N. Mehboob, M. Kriegisch, A. Bachmaier, R. Pippan, "Frequency dependence of the coercivity of soft magnetic materials," *IEEE Transactions on Magnetics*, vol. 48, pp. 1473-1476, 2012.

[14] "Permanent Magnet Demagnetization Curves," [Online]. Available: https://www.kjmagnetics.com/images/blog/demag.curves2d.gif. [Accessed: 02-Jul-2017].

[15] "Demagnetization (BH) Curves for Neodymium Magnets," [Online]. Available: https://www.kjmagnetics.com/bhcurves.asp. [Accessed: 02-Jul-2017].

[16] "Magnetization Direction for Neodymium Magnets," [Online]. Available: https://www.kjmagnetics.com/magdir.asp. [Accessed: 02-Jul-2017].

[17] "Slotted vs. Slotless Motor Technology," [Online]. Available: https://www.servo2go.com/information.php?menu=TS&page=10032. [Accessed: 02-Jul-2017].

[18] "Magnetic Circuits," [Online]. Available: http://nptel.ac.in/courses/108105053/pdf/L-21(TB)(ET)%20((EE)NPTEL).pdf. [Accessed: 02-Jul-2017].

[19] "Brush Linear Motors," [Online]. Available: https://www.h2wtech.com/category/brush-linear#productInfo1. [Accessed: 02-Jul-2017].

[20] I. Boldea, Syed A. Nasar, *Linear Electric Actuators and Generators.* Cambridge University Press. pp. 34-35, New York, 1997.

[21] R. J. Kaye, E. Masada, *Comparison of Linear Synchronous and Induction Motors.* Urban Maglev Technology Development Program Colorado Maglev Project, Report Number: FTA-DC-26-7002.2004.01 SAND2004-2734P, pp. 7-8, 2004.

[22] R. J. Kaye, E. Masada, *Comparison of Linear Synchronous and Induction Motors.* Urban Maglev Technology Development Program Colorado Maglev Project, Report Number: FTA-DC-26-7002.2004.01 SAND2004-2734P, pp. 10-11, 2004.

[23] "Linear Induction Motors," [Online]. Available: https://www.h2wtech.com/category/linear-induction#productInfo1. [Accessed: 02-Jul-2017].

[24] "Series Linear Synchronous Motors," [Online]. Available: http://www.smwe.cz/index.php?id=25. [Accessed: 02-Jul-2017].

[25] "LP Cylindrical Linear Motors," [Online]. Available: http://www.oswald.de/en/products/lp-cylindrical-linear-motors/. [Accessed: 02-Jul-2017].

[26] "Linear Solenoid Actuator," [Online]. Available: http://www.electronics-tutorials.ws/io/io_6.html. [Accessed: 02-Jul-2017].

[27] "Voice Coil Actuators," [Online]. Available: http://ariwatch.com/VS/VoiceCoils/. [Accessed: 02-Jul-2017].

[28] D. K. Chembe, J. M. Strauss, "Armature reaction magnetic field prediction for a moving-coil tubular permanent magnet linear oscillatory machine," 25th Southern African Universities Power Engineering Conference – SAUPEC, Stellenbosch, 2017.

[29] "PWM," [Online]. Available: https://www.arduino.cc/en/Tutorial/PWM. [Accessed: 02-Jul-2017].

[30] X. Li, W. Xu, C. Ye, J. Zhu, "Novel hybrid-flux-path moving-iron linear oscillatory machine with magnets on stator," *IEEE Transactions on Magnetics*, vol. 53, 2017.

[31] C. Pompermaier, K. Kalluf, A. Zambonetti, M. V. Ferreira da Luz and I. Boldea, "Small linear PM oscillatory motor: magnetic circuit modeling corrected by axisymmetric 2-D FEM and experimental characterization," *IEEE Transactions on Industrial Electronics*, vol. 59, pp. 1389-1396, 2012.

[32] J. Wang, D. Howe, Z. Lin, "Design Optimization of Short-Stroke Single-Phase Tubular Permanent-Magnet Motor for Refrigeration Applications," *IEEE Transactions on Industrial Electronics*, vol. 57, pp. 327-334, 2010.

[33] H. Liang, Z. Jiao, L. Yan, L. Zhao, S. Wu, Y. Li, "Design and analysis of a tubular linear oscillating motor for directly-driven EHA pump," *Sensors and Actuators A*, vol. 210, pp. 107-118, 2014.

[34] P. Smith, R. W. Zappe, *Valve Selection Handbook.* Elsevier, p. 1, 2004.

[35] T. C. Dickinson, *Valves, Piping and Pipelines Handbook.* Elsevier, pp. 185-195, 1999.

[36] "miniValve Products," [Online]. Available: http://www.minivalve.com/newsite/index.php/en/products-and-technology/products/catalog-valves. [Accessed: 03-Jul-2017].

[37] "2.5 mm Check Valve for Plastic Installation," [Online]. Available: http://www.leeimh.com/plastic/check-valves/check-valve-25p.htm. [Accessed: 03-Jul-2017].

[38] "Halbach Arrays," [Online]. Available: https://www.kjmagnetics.com/blog.asp?p=halbach-arrays. [Accessed: 04-Jul-2017].

[39] F. H. Kharadi, M. S. Jadhav, S. D. Kanhurkar, P. A. Pereira, Dr.V. K. Bhojwani, S. Phadkule, "Selection of high performing geometry in flexure bearings for linear compressor applications using FEA," *International Journal of Scientific & Technology Research*, Vol. 4, Issue 01, pp. 170-173, 2015.

[40] X. Chen, Z. Q. Zhu, "Analytical determination of optimal split ratio of E-core permanent magnet linear oscillating actuators," *IEEE Transactions on Industrial Electronics*, vol. 47, no. 1, pp. 25-33, 2011.

[41] I. Boldea, Syed A. Nasar, *Linear electric actuators and generators.* Cambridge University Press, pp. 36-39, New York, 1997.

[42] H. Yamada, T. Hamajima, S. Xiang, N. Nishizawa, "Six-phase cylindrical linear pulse motor as linear oscillatory actuator," *IEEE Transactions on Magnetics.*, vol. 23, no. 5, pp. 2841-2843, 1987.

[43] D. Ebihara, M. Watada, "Development of a single-winding linear oscillatory actuator," *IEEE Transactions on Magnetics*, vol. 28, no. 5, pp. 3030-3032, 1992.

[44] M. Watada, K. Yanashima, Y. Oishi, D. Ebihara, "Improvement on characteristics of linear oscillatory actuator for artificial hearts," *IEEE Transactions on Magnetics*, vol. 29, no. 6, pp. 3061-3363, 1993.

[45] R. E. Clark, D. S. Smith, P.H. Mellor, D. Howe, “Design optimisation of moving-magnet actuators for reciprocating electro-mechanical systems,” *IEEE Transactions on Magnetics,* vol. 31, no. 6, pp. 3746-3748, 1995.

[46] Y. Abe , A. Nakagawa , M. Watada, S. Torii , K. Yamane , D. Ebihara, “Basic characteristics of linear oscillatory actuator for liquid hydrogen pump,” *IEEE Transactions on Magnetics,* vol. 32, no. 5, pp. 5025-5027, 1996.

[47] S. Yoon, I. Jung, K. Kim, D. Hyun, “Dynamic analysis of a reciprocating linear actuator for gas compression using finite element method,” *IEEE Transactions on Magnetics,* vol. 33, no. 5, pp. 4113-4115, 1997.

[48] J. Wang, G. W. Jewell, D. Howe, “A general framework for the analysis and design of tubular linear magnet machines,” *IEEE Transactions on Magnetics,* vol. 35, no. 3, pp. 1986-2000, 1999.

[49] R. E. Clark, D. Howe, G. W. Jewell, “The influence of magnetization pattern on the performance of a cylindrical moving-magnet linear actuator,” *IEEE Transactions on Magnetics,* vol. 36, no. 5, pp. 3571-3574, 2000.

[50] N. Bianchi, “Analytical field computation of a tubular permanent-magnet linear motor,” *IEEE Transactions on Magnetics,* vol. 36, no. 5, pp. 3798-3801, 2000.

[51] K. Park, E. Hong, H. K. Lee, “Linear motor for linear compressor,” *International Compressor Engineering Conference,* Paper 1544, 2002.

[52] S. Jang, J. Choi, S. Lee, H. Cho, W. Jang, “Analysis and experimental verification of moving-magnet linear actuator with cylindrical Halbach array,” *IEEE Transactions on Magnetics,* vol. 40, no. 4, pp. 2068-2070, 2004.

[53] T. Mizuno, M. Kawai, F. Tsuchiya, M. Kosugi, H. Yamada, “An examination for increasing the motor constant of a cylindrical moving magnet-type linear actuator,” *IEEE Transactions on Magnetics,* vol. 41, no. 10, pp. 3976-3978, 2005.

[54] S. M. Jang, J. Y. Choi, H. W. Cho, W. B. Jang, B. H. Kim, "The influence of mechanical resonance on the dynamic performance of a tubular linear actuator with Halbach array," *ICEMS 2005, Proceedings of the Eighth International Conference on Electrical Machines and Systems,* pp. 264-269, 2005.

[55] R. B. Ummaneni, R. Nilssen, J. E. Brennvall, "Force analysis in design of high power linear permanent magnet actuator with gas springs in drilling applications," *Electric Machines & Drives Conference,* pp. 285-288, 2007.

[56] Z. Q. Zhu, X. Chen, D. Howe, S. Iwasaki, "Electromagnetic modeling of a novel linear oscillating actuator," *IEEE Transactions on Magnetics*, vol. 44, no. 11, pp. 3855-3858, 2008.

[57] Z. Q. Zhu, X. Chen, "Analysis of an E-core interior permanent magnet linear oscillating actuator," *IEEE Transactions on Magnetics,* vol. 45, no. 10, pp. 4384-4387, 2009.

[58] N. C. Tsai, C. W. Chiang, "Design and analysis of magnetically-drive actuator applied for linear compressor," *Mechatronics* 20, pp. 596–603, 2010.

[59] Y. Son, Y. You, B. Kwon, "Optimal design to increase thrust force in electro-magnetic linear actuator for fatigue and durability test machine," *IEEE Transactions on Magnetics,* vol. 47, no. 10, pp. 4294-4297, 2011.

[60] Q. Lu, M. Yu, Y. Ye, Y. Fang, and J. Zhu, "Thrust force of novel PM transverse flux linear oscillating actuators with moving magnet," *IEEE Transactions on Magnetics,* vol. 47, no. 10, pp. 4211-4214, 2011.

[61] F. Poltschak, "A high efficient linear motor for compressor applications," *2014 International Symposium on Power Electronics, Electrical Drives, Automation and Motion,* pp. 1356-1361, 2014.

[62] T. Wang, Z. Jiao, L. Yan, C. Y. Chen and I. M. Chen, "Design and analysis of an improved Halbach tubular linear motor with non-ferromagnetic mover tube for direct-driven EHA," *Proceedings of 2014 IEEE Chinese Guidance, Navigation and Control Conference,* pp. 797-812, 2014.

[63] K. Li, X. Zhang, H. Chen, "Design optimization of a tubular permanent magnet machine for cryocoolers," *IEEE Transactions on Magnetics*, vol. 51, no. 5, 2015.

[64] Q. Lu, Y. Ye, M. Yu, "Model and analysis of integrative transverse-flux linear compressor," 2015, *Tenth International Conference on Ecological Vehicles and Renewable Energies*, pp. 1-8, 2015.

[65] M. Xia, X. Chen, "Analysis of resonant frequency of moving magnet linear compressor of Stirling cryocooler," *International Journal of Refrigeration*, vol. 33, pp. 739-744, 2010.

[66] C. R. Bradshaw, E. A. Groll, S. V. Garimella, "Sensitivity analysis of a comprehensive model for a miniature-scale linear compressor for electronics cooling," *International Journal of Refrigeration*, vol. 36, pp. 1998-2006, 2013.

[67] J. K. Kim, C. G. Roh, H. Kim, J. H. Jeong, "An experimental and numerical study on an inherent capacity modulated linear compressor for home refrigerators," *International Journal of Refrigeration*, vol. 34, pp. 1415-1423, 2011.

[68] J. K. Kim, J. H. Jeong, "Performance characteristics of a capacity modulated linear compressor for home refrigerators," *International Journal of Refrigeration*, vol. 36, pp. 776-785, 2013.

[69] J. K. Kim, J. H. Jeong, "Dynamic response of a capacity-modulated linear compressor to supply voltage disturbances," *International Journal of Refrigeration*, vol. 40, pp. 84-96, 2014.

[70] K. Liang, R. Stone, M. Dadd, P. Bailey, “A novel linear electromagnetic-drive oil-free refrigeration compressor using R134a,” *International Journal of Refrigeration*, vol. 40, pp. 450-459, 2014.

[71] K. Liang, R. Stone, M. Dadd, P. Bailey, “Piston position sensing and control in a linear compressor using a search coil,” *International Journal of Refrigeration*, vol. 66, pp. 32-40, 2016.

[72] K. Liang, R. Stone, M. Dadd, P. Bailey, “The effect of clearance control on the performance of an oil-free linear refrigeration compressor and a comparison between using a bleed flow and a DC current bias,” *International Journal of Refrigeration*, vol. 69, pp. 407-417, 2016.

[73] P. S. Dainez, J. de Oliveira, A. Nied, M. S. M. Cavalca, “A linear resonant compressor model based on a new linearization method of the gas pressure force,” *International Journal of Refrigeration*, vol. 48, pp. 201-209, 2014.

[74] H. Dang, L. Zhang, N. Tan, “Dynamic and thermodynamic characteristics of the moving-coil linear compressor for the pulse tube cryocooler. Part A: Theoretical analyses and modeling,” *International Journal of Refrigeration*, vol. 69, pp. 480-496, 2016.

[75] J. Park, S. Jeong, J. Cha, “Development and experimental investigation of Stirling-type pulse tube refrigerator (PTR) below 20 K; cold compressor and colder expander, ” *International Journal of Refrigeration*, vol. 75, pp. 64-76, 2017.

[76] M. Park, J. Lee, H. Kim, Y. Ahn, “Experimental and numerical study of heat transfer characteristics using the heat balance in a linear compressor,” *International Journal of Refrigeration*, vol. 74, pp. 550-559, 2017.